Comenius University in Bratislava
Faculty of Mathematics, Physics and Informatics

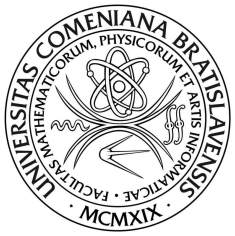

Nonlinear convection during phase change

Dissertation thesis

Study programme: 9.1.9 Applied mathematics

Supervising institution: Department of Applied Mathematics and Statistics

Supervisor: Doc. RNDr. Peter Guba, PhD.

Bratislava 2014 Mgr. Juraj Kyselica

Univerzita Komenského v Bratislave
Fakulta matematiky, fyziky a informatiky

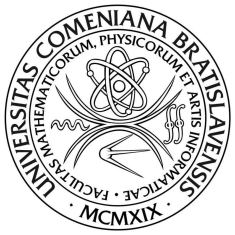

Nelineárna konvekcia pri fázovej premene

Dizertačná práca

Študijný odbor: 9.1.9 Aplikovaná matematika

Školiace pracovisko: Katedra aplikovanej matematiky a štatistiky

Školiteľ: Doc. RNDr. Peter Guba, PhD.

Bratislava 2014 Mgr. Juraj Kyselica

Hereby I declare that this dissertation was written on my own with all the relevant references listed in bibliography.

Bratislava, April 29, 2014 .....

Juraj Kyselica

I would like to express my sincere gratitude to my supervisor

Doc. Mgr. Peter Guba, PhD.

for his kind support, guidance and many inspiring discussions during the work on this dissertation.

Abstract

We study the solidification of a binary alloy over a horizontally moving substrate. Both cases without a mushy layer and with the mushy layer present in the system are analysed, the phase interfaces being two-dimensional. The self-similar solutions of the governing boundary-layer equations are found and analysed via the asymptotic methods. The main goal of the thesis is to determine how the boundary-layer flow influences the physical characteristics of the solidifying system. Some of the results apply also to the systems with planar interfaces.

Keywords: Solidification of binary alloys • Mushy layers • Boundary layers • Free-boundary problems • Self-similar solutions • Asymptotic approximations

AMS Subject Classification: 80A22 • 35C06 • 76M45

Abstrakt

V dizertačnej práci sa zaoberáme tuhnutím binárnej zmesi nad horizontálne posúvaným ochladeným substrátom. Predmetom štúdia je situácia keď je v systéme prítomná len tuhá a kvapalná fáza a tiež situácia keď je tuhá fáza oddelená od kvapalnej fázy dendritickou zónou. V práci sú odvodené samopodobné riešenia príslušných riadiacich hraničnо-vrstvových rovníc v limite malého Prandtlovho čísla. Následne sú študované ďalšie asymptotické aproximácie týchto riešení s cieľom pochopiť vplyv toku, generovaného v kvapalnej fáze posúvaním substrátu, na vlastnosti tuhnúceho systému. Niektoré výsledky sú aplikovateľné aj na situácie s rovinnými fázovými rozhraniami.

Kľúčové slová: tuhnutie binárneho systému • dendritická zóna • hraničná vrstva • úloha s voľnou hranicou • samopodobné riešenie • asymptotické aproximácie

AMS klasifikácia: 80A22 • 35C06 • 76M45

Contents

List of symbols

Operators

$\boldsymbol{u} \cdot \boldsymbol{v}$	inner product of vectors $\boldsymbol{u}$ and $\boldsymbol{v}$
$\boldsymbol{\nabla}\phi$	gradient of a scalar field ϕ
$\nabla^2\phi$	Laplace operator
$\boldsymbol{\nabla} \cdot \boldsymbol{u}$	divergence of a vector field $\boldsymbol{u}$
$\boldsymbol{u} \cdot \boldsymbol{\nabla}$	advective operator with respect to the vector field $\boldsymbol{u}$
$\dfrac{\mathrm{D}\phi}{\mathrm{D}t} \equiv \dfrac{\partial\phi}{\partial t} + (\boldsymbol{u} \cdot \boldsymbol{\nabla})\phi$	material derivative following the vector field $\boldsymbol{u}$
$\oint_S \phi \,\mathrm{d}S$	surface integral over a closed surface S

Functions

$F(x) = \pi^{1/2} x \,\mathrm{e}^{x^2} \operatorname{erfc}(x)$

$G(x) = \pi^{1/2} x \,\mathrm{e}^{x^2} \operatorname{erf}(x)$

$H(x) = (\mathrm{e}^{x^2} - 1)/G(x)$

$\Lambda(\lambda) \equiv \lambda + Pr\dfrac{1 - \mathscr{U}}{2\lambda}.$

Dimensionless numbers

$Pr = \dfrac{\nu}{\kappa}$ (Prandtl number)

$\varepsilon = \dfrac{D}{\kappa}$ (inverse Lewis number)

$\mathscr{S} = \dfrac{L}{C_p \Delta T}$ (Stefan number)

$\mathscr{C} = \dfrac{C_0}{\Delta C}$ (concentration ratio)

$\Gamma = \hat{\Gamma}\dfrac{\Delta C}{\Delta T}$ (dimensionless liquidus slope)

$\mathscr{U} = \dfrac{U_\infty}{U_0}$ (velocity ratio)

where

$\Delta T = T_\infty - T_0,$

$\Delta C = C_0 - C_\infty$

Introduction

The solidification of fluids is an integral part of many natural and industrial processes. Among typical examples is the formation of snowflakes and icicles in winter or the sea ice in polar areas. The phase-change processes play an important role also in material engineering during production of new materials such as metal castings and semiconductors. From the point of applications in material engineering, an important class of problems is that of solidification of multi-component systems (alloys).

It is a well known phenomenon that a material solidifying from an alloy usually has a different composition than the original system. For example, the ice growing from sea water is almost pure. The way in which the liquid material solidifies can affect the quality of the final product. A typical example is the appearance of structural defects, called freckles, during solidification of metal alloys (see Fowler 1985). To control the quality of solidified products, it is necessary to understand the coupling between fluid flow and solidification involved.

A mathematical model of diffusion-driven solidification of a binary alloy cooled below was studied by Worster (1986) as an extension of the classical Stefan problem for a single component system. The interface between the solid and liquid phases, characterised by the local conservation of heat and solute, was assumed planar. The rate of solidification in the model was controlled by the diffusive transport of solute away from the interface. Analytical self-similar solutions were found, with square-root time growth of the interface. Since the diffusion of solute is typically much slower that the diffusion of heat, a region of so-called constitutional supercooling often forms ahead of the solid/liquid interface, where the temperature of the liquid phase is below the local liquidus (freezing) temperature. Under such conditions a planar solid/liquid interface may become morphologically unstable, thus giving rise to the formation of highly convoluted structures, called dendrites. As a result, a so-called mushy layer forms, which is a region between the solid and liquid phases with a complicated microstructure. From the macroscopic point of view, the mushy layer is a reactive porous medium whose permeability changes in space and time upon the internal solidification/melting of its dendrites. Worster (1986) developed a model of a mushy layer, based on the local conservation of heat and solute, as an extension of the model with planar solid/liquid interface. The mushy layer was separated from the solid and liquid regions by planar interfaces with square-root time growth. The mathematical model was dimensional, with a large number of physical parameters — he assumed that the solid and liquid phases had different thermal properties. Therefore, the nonlinear, free-boundary problem governing the mushy

layer could not be solved explicitly but only numerically via the shooting method. Gewecke & Schulze (2011*b*) assumed the equal thermal properties of the solid and liquid phases, along with the negligible latent-heat release. These assumption allowed them to find explicit self-similar solutions to the governing equations.

The self-similar form of solutions derived by Worster (1986) and Gewecke & Schulze (2011*b*) was a consequence of the semi-infinity of the solidifying system in the vertical direction, i.e. the direction perpendicular to the planar interfaces. Gewecke & Schulze (2011*a*) studied the dynamics of a mushy layer in a vertically-bounded region. Due to the finite extent of the solidifying system, they could not use the self-similar approach. However, due to the hyperbolic character of the equation governing the liquid fraction in the mushy layer, they were able to study the problem via the method of characteristics. The main finding was that the mush/liquid interface retreated in a finite time in case when the solute diffusion was not neglected.

Of different nature is a so-called directional solidification in which the solidifying liquid is pulled at constant speed through a constant temperature gradient and the solid-liquid interface is stationary. In recent years, the models of directional solidification were studied extensively in context of morphological and convective instabilities (see Worster 2000 or Davis 2001 for general reviews). Guba & Worster (2006*b*) studied nonlinear oscillatory convection in mushy layers by methods of bifurcation analysis. Nonlinear interactions between steady and oscillatory convection were analysed by Guba & Worster (2010).

In addition to the studies devoted to the solidification of binary alloys, in recent years, experimental attempts to understand the behaviour of the solidifying ternary alloys were made by Aitta, Huppert & Worster (2001), followed by the theoretical studies by Anderson (2003), Anderson & Schulze (2005) and Guba & Anderson (in preparation).

Another experimental configuration in which the interface is stationary and that is also common in material engineering is the one in which a cooled horizontal boundary (substrate) is moving at a constant speed in horizontal direction in an imposed vertical temperature gradient (continuous strip and spin casting). There are two main features that distinguish such a configuration from those with a stationary cooled boundary or those of directional solidification: (*i*) the solidifying interface is not planar; (*ii*) there is a strong two-dimensional flow in the liquid phase. Such a configuration was previously addressed as a local approximation of spin casting (see the review by Steen & Karcher 1997). Löfgren & Åkerstedt (2001) studied the initial solidification of a pure liquid-metal film flow over a moving boundary. The problem of a steady two-dimensional boundary-layer flow of a binary alloy over a moving substrate was studied by Löfgren (2001). He obtained self-similar solutions for the velocity, temperature and solute concentration fields in the limit of small Prandtl number, which is typical of liquid metal flows. The interface was shown to have a square-root growth in the horizontal direction. The self-similar analysis was facilitated by the assumption of semi-infinite domain in vertical direction and that of small interfacial slope so that boundary-layer reduction was possible. An extension of the problem to include a mushy region was considered by Cheung, Shiah & Tangthieng (2002) and by Cheung & Tangthieng (2003). The mushy layer consisted of two sep-

arate layers: a packing region, with solid phase moving with the substrate, and a dispersed region, where solid phase was free to move with the fluid. The self-similar solutions were found numerically. However, the relationship between the local liquid fraction and temperature was prescribed through the lever rule, not by the local conservation of solute as by Worster (1986).

The aim of this thesis is to combine the approach of Löfgren (2001) with that of Worster (1986) in order to formulate the problem studied by Cheung *et al.* (2002), such that the local liquid fraction will be given by the local conservation of solute. Unlike Cheung *et al.* (2002), we shall consider a simplified situation with the mushy layer consisting only of the packing region. Our task will be to find closed-form self-similar solutions to the governing equations and, using these solutions, study how the forced boundary layer flow influences the main physical characteristics of the mushy layer – the local liquid fraction and the positions of solid/mush and mush/liquid interfaces. Moreover, the problem studied in the present thesis, together with that by Löfgren (2001), has its importance because it provides analytical self-similar solutions to a solidification problem with a non-planar interface and a two-dimensional advection in the liquid. Generally, such problems are rare. As another example can serve the study made by Guba & Worster (2006*a*) of a two dimensional convection in a laterally solidifying mushy region.

The structure of the thesis is as follows. In the first part of Chapter 1, we review the basic facts concerning mathematical modelling of binary alloy solidification. First, we discuss the extended Stefan problem for a solidifying binary alloy with a sharp interface separating the solid and liquid phases. Then we discuss the situation when the mushy layer appears as a consequence of constitutional supercooling; we present a general system of partial differential equations governing the dynamics of solidifying system in such a situation. In the second part, we focus on a general formulation of the mushy-layer equations that is valid in an arbitrary frame of reference. Such formulation is of importance in cases when the interface velocities are distinct from both the velocity of the dendrites and the velocity of the interdendritic fluid — cf. Schulze & Worster 2005. Since, unlike Schulze & Worster (2005), we assume solute diffusion in the liquid phase, in addition to the conditions at the mush/liquid interface derived by the authors, we also derive the conditions at the solid/mush interface using a similar approach. The conditions at the solid/mush interface were not discussed by Schulze & Worster (2005) since the solid phase was not present in the system under the assumption of negligible solute diffusion.

In Chapter 2, we focus on the situation that is of interest in this thesis – we discuss the experimental configuration in which a cooled horizontal boundary (substrate) is moving at a constant speed in horizontal direction in an imposed vertical temperature gradient. The formulation of the governing equations in the liquid phase ahead of the mushy layer is the same as that used by Löfgren (2001), while the governing equations in the mushy layer, under the assumption of a general flow of the interdendritic fluid, together with the conditions at the mush/liquid interface, are the same as those used by Schulze & Worster (2005) and discussed in Chapter 2. However, unlike the authors, we take into account solute diffusion in the liquid portion of the mushy layer. After the boundary-layer reduction, the governing equations, together with

the interfacial conditions, turn out to be the same as those used by Worster (1986) and Gewecke & Schulze (2011*b*), with their time variable replaced by our horizontal spatial variable.

Before we analyse the problem with a mushy layer, in Chapter 3, we discuss the problem with solid/liquid interface similar to that studied by Löfgren (2001). However, we use different dimensionless scalings of the governing equations and focus our attention to the parametric analysis that was not addressed by Löfgren (2001), namely the influence of the velocity ratio on the solidification. The contents of this chapter are based on a paper by Kyselica & Guba (2014) (see Appendix).

In Chapter 4, we discuss the self-similar formulation of the mushy-layer problem, formulated in Chapter 2, with solute diffusion taken into account. We extend the results of Gewecke & Schulze (2011*a*) about the condition regarding the concentration and its gradient at the solid/mush interface to the cases when the Stefan number is positive — the results also apply to the problems with planar interfaces. For positive values of Stefan number, we also make some remarks about the liquid fraction and its gradient at the solid/mush interface. In the second part of the chapter, we study the regular limit of negligible Stefan number in order to derive explicit solutions to the mushy-layer equations. We also derive algebraic equations for the growth constants that determine the self-similar positions of the interfaces. Some approximate results are also discussed in order to get better understanding of the structure of the solutions and their parametric dependence.

In Chapter 5, we discuss the situation when the solute diffusion is neglected. First we analyse the model of a mushy layer that conserves solute globally and is similar to that discussed by Huppert & Worster (1985). Then we compare the results with those derived for the local conservation model with negligible solute diffusion. We derive an explicit relationship between the liquid fractions in the global and local models in the limit of negligible Stefan number.

In Conclusions, we make some final remarks about the results presented in this thesis, along with the open questions that have not been addressed and could provide motivation for further research. In Appendix, we also include a copy of a paper by Kyselica (2013), dedicated to the numerical solution of a Stefan problem for a binary alloy with initially perturbed solid/liquid interface.

Chapter 1

Solidification of binary alloys

1.1 Phase diagram

Essential for the study of dynamics of any solidifying system is the equilibrium phase diagram. We will assume a binary system comprising two components A and B — the component B will be referred to as *solute*. The phase diagram then specifies all the possible states that the system can rest in, in dependence on its temperature and concentration (in wt. % of B). The assumption of thermodynamic equilibrium means that, with concentration and pressure given, the temperature does not change in time. A typical binary phase diagram is depicted in figure 1.1

There are two special boundaries in the phase diagram:

(i) *Liquidus* curve, $T = T_L(C)$ or $C = C_L(T)$, which separates the region where the system is completely liquid (L) from the region where solid and liquid phases coexist (L + CSA and L + CSB).

(ii) *Solidus* curve, $T = T_S(C)$ or $C = C_S(T)$, which separates the regions L + CSA and L + CSB from the region where the system is completely solid (CSA and CSB).

The liquidus curve represents the freezing temperature as a function of concentration (under the liquidus, the solid phase is present in the system); similarly, the solidus curve represents the temperature at which the solid phase partially solidifies. Both liquidus and solidus curves intersect at *eutectic point* (C_E, T_E), below which the system is completely liquid irrespective of the concentration.

In figure 1.1 we see that for $C < C_E$ the liquidus curve is decreasing, while it is increasing for $C > C_E$. Thus, when $C < C_E$, the freezing temperature is highest when there is only the component A present in the system (i.e. when $C = 0$); when $C > C_E$, the freezing temperature is highest when there is only component B present (i.e. when $C = 1$). Therefore the eutectic temperature represent the lowest temperature at which the binary system can be completely liquid. Moreover, once the system lies in one of the regions $C \leq C_E$ or $C \geq C_E$, it resides in that region for all the time.

Consider the case when the system is in equilibrium and the point (C, T) lies in one of the regions L + CSA or L + CSB. As a result, the solid portion of the system

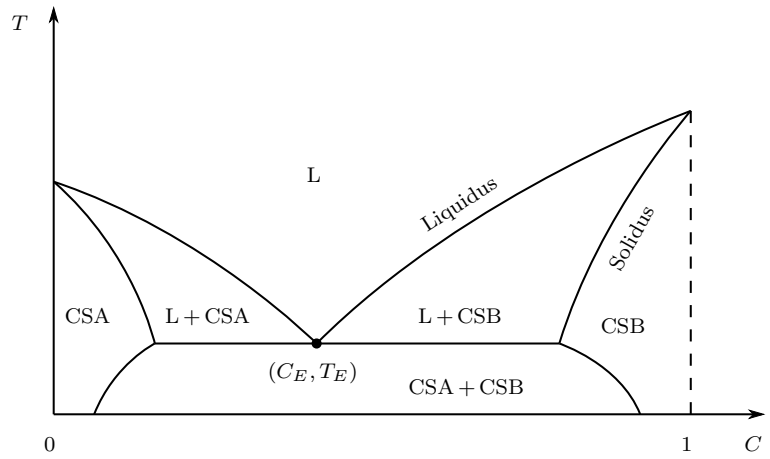

Figure 1.1: A typical equilibrium phase diagram for a binary system comprising two components A and B. Each region in the diagram defines the state of the system with respect to the temperature T and concentration C: L – liquid solution; CSA – solid solution in which the molecules of B are incorporated in the crystal lattice of A; CSB – solid solution in which the molecules of A are incorporated in the crystal lattice of B; L + CSA, L + CSB – the region of coexistence of the liquid solution L with CSA or CSB, respectively; CSA + CSB – composite solid phase, in which the grains of CSA are interspersed among the grains of CSB.

has the concentration equal to $C_S(T)$ and the liquid portion has the concentration equal to $C_L(T)$. The averaged concentration is then given by

$$\bar{C} \equiv \chi C_L + (1 - \chi) C_S, \tag{1.1}$$

where $0 \leq \chi \leq 1$ is the local volume fraction of the liquid phase. From (1.1) we obtain

$$\chi = \frac{\bar{C} - C_S}{C_L - C_S}. \tag{1.2}$$

An important assumption in the modelling of phase changes is that the system is always close to equilibrium. For that reason the temperature is continuous at the solid-liquid interfaces. However, the concentration is discontinuous with a jump from the value $C_L(T)$ to the value $C_S(T)$, owing to the fact that, in general, the composition of the solid phase is different than that of liquid phase. Therefore, one of the components must be rejected, thus increasing its concentration ahead of the interface. The solid phase solidifying at the temperature T has the concentration given by the solidus curve, i.e. $C = C_S(T)$. In the rest of our work, we will use a linear approximation of the equilibrium phase diagram (see figure 1.2) given by

$$T_L(C) \equiv T_m - \Gamma C, \quad \Gamma > 0,\ C \leq C_E, \tag{1.3}$$

where T_m represents the melting temperature of a pure substance and Γ is the liquidus slope. In what follows, we will assume, without a loss of generality, that the concentration is subeutectic, i.e. $C < C_E$. Additionally, we will consider vertical solidus curve $C_S = 0$ so that the solid phase consists of pure substance A. That results in the increasing concentration of solute in the liquid phase towards the solidifying interface.

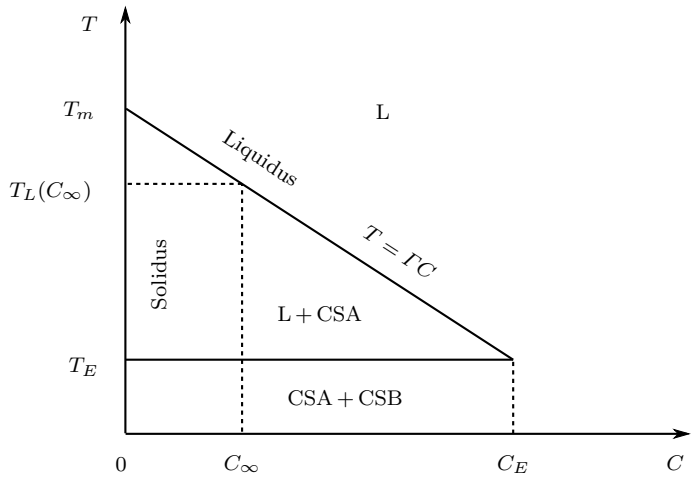

Figure 1.2: Linear approximation of the equilibrium phase diagram.

During solidification, randomly moving liquid molecules become attached and incorporated into the crystalline lattice of the solid. Their loss of entropy results in the release of *latent heat* which must be transported away from the solidifying interface if solidification is to proceed (cf. Worster 2000). We will denote L the latent heat per unit mass of solid phase, the dimension of L is therefore $[L] = \text{J kg}^{-1}$.

1.2 Stefan problem for a binary alloy

In this section, we will formulate an analogy of the well-known *Stefan problem*, originally formulated for pure melts, for a situation, when the solidifying system is a binary alloy. To facilitate the comparison with the problems formulated in subsequent chapters, we will formulate the Stefan problem in two-dimensions. Consider a two-dimensional region

$$-\infty < x < \infty,\ 0 \leq z < \infty$$

filled with a binary alloy that is initially completely liquid, with spatially homogenous concentration $C \equiv C_\infty < C_E$ and temperature $T \equiv T_\infty > T_L(C_\infty)$. At some initial time instant, $t = 0$, say, the temperature at the bottom boundary $z = 0$ is suddenly lowered to, and subsequently maintained at, a value $T_0 \in (T_E, T_L(C_\infty))$. As a consequence, the systems begins to solidify: at each time instant, there is a solid phase in the system bounded below by the bottom boundary $z = 0$ and above by a phase interface located at

$$z = h(x, t). \tag{1.4}$$

A typical situation is depicted in figure 1.3.

Governing equations

The temperature field $T = T(x, z, t)$ in the solid and liquid phases is governed by the standard heat equation of the form

$$\frac{\partial T}{\partial t} = \kappa \nabla^2 T, \quad \text{for} \quad z > 0, \tag{1.5}$$

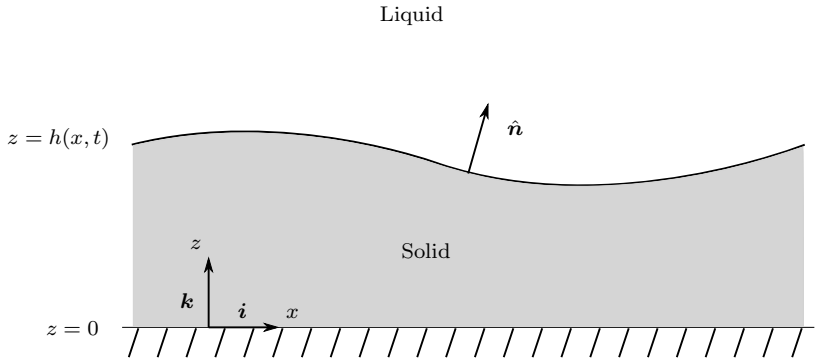

Figure 1.3: Interface between the solid and liquid phases during a two-dimensional diffusion-driven solidification of a binary alloy; $\hat{\boldsymbol{n}}$ is the unit outward-normal vector to the interface, $\boldsymbol{i} = (1,0)^T$ and $\boldsymbol{k} = (0,1)^T$.

where κ is thermal diffusivity, defined as $\kappa \equiv k/(\rho C_P)$, with k denoting the thermal conductivity, ρ the density (which we shall treat as constant) and C_P the thermal capacity. For simplicity, we shall consider equal thermal properties of the solid and liquid phases. The concentration field in the liquid phase is governed by the solute diffusion equation of the form

$$\frac{\partial C}{\partial t} = D\nabla^2 C, \quad \text{for} \quad z > h, \tag{1.6}$$

with D being the diffusivity of solute in the liquid phase. The boundary conditions imposed are

$$z = 0: \quad T = T_0, \tag{1.7a}$$
$$z \to \infty: \quad T \to T_\infty, \tag{1.7b}$$
$$C \to C_\infty, \tag{1.7c}$$

and the initial conditions

$$t = 0: \quad T \equiv T_\infty, \tag{1.8a}$$
$$C \equiv C_\infty. \tag{1.8b}$$

Conservation laws at the solid/liquid interface

The solidification problem as stated above is a problem with a moving boundary (the position of the interface is time-dependent), with the moving boundary itself being part of the solution. Therefore, to close the problem, some conditions at the moving boundary need to be imposed. The first condition is the Stefan condition

$$\rho L \frac{\partial h}{\partial t} \boldsymbol{k} \cdot \boldsymbol{n}_h = k \left(\boldsymbol{n}_h \cdot \boldsymbol{\nabla} T|_{h^-} - \boldsymbol{n}_h \cdot \boldsymbol{\nabla} T|_{h^+} \right), \tag{1.9}$$

representing the conservation of heat at the interface, $\boldsymbol{n}_h$ being the unit outward-normal vector to the interface. The left hand-side represents the rate at which the latent heat is released during solidification. The first term at the right hand-side

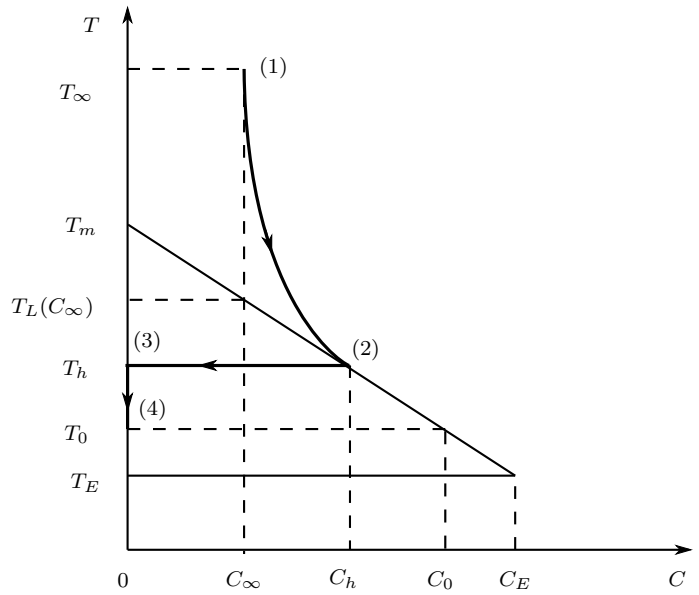

Figure 1.4: Typical evolution of a solidifying system in a (C, T) space. The particular points shown are, together with the corresponding z-coordinates: (1) $z \to \infty$, (2) $z = h^+$, (3) $z = h^-$ and (4) $z = 0$. The points (2) and (3) correspond to a jump in concentration across the interface.

is minus the heat flux from the interface to the solid phase and the second one is the heat flux from the liquid phase towards the interface. The right hand-side of (1.9) thus represents the difference between the heat fluxes on the liquid and solid sides of the interface. Since the left hand-side of (1.9) is always non-negative during solidification, the heat conducted from the interface to the solid is never less than the heat flux from the liquid.

The second condition at the interface is

$$C_{h^+}\frac{\partial h}{\partial t}\boldsymbol{k}\cdot\boldsymbol{n}_h = -D\boldsymbol{n}_h\cdot\boldsymbol{\nabla}C|_{h^+}. \tag{1.10}$$

This condition expresses the balance between the rate at which the solute is rejected during solidification (the left hand-side) and the rate of diffusion of solute away from the interface at the liquid side of the interface (the right hand-side). In addition to the two condition stated above, we assume that the temperature is continuous across the interface, i.e.

$$T_{h^-} = T_{h^+} \equiv T_h, \tag{1.11}$$

and that the interface sits in local thermodynamic equilibrium, i.e. the interfacial temperature and concentration are coupled via the liquidus relationship

$$T_h = T_m - \Gamma C_{h^+}. \tag{1.12}$$

A typical evolution of a solidifying binary alloy is depicted in figure 1.4.

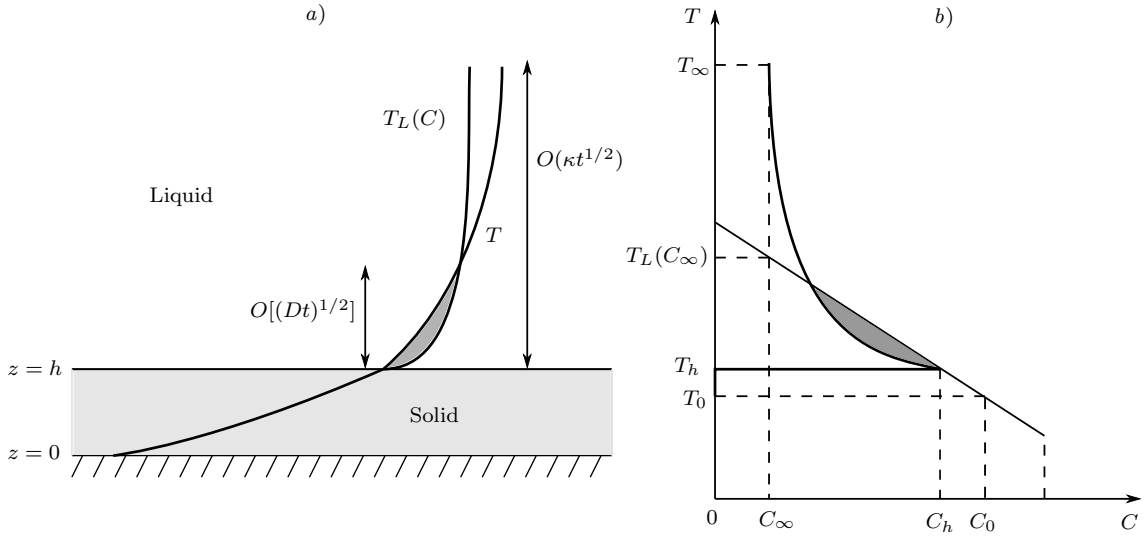

Figure 1.5: (a) Schematic plot of the region of constitutional supercooling ahead of the solid/liquid interface. (b) The effect of constitutional supercooling from the point of phase diagram.

1.2.1 Constitutional supercooling and the morphological instability

Since, typically, heat diffuses more rapidly than solute, a region of so-called constitutional supercooling often forms. The character of the diffusion equations (1.5) and (1.6) implies that there is a thermal boundary layer of thickness $O(\kappa t^{1/2})$ and a concentration boundary layer of thickness $O[(Dt)^{1/2}]$ ahead of the solid/liquid interface. Since, typically, $D \ll \kappa$, the concentration boundary layer resides in the thermal one, see figure 1.5(a). As a consequence, the local freezing temperature (i.e. the liquidus temperature corresponding to the concentration at the particular point) ahead of the interface rises more rapidly than the local temperature. Since both these temperatures are equal at the interface, there is a region close to the interface where the temperature is under the local freezing temperature — the region of constitutional supercooling. In figure 1.5(b) we see that the constitutional supercooling appears as soon as the inequality

$$\boldsymbol{n}_h \cdot \boldsymbol{\nabla} T|_{z=h^+} < \boldsymbol{n}_h \cdot \boldsymbol{\nabla} T_L(C)|_{z=h^+} = -\Gamma\, \boldsymbol{n}_h \cdot \boldsymbol{\nabla} C|_{z=h^+} \tag{1.13}$$

is satisfied. The presence of the region of constitutional supercooling usually gives rise to morphological instabilities of a planar interface. As a consequence, so-called mushy layers may form, which we shall discuss in the next section.

1.3 Mushy layers

1.3.1 Mushy layer as a reactive porous medium

So far we have been discussing the situation when there were solid and liquid phases present in the system, separated with a simple interface. However, as a con-

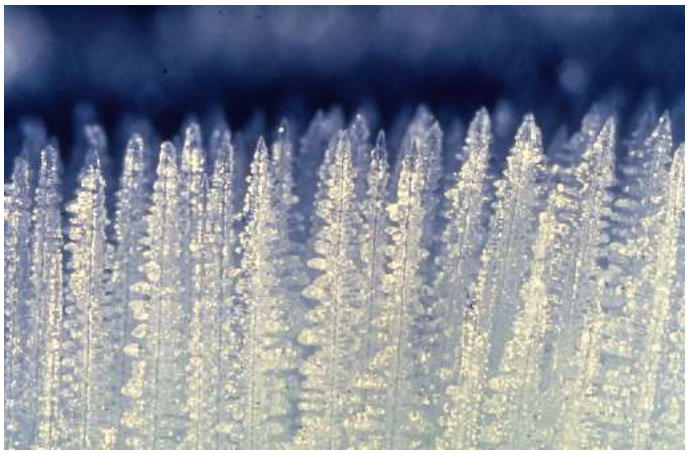

Figure 1.6: An example of a typical microstructure of an interface between mushy layer and the liquid phase. The example corresponds to the aqueous solution of ammonium chloride (NH_4Cl). The solid dendrites are composed of pure NH_4Cl. The horizontal length of depicted portion of the mush is 8×10^{-3} m, with a typical inter-dendritic length equal to 3×10^{-4} m. Source: Huppert (1990).

sequence of morphological instability, the interface can become highly convoluted, leading to formation of so-called *mushy layer*, a region of coexistence of the solid and liquid phases. From the microscopic point of view, the mushy layer typically consists of dendritic crystals, as shown in figure 1.6.

The distances between dendrites are typically very small compared to the overall size of the mushy layer. Therefore, from the macroscopic point of view, the mushy layer can be treated as a reactive porous medium. In this context, the term reactive means that the local permeability of the mushy layer can change due to the internal solidification and dissolution. The mushy layer is separated from the solid and liquid phase by interfaces: the solid/mush interface, located at $z = a(x,t)$ and the mush/liquid interface, located at $z = b(x,t)$. The properties of the mushy layer are given as averages (integrals) of the corresponding physical variables across control volumes that are large compared to the typical interdendritic spacing but are small compared to the thickness of the mushy layer.

The key variable describing the local properties of the mushy layer is the local volume fraction of the liquid phase

$$\chi = \chi(x,z,t) \in \langle 0,1 \rangle.$$

Using χ, we can define the local volume fraction of the solid phase as

$$\phi \equiv 1 - \chi.$$

The thermal properties of the mush can then be approximated as (cf. Worster 1986)

$$\begin{aligned} k_m &\equiv \chi k_l + (1-\chi) k_s, \\ (\rho C_p)_m &\equiv \chi \rho_l C_{pl} + (1-\chi) \rho_s C_{ps}, \end{aligned}$$

with subscripts l and s denoting the liquid and solid phases, respectively. Since in this thesis we shall consider equal thermal properties of the solid and liquid phases, we

obtain $k_m \equiv k$ and $(\rho C_p)_m \equiv \rho C_p$. However, we will present the governing equations in their general form. As in the situation with solid/liquid interface, we denote $T(x, z, t)$ the temperature field in the mushy layer and $C(x, z, t)$ the concentration field expressing the concentration of solute in the liquid portion of the mushy layer. We assume that solid is free of solute, i.e. $C \equiv 0$ there.

Let V be any bounded region in the mushy layer. The total volume of liquid and solid in V, respectively, can be expressed as

$$|V_{\text{liquid}}| = \int_V \chi \, \mathrm{d}V, \quad \text{and} \quad |V_{\text{solid}}| = \int_V \phi \, \mathrm{d}V$$

and the total amount of solute in V as

$$|V_{\text{solute}}| = \int_V \chi C \, \mathrm{d}V$$

where $\bar{C} \equiv \chi C$ is the bulk concentration.

The formation of mushy layer can be interpreted from the thermodynamical point of view. The dendrites are growing in order to increase the contact area between the solid and liquid phases and thus enhance the release of latent heat and solute. The enhanced latent-heat release results in the local increase of temperature; the enhanced solute rejection results in the local decrease of melting temperature due to the liquidus relationship that holds at the local solid/mush interfaces. Both these effects suppress the constitutional supercooling. Thus the growth of the mushy layer and the morphological instability in general occur in order to reduce the constitutional supercooling present ahead of the interface. Moreover, it is natural to assume that the mushy layer grows until the constitutional supercooling is completely eliminated. That means that the inequality (1.13) expressing the constitutional supercooling is in fact an equality in the mushy layer so that the condition of thermodynamical equilibrium

$$T = T_m - \Gamma C \tag{1.14}$$

holds throughout the whole mushy layer.

1.3.2 Governing equations

The equations governing the temperature and concentration fields in the mushy layer express the local conservation of heat and solute on the scales that are small compared to the overall extent of the mushy layer, but are large enough to encompass its microstructure. These equations are

$$(\rho C_P)_m \frac{\partial T}{\partial t} = \boldsymbol{\nabla} \cdot (k_m \boldsymbol{\nabla} T) - \rho_S L \frac{\partial \chi}{\partial t}, \tag{1.15a}$$

$$\chi \frac{\partial C}{\partial t} = D \boldsymbol{\nabla} \cdot (\chi \boldsymbol{\nabla} C) - C \frac{\partial \chi}{\partial t}. \tag{1.15b}$$

It the above equations, the effects of internal solidification are represented by source terms. The first equation represents the local conservation of heat. The term $-\rho_S L \partial\chi/\partial t$ can be expressed equivalently as $\rho_S L \partial\phi/\partial t$ and can be interpreted as

the rate at which the latent heat is released during internal solidification. Note that $\partial\phi/\partial t > 0$ means the mushy layer is solidifying locally (new dendrites are growing); conversely, $\partial\phi/\partial t < 0$ when the solid portion of the mushy layer is melting. The second equation represents the local conservation of solute. The term $-C\partial\chi/\partial t$, which can be written equivalently as $C\partial\phi/\partial t$, expresses the rate at which the solute is rejected upon local solidification.

1.3.3 Conservation laws at the solid/mush and mush/liquid interfaces

The conditions expressing the conservation heat and solute at the solid/mush interface are

$$\rho_s L\chi_{a^+}\frac{\partial a}{\partial t}\boldsymbol{k}\cdot\boldsymbol{n}_a = k_s\boldsymbol{n}_a\cdot\boldsymbol{\nabla}T|_{a^-} - k_m\boldsymbol{n}_a\cdot\boldsymbol{\nabla}T|_{a^+}, \tag{1.16a}$$

$$C_{a^+}\chi_{a^+}\frac{\partial a}{\partial t}\boldsymbol{k}\cdot\boldsymbol{n}_a = -D\chi_{a^+}\boldsymbol{n}_a\cdot\boldsymbol{\nabla}C|_{a^+} \tag{1.16b}$$

and that expressing the conservation of heat and solute at the mush/liquid interface are

$$\rho_s L(1-\chi_{b^-})\frac{\partial b}{\partial t}\boldsymbol{k}\cdot\boldsymbol{n}_b = k_m\boldsymbol{n}_b\cdot\boldsymbol{\nabla}T|_{b^-} - k_l\boldsymbol{n}_b\cdot\boldsymbol{\nabla}T|_{b^+}, \tag{1.17a}$$

$$C_b(1-\chi_{b^-})\frac{\partial b}{\partial t}\boldsymbol{k}\cdot\boldsymbol{n}_b = D\left(\chi_{b^-}\boldsymbol{n}_b\cdot\boldsymbol{\nabla}C|_{b^-} - \boldsymbol{n}_b\cdot\boldsymbol{\nabla}C|_{b^+}\right). \tag{1.17b}$$

where $\boldsymbol{n}_a$ and $\boldsymbol{n}_b$ are the outward unit vectors normal to the corresponding interfaces, defined as

$$\boldsymbol{n}_a = \frac{1}{n_a}\left[-\frac{\partial a}{\partial x}, 1\right]^{\mathrm{T}}, \quad \boldsymbol{n}_b = \frac{1}{n_b}\left[-\frac{\partial b}{\partial x}, 1\right]^{\mathrm{T}},$$

with $n_a := (a_x^2+1)^{1/2}$ and $n_b := (b_x^2+1)^{1/2}$.

Another conditions that we assume to be valid at the interfaces (and that we have already used when formulating the condition 1.17b) are that of continuity of the temperature field across both interfaces and the continuity of concentration field across the mush/liquid interface

$$T_{a^-} = T_{a^+} \equiv T_a, \tag{1.18a}$$

$$T_{b^-} = T_{b^+} \equiv T_b, \tag{1.18b}$$

$$C_{b^-} = C_{b^+} \equiv C_b, , \tag{1.18c}$$

with the unknown interfacial values T_a, T_b and C_b being parts of solution.

The governing equations in the liquid and solid phases are the same as that in the Stefan problem with solid/liquid interface. However, unlike the Stefan problem, the mushy layer equations comprise one new variable — the local liquid fraction χ. The system of differential equations for the mushy layer, as stated above, is not complete. One more condition is required to close the system. The additional condition to be imposed is the one of *marginal equilibrium* at the mush/liquid interface of the form

$$\boldsymbol{n}_b\cdot\boldsymbol{\nabla}T|_{b^+} = \boldsymbol{n}_b\cdot\boldsymbol{\nabla}T_L(C)|_{b^+} = -\Gamma\boldsymbol{n}_b\cdot\boldsymbol{\nabla}C|_{b^+}. \tag{1.19}$$

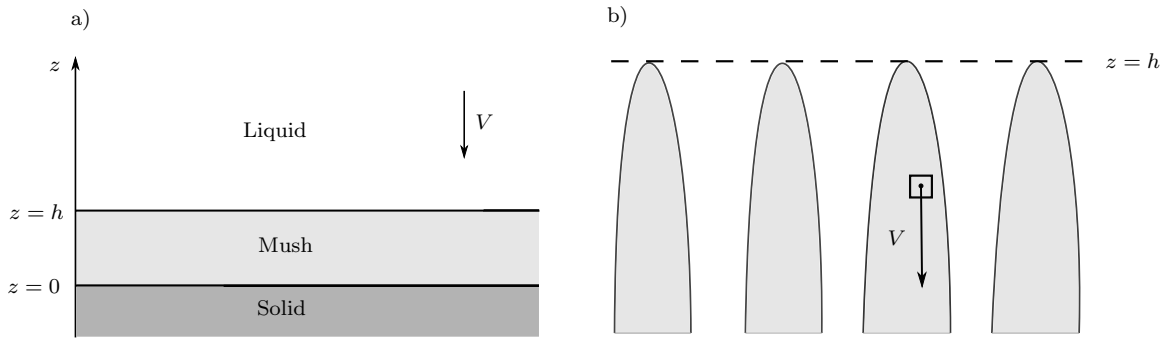

Figure 1.7: (*a*) Schematic plot of directional solidification of a binary alloy, in which the whole systems is pulled downwards at speed V in an imposed temperature gradient. The positions of solid/mush and mush/liquid interfaces are fixed in space. (*b*) Relative motion of a fixed solid material element relative to the stationary mush/liquid interface during direction solidification.

The condition ensures that none of the liquid ahead the mush/liquid interface is constitutionally supercooled (see Worster 1986 for further discussion of this condition and its relation to the morphological instability of the interface). In fact, (1.19) states that the mushy layer grows in such a way that the inequality (1.13) becomes an equality at the mush/liquid interface.

1.4 Mushy-layer equations in general frames of reference

From the point of applications of solidification in material engineering, of special interest are the solidifying systems with constant solidification rate V. Such a solidification rate can be obtained by pulling the whole system downwards at speed V in an imposed temperature gradient such that the positions of solid/mush and mush/liquid interfaces are fixed in space. The situation just described is usually referred to as directional solidification — see figure 1.7*a*.

While the position of the interface does not change during directional solidification, the solid phase formed is pulled downwards at the speed V. This is also true for the dendrites in the mushy layer. The situation is schematically depicted in 1.7*b*.

Though in the problem of directional solidification stated above the liquid phase flows towards the mush/liquid interface, the liquid material elements do not move relative to the dendrites of the mushy layer. With respect to the frame of reference moving with the solid, the interfaces are moving at constant speed V vertically upwards with the liquid phase being stationary. Usually, when one is studying a flow in a mushy layer, it is in fact the flow relative the solid phase that is important. Therefore it is instructive to formulate the local conservation laws with respect to a frame of reference connected with the solid phase of the mushy layer.

It is clear from the discussion in the previous paragraph, that when formulating a general mathematical model of a mushy layer with flow, one has to take into account that the speed of solid phase, the flow velocity and the rate at which the interfaces

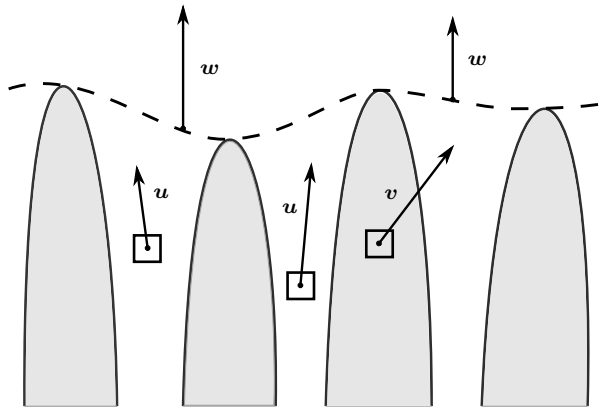

Figure 1.8: Definition sketch representing the three velocities $\boldsymbol{u}$, $\boldsymbol{v}$ and $\boldsymbol{w}$. For the definitions of these quantities, see text.

propagate can be different when measured in a frame of reference connected with an external observer — the laboratory frame of reference. To make this explicit, we define the following quantities, all with respect to the laboratory frame of reference:

- $\boldsymbol{u}$ velocity of the fluid flow in the mushy layer; in component form, $\boldsymbol{u} = (u, v)$;
- $\boldsymbol{v}$ speed of material points embedded in the dendrites (i.e. the speed of solid material elements);
- $\boldsymbol{w}$ rate of propagation of the interface.

In what follows, we will assume that the dendrites do not move with respect to each other so that $\boldsymbol{v}$ is constant throughout the mushy layer. The situation is schematically depicted in figure 1.8. In general, the velocities $\boldsymbol{u}$ and $\boldsymbol{w}$ are independent. For example, in directional solidification $\boldsymbol{v} = -V\boldsymbol{k}$ and $\boldsymbol{w} = \boldsymbol{0}$; in diffusion-driven solidification with a planar interface $\boldsymbol{v} = \boldsymbol{0}$ and $\boldsymbol{w} = t^{-1/2}\boldsymbol{k}$. In general, the growth rate of the interface can be expressed as $\boldsymbol{w} = (\partial h/\partial t)\boldsymbol{k}$ and does not have to be constant.

We distinguish between two cases that can occur according to the sign of the relative velocity of the interface and the solid material points: when $(\boldsymbol{w} - \boldsymbol{v}) \cdot \boldsymbol{n} > 0$, the mush/liquid interface is a *freezing* interface; when $(\boldsymbol{w} - \boldsymbol{v}) \cdot \boldsymbol{n} < 0$, it is a *melting* interface. We will consider only the cases when the interface is freezing.

Another important vector quantities describing the mushy layer are the *total mass flux*, defined as

$$\boldsymbol{q} \equiv \chi\boldsymbol{u} + \phi\boldsymbol{v}, \tag{1.20}$$

and the *Darcy velocity* $\chi(\boldsymbol{u} - \boldsymbol{v})$, which can be expressed equivalently as

$$\chi(\boldsymbol{u} - \boldsymbol{v}) = \boldsymbol{q} - \boldsymbol{v}. \tag{1.21}$$

The vector field $\boldsymbol{u} - \boldsymbol{v}$ is the local flow of the liquid phase relative to the solid phase.

In next sections, we shall present the derivation of governing equations describing the conservation of mass, heat and solute in general inertial frames of reference. The equations presented here were introduced by Schulze & Worster (2005) under the assumptions that the material properties of liquid and solid phases were the same and

that the diffusion of solute was negligible. However, unlike Schulze & Worster (2005), we shall relax the latter assumption and take the solute diffusivity into account.

In the derivations, we will use the following vector identity

$$\boldsymbol{\nabla}\cdot(A\boldsymbol{B}) = (\boldsymbol{B}\cdot\boldsymbol{\nabla})A + A\boldsymbol{\nabla}\cdot\boldsymbol{B}, \tag{1.22}$$

valid for any smooth scalar field A and any smooth vector field $\boldsymbol{B}$. We will also make use of the Reynolds transport theorem (see Aris 1990). Consider a smooth flow field $\boldsymbol{U}$ and a time-dependent material volume $V(t)$ (i.e. a region of fluid deformed by the flow). Then the time derivative of the integral of some smooth function f (scalar or vector) can be expressed in the following way

$$\frac{\mathrm{d}}{\mathrm{d}t}\int_{V(t)} f\,\mathrm{d}V = \int_{V(t)}\left[\frac{\mathrm{D}f}{\mathrm{D}t} + f\boldsymbol{\nabla}\cdot\boldsymbol{U}\right]\mathrm{d}V, \tag{1.23}$$

where

$$\frac{\mathrm{D}f}{\mathrm{D}t} \equiv \frac{\partial f}{\partial t} + (\boldsymbol{U}\cdot\boldsymbol{\nabla})f \tag{1.24}$$

is the material (Lagrangian) derivative of f following the fluid element moving with velocity $\boldsymbol{U}$. We will denote the material derivatives with respect to the vector fields $\boldsymbol{u}$, $\boldsymbol{v}$ and $\boldsymbol{q}$ as $\mathrm{D}^l f/\mathrm{D}t$, $\mathrm{D}^s f/\mathrm{D}t$ and $\mathrm{D}f/\mathrm{D}t$, respectively.

1.4.1 Governing equations

Conservation of mass

Consider an arbitrary time-independent (i.e. fixed in space) volume V, lying in the mushy layer. According to the conservation of mass, the total outflow of mass per unit of time through the boundary ∂V must be zero, in other words

$$\begin{aligned} 0 &= \rho\oint_{\partial V}\chi\boldsymbol{u}\cdot\boldsymbol{n}\,\mathrm{d}S + \rho\oint_{\partial V}\phi\boldsymbol{v}\cdot\boldsymbol{n}\,\mathrm{d}S \\ &= \rho\oint_{\partial V}\boldsymbol{q}\cdot\boldsymbol{n}\,\mathrm{d}S, \end{aligned}$$

where $\boldsymbol{n}$ is the unit outward vector normal to the boundary ∂V. The first integral in the first line represents the total volume of the liquid per unit of time that is transported away from V. Similarly, the second integral represents the total amount of the solid phase per unit of time that is transported away from V. If we use the divergence theorem and the assumption that the volume V was arbitrary, we get the formulation of the mass conservation in the following form

$$\boldsymbol{\nabla}\cdot\boldsymbol{q} = 0. \tag{1.25}$$

Thus, from the point of mass transport, the field $\boldsymbol{q}$ plays the same role as the velocity field for the flow of an incompressible fluid. Note that $\boldsymbol{\nabla}\cdot\boldsymbol{u} \neq 0$, since it is not only the flow field $\boldsymbol{u}$ but also the field $\boldsymbol{v}$ that contribute to the overall transport of mass within the mushy layer.[1]

[1]The non-vanishing divergence of the liquid flow field $\boldsymbol{u}$ is a consequence of the fact that $\boldsymbol{u}$ was defined on scales that were large compared to the typical interstitial length scales (the distances

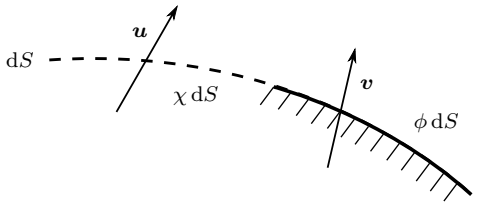

Figure 1.9: Schematic plot of the mass transport through an element $\mathrm{d}S$ of the boundary ∂V.

Conservation of heat

Let $V(t)$ be an arbitrary bounded region that is stationary relative to the solid phase of the mushy layer. Relative to the laboratory (stationary) frame of reference, in which the fields $\boldsymbol{u}$, $\boldsymbol{v}$ and $\boldsymbol{q}$ were defined, each point of $V(t)$ is moving at speed $\boldsymbol{v}$. The total heat change in $V(t)$ during a small time interval Δt can be expressed, using the Reynolds transport theorem and 1.22, in the following way

$$\begin{aligned}
\Delta Q &= \int_{V(t+\Delta t)} \rho C_P T(\boldsymbol{x}, t+\Delta t)\,\mathrm{d}V - \int_{V(t)} \rho C_P T(\boldsymbol{x}, t)\,\mathrm{d}V \\
&\approx \Delta t \frac{\mathrm{d}}{\mathrm{d}t} \int_{V(t)} \rho C_P T\,\mathrm{d}V \\
&= \Delta t \rho C_P \int_{V(t)} \left[\frac{\partial T}{\partial t} + (\boldsymbol{v}\cdot\boldsymbol{\nabla})T \right] \mathrm{d}V \\
&= \Delta t \rho C_P \left[\int_{V(t)} \frac{\partial T}{\partial t}\,\mathrm{d}V + \oint_{\partial V(t)} T\boldsymbol{v}\cdot\boldsymbol{n}\,\mathrm{d}S \right].
\end{aligned} \tag{1.26}$$

Since $V(t)$ was fixed relative to the solid phase, the total amount of solid phase in $V(t)$ changes only through internal solidification/melting. The increase of the total amount of the solid phase during the time interval of length Δt is equal to

$$\begin{aligned}
\Delta M_{\mathrm{solid}} &= \rho \left[\int_{V(t+\Delta t)} \phi(\boldsymbol{x}, t+\Delta t)\,\mathrm{d}V - \int_{V(t)} \phi(\boldsymbol{x}, t)\,\mathrm{d}V \right] \\
&\approx \Delta t \rho \frac{\mathrm{d}}{\mathrm{d}t} \int_{V(t)} \phi\,\mathrm{d}V \\
&= \Delta t \rho \int_{V(t)} \left[\frac{\partial \phi}{\partial t} + (\boldsymbol{v}\cdot\boldsymbol{\nabla})\phi \right] \mathrm{d}V \\
&\equiv \Delta t \rho \int_{V(t)} \frac{\mathrm{D}^s \phi}{\mathrm{D}t}\,\mathrm{d}V.
\end{aligned} \tag{1.27}$$

The amount of latent heat released in $V(t)$ during the time interval Δt is then equal to $L\Delta M_{\mathrm{solid}}$.

between single dendrites). If one would think instead of a fluid flow in a region whose size was small compared to the intersticial length scales, the mass transport would be fully determined by the flow field $\boldsymbol{u}$.

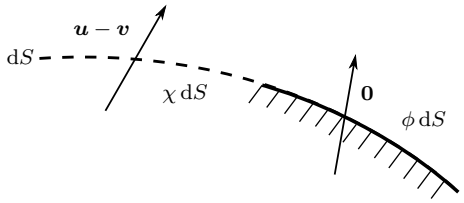

Figure 1.10: Schematic plot of an element $\mathrm{d}S$ of the boundary ∂V. The advective transport of heat depends only upon the relative velocity of the liquid phase relative to the solid phase. This relative velocity is given as $\boldsymbol{u}-\boldsymbol{v}$. Moreover, the solid portion of the boundary does not contribute to the advective transport.

As a next step, we express the amount of heat that enters $V(t)$ by diffusion and advection through the boundary. The local rate of heat flow is given as

$$\begin{aligned}\boldsymbol{Q} &= -k\boldsymbol{\nabla}T + \rho C_P T\chi(\boldsymbol{u}-\boldsymbol{v}) \\ &= -k\boldsymbol{\nabla}T + \rho C_P T(\boldsymbol{q}-\boldsymbol{v}).\end{aligned} \tag{1.28}$$

The advective term[2] $\rho C_P T\chi(\boldsymbol{u}-\boldsymbol{v})$ represents the advection of heat relative to the solid phase. Since $V(t)$ is stationary relative to the solid phase, the motion of the solid phase does not contribute to the heat transport – see figure 1.10 for a schematic plot. The amount of heat that enters $V(t)$ during the time interval Δt is then equal to

$$\begin{aligned}Q_{\text{in}} &= \Delta t \oint_{\partial V(t)} \boldsymbol{Q}\cdot(-\boldsymbol{n})\,\mathrm{d}S \\ &= \Delta t\left[k\int_{V(t)}\nabla^2 T\,\mathrm{d}V - \rho C_P\oint_{\partial V(t)} T(\boldsymbol{q}-\boldsymbol{v})\cdot\boldsymbol{n}\,\mathrm{d}S\right].\end{aligned} \tag{1.29}$$

The conservation of heat in $V(t)$ can then be expressed as

$$\Delta Q = Q_{\text{in}} + L\Delta M_{\text{solid}}. \tag{1.30}$$

Inserting (1.26), (1.27) and (1.29) in (1.30) yields

$$\rho C_P\left[\int_{V(t)}\frac{\partial T}{\partial t}\,\mathrm{d}V + \oint_{\partial V(t)} T\boldsymbol{q}\cdot\boldsymbol{n}\,\mathrm{d}S\right] = \int_{V(t)}\left[k\nabla^2 T + \rho L\frac{\mathrm{D}^s\phi}{\mathrm{D}t}\right]\mathrm{d}V. \tag{1.31}$$

We can re-write the surface integral on the left hand-side using the divergence theorem, together with (1.22) and (1.25), as

$$\oint_{\partial V(t)} T\boldsymbol{q}\cdot\boldsymbol{n}\,\mathrm{d}S = \int_{V(t)}(\boldsymbol{q}\cdot\boldsymbol{\nabla})T\,\mathrm{d}V. \tag{1.32}$$

[2]When the heat transport is not only by diffusion but also by advection, the rate of heat flux is given by

$$\boldsymbol{Q} = -k\boldsymbol{\nabla}T + \rho C_P\boldsymbol{u}T.$$

Since $V(t)$ was arbitrary, the temperature field in the mushy layer must obey the following advection-diffusion equation

$$\rho C_P \frac{\mathrm{D}T}{\mathrm{D}t} = k\nabla^2 T + \rho L \frac{\mathrm{D}^s \phi}{\mathrm{D}t},$$

or

$$\frac{\mathrm{D}T}{\mathrm{D}t} = \kappa \nabla^2 T + \frac{L}{C_P} \frac{\mathrm{D}^s \phi}{\mathrm{D}t}. \tag{1.33}$$

Conservation of solute

For the sake of generality, we will assume that the solute is not completely rejected upon solidification so that $C_S \neq 0$, with C_S being constant throughout the mush. Let V be an arbitrary region fixed in space. The total amount M of solute in V is equal to

$$\rho \int_V \bar{C} \, \mathrm{d}S \equiv \rho \int_V (\chi C + \phi C_S) \, \mathrm{d}S. \tag{1.34}$$

We can express the change of M in a small time interval of length Δt as

$$\begin{aligned} \Delta M &= \Delta t \rho \frac{\mathrm{d}}{\mathrm{d}t} \int_V \bar{C} \, \mathrm{d}V \\ &= \Delta t \rho \int_V \left[\frac{\partial \chi}{\partial t} C + \chi \frac{\partial C}{\partial t} + \frac{\partial \phi}{\partial t} C_S \right] \mathrm{d}V \\ &= \Delta t \rho \int_V \left[\chi \frac{\partial C}{\partial t} - (C - C_S) \frac{\partial \phi}{\partial t} \right] \mathrm{d}V. \end{aligned} \tag{1.35}$$

The amount of solute that enters V by advection through its boundary is

$$\begin{aligned} M_{\text{advection}} &= \Delta t \rho \left[\oint_{\partial V} C \chi \boldsymbol{u} \cdot (-\boldsymbol{n}) \, \mathrm{d}S + \oint_{\partial V} C_S \phi \boldsymbol{v} \cdot (-\boldsymbol{n}) \, \mathrm{d}S \right] \\ &= -\Delta t \rho \int_V \boldsymbol{\nabla} \cdot (C \chi \boldsymbol{u} + C_S \phi \boldsymbol{v}) \, \mathrm{d}V. \end{aligned} \tag{1.36}$$

The first surface integral represents the amount of solute contained in the liquid entering V. Similarly, the second surface integral represents the amount of solute contained in the solid entering V. The amount of solute diffusing into V is equal

$$M_{\text{diffusion}} = \Delta t \rho \int_V D \boldsymbol{\nabla} \cdot (\chi \boldsymbol{\nabla} C) \, \mathrm{d}V. \tag{1.37}$$

If we set $A = C$ and $\boldsymbol{B} = \chi \boldsymbol{u}$ in (1.22), we obtain

$$\begin{aligned} \boldsymbol{\nabla} \cdot (C \chi \boldsymbol{u}) &= \chi (\boldsymbol{u} \cdot \boldsymbol{\nabla}) C + C \boldsymbol{\nabla} \cdot (\chi \boldsymbol{u}) = \chi (\boldsymbol{u} \cdot \boldsymbol{\nabla}) C - C \boldsymbol{\nabla} \cdot (\phi \boldsymbol{v}) \\ &= \chi (\boldsymbol{u} \cdot \boldsymbol{\nabla}) C - C (\boldsymbol{v} \cdot \boldsymbol{\nabla}) \phi. \end{aligned}$$

In the second equality, we used that $\boldsymbol{\nabla} \cdot (\chi \boldsymbol{u}) = -\boldsymbol{\nabla} \cdot (\phi \boldsymbol{v})$, which is a direct consequence of (1.25). In the last equality, we used (1.22) and the fact that $\boldsymbol{v}$ is constant and therefore is divergence-free. In an analogous way we obtain

$$\boldsymbol{\nabla} \cdot (C_S \phi \boldsymbol{v}) = C_S (\boldsymbol{v} \cdot \boldsymbol{\nabla}) \phi.$$

Inserting the last two equalities into (1.36), we get

$$M_{\text{advection}} = \Delta t \rho \left[\int_V (C - C_S)(\boldsymbol{v} \cdot \boldsymbol{\nabla}) \phi \, \mathrm{d}V - \int_V \chi (\boldsymbol{u} \cdot \boldsymbol{\nabla}) C \, \mathrm{d}V \right]. \tag{1.38}$$

The conservation of solute can be expressed as

$$\Delta M = M_{\text{diffusion}} + M_{\text{advection}},$$

from which, after inserting (1.35), (1.37) and (1.38) and since V was arbitrary, we finally get the advection-diffusion equation for the concentration field

$$\chi \frac{\mathrm{D}^l C}{\mathrm{D}t} = D \boldsymbol{\nabla} \cdot (\chi \boldsymbol{\nabla} C) + (C - C_S) \frac{\mathrm{D}^s \phi}{\mathrm{D}t}. \tag{1.39}$$

The last equation can be expressed equivalently as

$$\frac{\mathrm{D}C}{\mathrm{D}t} - \phi \frac{\mathrm{D}^s C}{\mathrm{D}t} = D \boldsymbol{\nabla} \cdot (\chi \boldsymbol{\nabla} C) + (C - C_S) \frac{\mathrm{D}^s \phi}{\mathrm{D}t}, \tag{1.40}$$

or

$$\frac{\mathrm{D}C}{\mathrm{D}t} = D \boldsymbol{\nabla} \cdot (\chi \boldsymbol{\nabla} C) + \frac{\mathrm{D}^s}{\mathrm{D}t} [\phi (C - C_S)]. \tag{1.41}$$

Darcy equation

The fluid flow in the mushy layer is governed by Darcy equation for a flow in a porous medium (see Schultze & Worster 2005) of the following form

$$\chi (\boldsymbol{u} - \boldsymbol{v}) = \frac{\Pi(\phi)}{\mu} (\rho \boldsymbol{g} - \boldsymbol{\nabla} P), \tag{1.42}$$

where $\Pi(\phi)$ is the permeability of the porous medium (mushy layer), which depends upon the local volume fraction of solid, μ is the dynamic viscosity, P is the pressure and $\boldsymbol{g} = (0, -g)^{\mathrm{T}}$ is the gravity.

1.4.2 Conditions at the interfaces

A thorough discussion of the interfacial conditions reviewed below can be found in Worster (2002).

Conservation of mass

The conservation of mass at the mush/liquid interface implies continuity of the normal mass fluxes

$$(\boldsymbol{q}_{b^-} - \boldsymbol{u}_{b^+}) \cdot \boldsymbol{n}_b = 0. \tag{1.43}$$

Note that in the liquid phase, the mass flux $\boldsymbol{q}$ is the same as the velocity field $\boldsymbol{u}$. Moreover, (1.43) is equivalent to

$$(\boldsymbol{u}_{b^+} - \boldsymbol{u}_{b^-}) \cdot \boldsymbol{n}_b = \phi_{b^-} (\boldsymbol{v} - \boldsymbol{u}_{b^-}) \cdot \boldsymbol{n}_b. \tag{1.44}$$

This last condition states that unless $\phi = 0$ at the interface (no phase change at the interface) or $\boldsymbol{v} \cdot \boldsymbol{n}_b = \boldsymbol{u}_{b^-} \cdot \boldsymbol{n}_b$ (a zero normal fluid velocity relative to solid material points), the normal velocity field is discontinuous across the interface.

Since $\phi = 1$ in the solid phase, the conservation of mass at the solid/mush interface implies

$$\chi_{a^+}(\boldsymbol{u}_{a^+} - \boldsymbol{v}) \cdot \boldsymbol{n}_a = 0, \tag{1.45}$$

so that the normal component of the Darcy velocity is zero there.

Conservation of heat

The conservation of heat at the mush/liquid interface implies

$$\rho L(1 - \chi_{b^-})(\boldsymbol{w}_b - \boldsymbol{v}) \cdot \boldsymbol{n}_b = k\,(\boldsymbol{\nabla} T|_{b^-} - \boldsymbol{\nabla} T|_{b^+}) \cdot \boldsymbol{n}_b. \tag{1.46}$$

The difference between (1.17a) and (1.46) is in term $\boldsymbol{w}_b - \boldsymbol{v}$, which expresses the rate of solidification as the difference between the rate of interfacial propagation and the speed of solid material points. In (1.17a), the solid was stationary, hence $\boldsymbol{v} = \boldsymbol{0}$ in that case. Since the temperature is continuous across the interface, the terms representing the advective transport of heat due to the fluid flow or that due to the motion of dendrites are not present in (1.46). In such case, the full conservation of heat across the mush/liquid interface would be

$$\begin{aligned} &\rho L(1 - \chi_{b^-})(\boldsymbol{w}_b - \boldsymbol{v}) \cdot \boldsymbol{n}_b + \underbrace{[-k\boldsymbol{\nabla} T|_{b^+} + \rho C_P T_{b^+}(\boldsymbol{u}_{b^+} - \boldsymbol{w}_b)]}_{\boldsymbol{Q}_{\boldsymbol{b}^+}} \cdot (-\boldsymbol{n}_b) \\ &= \underbrace{[-k\boldsymbol{\nabla} T|_{b^-} + \rho C_P T_{b^-}(\boldsymbol{q}_{b^-} - \boldsymbol{w}_b)]}_{\boldsymbol{Q}_{\boldsymbol{b}^-}} \cdot (-\boldsymbol{n}_b), \end{aligned} \tag{1.47}$$

where $\boldsymbol{Q}_{\boldsymbol{b}^+}$ and $\boldsymbol{Q}_{\boldsymbol{b}^-}$ are the local heat fluxes on the liquid and solid sides of the interface, respectively. The advective components of these vectors depend upon the mass flow relative to the interface; the term $\rho C_P T_{b^-}(\boldsymbol{q}_{b^-} - \boldsymbol{w}_b) \cdot (-\boldsymbol{n}_b)$ represents the advective heat flux from the interface to mushy layer and the term $\rho C_P T_{b^+}(\boldsymbol{u}_{b^+} - \boldsymbol{w}_b) \cdot (-\boldsymbol{n}_b)$ represents the advective heat flux from the liquid phase toward the interface. Since we assume that the temperature field is continuous, we get from (1.43) that the difference of the advective fluxes in (1.47) vanishes.

Analogously, the conservation of heat at the solid/mush interface leads to

$$\rho L \chi_{a^+}(\boldsymbol{w}_a - \boldsymbol{v}) \cdot \boldsymbol{n}_a = k\,(\boldsymbol{\nabla} T|_{a^-} - \boldsymbol{\nabla} T|_{a^+}) \cdot \boldsymbol{n}_a. \tag{1.48}$$

Conservation of solute

The conservation of solute at the mush/liquid interface is expressed by the following condition

$$(C_b - C_S)(1 - \chi_{b^-})(\boldsymbol{w}_b - \boldsymbol{v}) \cdot \boldsymbol{n}_b = D\,(\chi_{b^-} \boldsymbol{\nabla} C|_{b^-} - \boldsymbol{\nabla} C|_{b^+}) \cdot \boldsymbol{n}_b. \tag{1.49}$$

Since we assume nontrivial solute diffusion, the concentration field is continuous across the interface, hence the advective transport of solute is not included in (1.49). The conservation of solute in full form would be

$$\chi_{b^-} C_{b^-}(\boldsymbol{u}_{b^-} - \boldsymbol{w}_b) \cdot \boldsymbol{n}_b + \phi_{b^-} C_S(\boldsymbol{v} - \boldsymbol{w}_b) \cdot \boldsymbol{n}_b - D\chi_{b^-} \boldsymbol{\nabla} C|_{b^-} \cdot \boldsymbol{n}_b$$

$$= -D\boldsymbol{\nabla}C|_{b^+} \cdot \boldsymbol{n}_b + C_{b^+}(\boldsymbol{u}_{b^+} - \boldsymbol{w}_b) \cdot \boldsymbol{n}_b. \tag{1.50}$$

The term $\chi_{b^-}C_{b^-}(\boldsymbol{u}_{b^-} - \boldsymbol{w}_b) \cdot \boldsymbol{n}_b$ is the advective flux of solute from the mushy layer towards the interface. In case $(\boldsymbol{v} - \boldsymbol{w}_b) \cdot \boldsymbol{n}_b < 0$, the expression $\phi_{b^-}C_S|(\boldsymbol{v} - \boldsymbol{w}_b) \cdot \boldsymbol{n}_b|$ represents the rate at which solute, contained within the dendrites, is transported into the mushy layer from the mush-side of the interface (the solid phase has the concentration C_S and the solid material elements are moving away from the interface into the mushy layer). In case $(\boldsymbol{v} - \boldsymbol{w}_b) \cdot \boldsymbol{n}_b > 0$ the interface is melting and the expression $\phi_{b^-}C_S(\boldsymbol{v} - \boldsymbol{w}_b) \cdot \boldsymbol{n}_b$ represents the rate at which the solute is released ahead of the interface. The condition (1.50) can be manipulated to yield

$$[C_b]^-_+(\boldsymbol{q}_{b^-} - \boldsymbol{w}_b) \cdot \boldsymbol{n}_b + \phi_{b^-}(C_{b^-} - C_S)(\boldsymbol{w}_b - \boldsymbol{v}) \cdot \boldsymbol{n}_b = D\left(\chi_{b^-}\boldsymbol{\nabla}C|_{b^-} - \boldsymbol{\nabla}C|_{b^+}\right) \cdot \boldsymbol{n}_b,$$

where we have used the mass conservation (1.43). In case when $D \neq 0$ the concentration field is continuous across the interface so that the first term in the above condition is zero. In case when $D = 0$ the concentration does not have to be continuous so that the conservation of solute reads

$$[C_b]^-_+(\boldsymbol{q}_{b^-} - \boldsymbol{w}_b) \cdot \boldsymbol{n}_b + \phi_{b^-}(C_{b^-} - C_S)(\boldsymbol{w}_b - \boldsymbol{v}) \cdot \boldsymbol{n}_b = 0.$$

Analogously, the conservation of solute at the solid/mush interface is expressed as

$$(C_a - C_S)\chi_{a^+}(\boldsymbol{w}_a - \boldsymbol{v}) \cdot \boldsymbol{n}_a = -D\chi_{a^+}\boldsymbol{n}_a \cdot \boldsymbol{\nabla}C|_{a^+}. \tag{1.51}$$

Chapter 2

Solidification over a horizontally-moving boundary

2.1 Introduction

In the previous chapter we reviewed the basics of mathematical modelling of a solidifying binary substance, with focus on the dynamics of mushy layers — the reactive porous regions, in which the solid and liquid phases coexists. The simplest case was that of diffusion-driven solidification with a planar solid/liquid interface. We have also briefly discussed the directional solidification, in which the solidifying system was pulled in vertical direction in an imposed temperature gradient, with the interface being stationary in the laboratory frame of reference. Such solidification is of importance from both the theoretical and experimental views, as it enables both the morphological stability analyses of the interface and the analyses of convection.

The experimental configuration that is of interest in our thesis and shall be discussed in detail in this chapter is the one in which a cooled horizontal boundary (substrate) is moving at a constant speed in horizontal direction in an imposed vertical temperature gradient. In what follows, we shall assume that the material properties of the solid and liquid phases are the same.

2.2 Mathematical formulation

We consider a steady-state solidification of a binary alloy over a cooled plate $z = 0$, moving horizontally at constant speed $U_0 > 0$. The temperature of the moving plate is maintained at a value T_0 that is above the eutectic temperature T_E and below the liquidus temperature $T_L(C_\infty)$ corresponding to the far-field solute concentration C_∞ at $z \to \infty$. The far-field temperature in the liquid is T_∞. The binary alloy occupies the region $x > 0$, $z > 0$. The experimental setting of the present problem is the same as that by Löfgren (2001); a new feature in the present analysis is the presence of a steady mushy layer separated from the solid and liquid phases by interfaces located at $z = a(x)$ and $z = b(x)$, respectively. A definition sketch for the problem under consideration is depicted in figure 2.1.

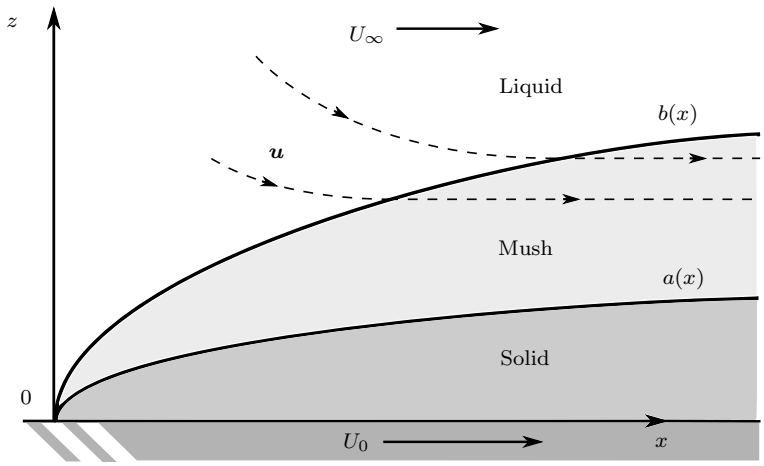

Figure 2.1: A definition sketch for the problem of solidification of a binary alloy over a horizontally moving boundary. A semi-infinite region $x > 0$, $z > 0$ is filled with a binary alloy of far-field solute concentration C_∞ and temperature T_∞ (for $z \to \infty$, x fixed). The cooled lower boundary lies in the plane $z = 0$ and is moving in horizontal direction at a constant speed U_0. The temperature of the cooled boundary is maintained at a value T_0. The stationary solid/mush and mush/liquid interfaces are located at $z = a(x)$ and $z = b(x)$.

2.2.1 Dimensional governing equations in the mushy layer

The speed of the material points embedded in the dendrites is

$$\boldsymbol{v} = U_0 \boldsymbol{i}, \tag{2.1}$$

while both interfaces are stationary so that

$$\boldsymbol{w} = \boldsymbol{0}. \tag{2.2}$$

We adopt the following assumptions to simplify the physical problem and to enable us to seek the solutions in a self-similar form:

i) We ignore the gravity as we do not assume any convective motions in the mush and liquid regions.

ii) We assume that there is no pressure gradient in the interstitial liquid of the mush.

Darcy equation

The above assumptions imply that there is no flow relative to the dendrites, since (1.42) reduces to

$$\chi(\boldsymbol{u} - \boldsymbol{v}) = \boldsymbol{0}, \tag{2.3}$$

so that in the mushy layer

$$\boldsymbol{q} = \boldsymbol{u} = \boldsymbol{v} \tag{2.4}$$

and the streamlines are parallel to the x-axis (see figure 2.1). Moreover, (2.4) implies that the incompressibility condition (1.25) is automatically satisfied.

Temperature field

The governing equation (1.33), describing the temperature field, becomes

$$\boldsymbol{v}\cdot\boldsymbol{\nabla}T=\kappa\nabla^2T-\frac{L}{C_P}\boldsymbol{v}\cdot\boldsymbol{\nabla}\chi,$$

or, after simplification,

$$U_0\frac{\partial T}{\partial x}=\kappa\left(\frac{\partial^2T}{\partial x^2}+\frac{\partial^2T}{\partial z^2}\right)-U_0\frac{L}{C_P}\frac{\partial\chi}{\partial x}. \tag{2.5}$$

Concentration field

The governing equation (1.39), describing the concentration field, transforms to

$$\chi\boldsymbol{v}\cdot\boldsymbol{\nabla}C=D\boldsymbol{\nabla}\cdot(\chi\boldsymbol{\nabla}C)-C\boldsymbol{v}\cdot\boldsymbol{\nabla}\chi$$

or, equivalently,

$$U_0\frac{\partial}{\partial x}(\chi C)=D\left[\frac{\partial}{\partial x}\left(\chi\frac{\partial C}{\partial x}\right)+\frac{\partial}{\partial z}\left(\chi\frac{\partial C}{\partial z}\right)\right]. \tag{2.6}$$

Liquidus relationship

Although we expressed the liquidus relationship in (1.14), we will use a more convenient form of the local thermodynamic equilibrium, namely

$$T=T_L(C)\equiv T_0-\hat{\Gamma}(C-C_0), \tag{2.7}$$

where $\hat{\Gamma}>0$ is the liquidus slope and C_0 is such that $T_0=T_L(C_0)$. However, the formulation stated in (2.7) is equivalent to that in (1.14). The corresponding phase diagram, along with the all relevant physical quantities, is depicted in figure 2.2.

Conditions at the interfaces

Since $\boldsymbol{q}=\boldsymbol{u}|_{b^-}=\boldsymbol{v}$, the condition (1.43) reduces to

$$(\boldsymbol{u}_{b^+}-\boldsymbol{v})\cdot\boldsymbol{n}_b=0, \tag{2.8}$$

so that the normal component of the velocity is continuous across the mush/liquid interface.

We denote by $\mathrm{D}a/\mathrm{D}t=-\boldsymbol{v}\cdot\boldsymbol{n}_a$ and $\mathrm{D}b/\mathrm{D}t=-\boldsymbol{v}\cdot\boldsymbol{n}_b$ the local velocities of the solid material elements relative to the (stationary) solid/mush and mush/liquid interfaces. Then the conservation of heat and solute at the mush/liquid interface, respectively, take the following form

$$\rho L(1-\chi_{b^-})\frac{\mathrm{D}b}{\mathrm{D}t}=(k\boldsymbol{\nabla}T|_{b^-}-k\boldsymbol{\nabla}T|_{b^+})\cdot\boldsymbol{n}_b, \tag{2.9a}$$

$$C_b(1-\chi_{b^-})\frac{\mathrm{D}b}{\mathrm{D}t}=D(\chi_{b^-}\boldsymbol{\nabla}C|_{b^-}-\boldsymbol{\nabla}C|_{b^+})\cdot\boldsymbol{n}_b. \tag{2.9b}$$

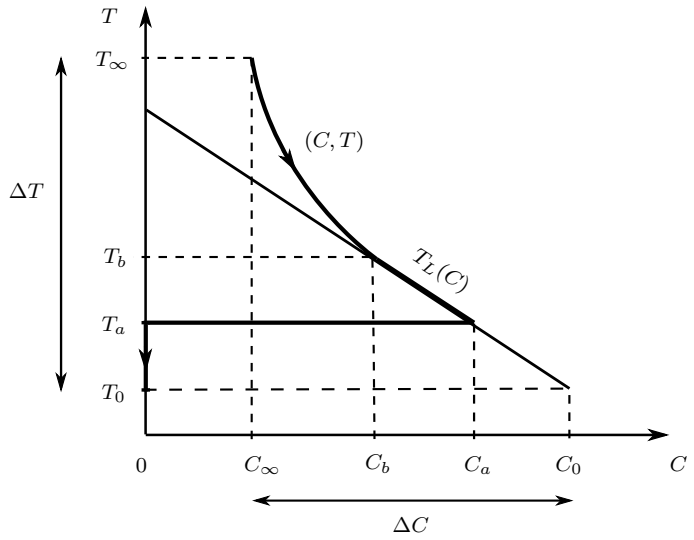

Figure 2.2: Approximate binary phase diagram for a system with a mushy layer, used in our thesis. For the description of particular symbols, see text. Shown is also a typical trajectory (C, T) of a solidifying system (solid lines with arrows).

and that at the solid/mush interface become

$$\rho L \chi_{a^+} \frac{\mathrm{D}a}{\mathrm{D}t} = (k\boldsymbol{\nabla} T|_{a^-} - k\boldsymbol{\nabla} T|_{a^+}) \cdot \boldsymbol{n}_a, \tag{2.10a}$$

$$C_{a^+} \chi_{a^+} \frac{\mathrm{D}b}{\mathrm{D}t} = -D\chi_{a^+} \boldsymbol{n}_a \cdot \boldsymbol{\nabla} C|_{a^+}. \tag{2.10b}$$

Note that, although the problem itself is stationary, the left hand-sides of $(2.9a,b)$ and $(2.10a,b)$ are non-zero: both interfaces are freezing since $(\boldsymbol{w} - \boldsymbol{v}) \cdot \boldsymbol{n}_i = -\boldsymbol{v} \cdot \boldsymbol{n}_i > 0$, $i = a, b$, hence there is a non-trivial latent heat and solute release.

Governing equations in the solid phase

The temperature field in the solid phase is governed by a stationary advection-diffusion equation of the following form

$$\boldsymbol{v} \cdot \boldsymbol{\nabla} T = \kappa \nabla^2 T, \tag{2.11}$$

or, equivalently,

$$U_0 \frac{\partial T}{\partial x} = \kappa \left(\frac{\partial^2 T}{\partial x^2} + \frac{\partial^2 T}{\partial z^2} \right). \tag{2.12}$$

The advective term results from the horizontal advection of heat caused by the pulling of the substrate (and hence the whole solid phase) at the constant speed U_0 in the x-direction.

Governing equations in the liquid phase

The temperature and concentration fields in the liquid phase are governed by the stationary advection-diffusion equations

$$\boldsymbol{u} \cdot \boldsymbol{\nabla} T = \kappa \nabla^2 T, \tag{2.13}$$

$$\boldsymbol{u}\cdot\boldsymbol{\nabla}C = D\nabla^2 C. \tag{2.14}$$

The stationary, Navier-Stokes equations for the velocity field $\boldsymbol{u}$ are

$$(\boldsymbol{u}\cdot\boldsymbol{\nabla})\boldsymbol{u} = -\frac{1}{\rho}\boldsymbol{\nabla}P + \nu\nabla^2\boldsymbol{u}, \tag{2.15}$$

$$\boldsymbol{\nabla}\cdot\boldsymbol{u} = 0, \tag{2.16}$$

where ν is the kinematic viscosity.

Boundary conditions

The boundary conditions imposed at the moving substrate, the mush/liquid interface and that at the far-field are

$$z = 0: \quad T = T_0, \tag{2.17a}$$

$$z = b: \quad u = U_0,\ v = 0, \tag{2.17b,c}$$

$$z \to \infty: \quad T \to T_\infty,\ C \to C_\infty, \tag{2.17d,e}$$

$$u \to U_\infty. \tag{2.17f}$$

The conditions (2.17*b,c*) require some additional comments. The mass conservation (1.43) can be expressed equivalently as

$$v = (u - U_0)\frac{\mathrm{d}b}{\mathrm{d}x}. \tag{2.18}$$

The conditions (2.17*b,c*) impose the continuity of both the normal and tangential mass fluxes across the mush/liquid interface and are consistent with the continuity of the normal mass flux, expressed by (1.43) and (2.18).

2.2.2 Dimensionless formulation

To render the governing equations dimensionless, we scale the velocities with U_0 and lengths with κ/U_0. In the rest of the thesis we will denote the dimensionless quantities by the same symbols as the dimensional ones. We define the dimensionless temperature and concentration, respectively, by

$$\theta = \frac{T - T_0}{\Delta T}, \quad \text{and} \quad \Theta = \frac{C_0 - C}{\Delta C}, \tag{2.19}$$

where

$$\Delta T = T_\infty - T_0, \quad \text{and} \quad \Delta C = C_0 - C_\infty. \tag{2.20}$$

Note that θ and Θ may vary from 0 to 1.

Mushy layer

The dimensionless governing equations in the mushy layer are

$$\frac{\partial \theta}{\partial x} = \frac{\partial^2 \theta}{\partial x^2} + \frac{\partial^2 \theta}{\partial z^2} - \mathscr{S}\frac{\partial \chi}{\partial x}, \tag{2.21a}$$

$$(\Theta - \mathscr{C})\frac{\partial \chi}{\partial x} + \chi\frac{\partial \Theta}{\partial x} = \varepsilon\left[\frac{\partial}{\partial x}\left(\chi\frac{\partial \Theta}{\partial x}\right) + \frac{\partial}{\partial z}\left(\chi\frac{\partial \Theta}{\partial z}\right)\right], \tag{2.21b}$$

$$\theta = \theta_L(\Theta) \equiv \Gamma\Theta. \tag{2.21c}$$

The dimensionless groups appearing in the above equations are the inverse Lewis number ε, the Stefan number $\mathscr{S}$, the concentration ratio $\mathscr{C}$ and the dimensionless liquidus slope Γ, defined respectively by

$$\varepsilon = \frac{D}{\kappa}, \quad \mathscr{S} = \frac{L}{C_p \Delta T}, \quad \mathscr{C} = \frac{C_0}{\Delta C}, \quad \Gamma = \hat{\Gamma}\frac{\Delta C}{\Delta T}. \tag{2.22a–d}$$

Note that the effective range of $\mathscr{C}$ is $(1, \infty)$ and that of Γ is $(0, 1)$. To see the latter, we first realize that $\hat{\Gamma} = (T_b - T_0)/(C_0 - C_b)$ and that

$$\frac{T_\infty - T_0}{C_0 - C_\infty} > \frac{T_b - T_0}{C_0 - C_b}. \tag{2.23}$$

The last inequality can be verified directly from figure 2.2.

Liquid phase

The dimensionless equations governing the temperature and concentration fields in the liquid phase are

$$u\frac{\partial \theta}{\partial x} + v\frac{\partial \theta}{\partial z} = \frac{\partial^2 \theta}{\partial x^2} + \frac{\partial^2 \theta}{\partial z^2}, \tag{2.24a}$$

$$u\frac{\partial \Theta}{\partial x} + v\frac{\partial \Theta}{\partial z} = \varepsilon\left(\frac{\partial^2 \Theta}{\partial x^2} + \frac{\partial^2 \Theta}{\partial z^2}\right). \tag{2.24b}$$

The dimensionless Navier-Stokes equations take the form

$$u\frac{\partial u}{\partial x} + v\frac{\partial u}{\partial z} = Pr\left(\frac{\partial^2 u}{\partial x^2} + \frac{\partial^2 u}{\partial z^2}\right), \tag{2.25a}$$

$$u\frac{\partial v}{\partial x} + v\frac{\partial v}{\partial z} = -\frac{\mathrm{d}p}{\mathrm{d}z} + Pr\left(\frac{\partial^2 v}{\partial x^2} + \frac{\partial^2 v}{\partial z^2}\right), \tag{2.25b}$$

$$\frac{\partial u}{\partial x} + \frac{\partial v}{\partial z} = 0, \tag{2.25c}$$

where

$$Pr = \frac{\nu}{\kappa} \tag{2.26}$$

is the dimensionless Prandtl number and p is the dimensionless pressure (note that p depends only on the z coordinate). However, as we shall see, the second equation will not be relevant due to boundary-layer reduction.

Solid phase

The dimensionless heat equation in the solid phase reads

$$\frac{\partial \theta}{\partial x} = \frac{\partial^2 \theta}{\partial x^2} + \frac{\partial^2 \theta}{\partial z^2}. \tag{2.27}$$

Conditions at the interfaces

The dimensionless conditions at mush/liqud interface are

$$\mathscr{S}(1-\chi_{b^-})\boldsymbol{i}\cdot(-\boldsymbol{n}_b) = (\boldsymbol{\nabla}\theta|_{b^-} - \boldsymbol{\nabla}\theta|_{b^+})\cdot\boldsymbol{n}_b, \tag{2.28a}$$
$$(\Theta_b - \mathscr{C})(1-\chi_{b^-})\boldsymbol{i}\cdot(-\boldsymbol{n}_b) = \varepsilon\,(\chi_{b^-}\boldsymbol{\nabla}\Theta|_{b^-} - \boldsymbol{\nabla}\Theta|_{b^+})\cdot\boldsymbol{n}_b \tag{2.28b}$$

and that at the solid/mush interface are

$$\mathscr{S}\chi_{a^+}\boldsymbol{i}\cdot(-\boldsymbol{n}_a) = (\boldsymbol{\nabla}\theta|_{a^-} - \boldsymbol{\nabla}\theta|_{a^+})\cdot\boldsymbol{n}_a, \tag{2.29a}$$
$$(\Theta_a - \mathscr{C})\chi_{a^+}\boldsymbol{i}\cdot(-\boldsymbol{n}_a) = -\varepsilon\chi_{a^+}\boldsymbol{n}_a\cdot\boldsymbol{\nabla}\Theta|_{a^+} \tag{2.29b}$$

Boundary conditions

The imposed dimensionless boundary conditions are

$$z = 0: \quad \theta = 0, \tag{2.30a}$$
$$z = b: \quad u = 1,\ v = 0, \tag{2.30b,c}$$
$$z \to \infty: \quad \theta \to 1,\ \Theta \to 1,\ u \to \mathscr{U}, \tag{2.30d,e,f}$$

where the dimensionless velocity ratio $\mathscr{U}$, defined by

$$\mathscr{U} = \frac{U_\infty}{U_0}, \tag{2.31}$$

represents the scaled far-field horizontal velocity.

2.2.3 Boundary-layer reduction and self-similar formulation

Our goal is to examine self-similar solutions to the problem just stated, with the dimensionless interfaces having a square-root growth of the form

$$a(x) = 2\lambda_a x^{1/2}, \quad b(x) = 2\lambda_b x^{1/2}, \tag{2.31a,b}$$

where λ_a and λ_b are unknown positive constants. We shall consider a self-similar variable ζ, defined by

$$\zeta = \frac{z}{2x^{1/2}}. \tag{2.32}$$

However, the system of partial differential equations hitherto presented does not admit a self-similar solution involving the variable ζ. To facilitate the self-similar analysis, we consider the limit

$$x \to \infty, \quad z/x^{1/2} = O(1), \tag{2.33}$$

so that $\boldsymbol{n}_a$, $\boldsymbol{n}_b \sim \boldsymbol{k}$ to the leading order. The physical motivation for such limit is that the horizontal gradients of temperature and concentration are small relative to the gradients in vertical direction – a procedure that is typical of boundary layer analyses in fluid dynamics (see, for example, Schlichting 1979). In the limit (2.33), a self-consistent boundary-layer approximation of the governing dimensionless equations and the interface conditions can be made formally via the following re-scaling

$$(x, z) \mapsto (l\hat{x}, l^{1/2}\hat{z}), \tag{2.34}$$

using a fictitious dimensionless scale l, taking the limit $l \to \infty$ with $\hat{x} = O(1)$, $\hat{z} = O(1)$, collecting the leading order terms and then returning back to the original variables x and z. Below we state the reduced system of governing equations and the corresponding conditions at the interfaces. The boundary conditions (2.30*a–f*) are not affected by the boundary-layer reduction.

Mushy layer

$$\frac{\partial \theta}{\partial x} = \frac{\partial^2 \theta}{\partial z^2} - \mathscr{S}\frac{\partial \chi}{\partial x}, \tag{2.35a}$$

$$(\Theta - \mathscr{C})\frac{\partial \chi}{\partial x} + \chi\frac{\partial \Theta}{\partial x} = \varepsilon\frac{\partial}{\partial z}\left(\chi\frac{\partial \Theta}{\partial z}\right), \tag{2.35b}$$

$$\theta = \Gamma\Theta. \tag{2.35c}$$

Liquid phase

$$u\frac{\partial \theta}{\partial x} + v\frac{\partial \theta}{\partial z} = \frac{\partial^2 \theta}{\partial z^2}, \tag{2.36a}$$

$$u\frac{\partial \Theta}{\partial x} + v\frac{\partial \Theta}{\partial z} = \varepsilon\frac{\partial^2 \Theta}{\partial z^2}, \tag{2.36b}$$

$$u\frac{\partial u}{\partial x} + v\frac{\partial u}{\partial z} = Pr\frac{\partial^2 u}{\partial z^2}, \tag{2.37a}$$

$$\frac{\partial u}{\partial x} + \frac{\partial v}{\partial z} = 0. \tag{2.37b}$$

Solid phase

$$\frac{\partial \theta}{\partial x} = \frac{\partial^2 \theta}{\partial z^2} \tag{2.38}$$

Mush/liquid interface

$$\mathscr{S}(1 - \chi_{b^-})\frac{\mathrm{d}b}{\mathrm{d}x} = \left.\frac{\partial \theta}{\partial z}\right|_{b^-} - \left.\frac{\partial \theta}{\partial z}\right|_{b^+}, \tag{2.39a}$$

$$(\mathscr{C} - \Theta_b)(1 - \chi_{b^-})\frac{\mathrm{d}b}{\mathrm{d}x} = \varepsilon\left(\left.\frac{\partial \Theta}{\partial z}\right|_{b^+} - \chi_{b^-}\left.\frac{\partial \Theta}{\partial z}\right|_{b^-}\right). \tag{2.39b}$$

Solid/mush interface

$$\mathscr{S}\chi_{a^+}\frac{\mathrm{d}a}{\mathrm{d}x} = \left.\frac{\partial\theta}{\partial z}\right|_{a^-} - \left.\frac{\partial\theta}{\partial z}\right|_{a^+}, \tag{2.40a}$$

$$(\mathscr{C}-\Theta_a)\chi_{a^+}\frac{\mathrm{d}a}{\mathrm{d}x} = \varepsilon\chi_{a^+}\left.\frac{\partial\Theta}{\partial z}\right|_{a^+}. \tag{2.40b}$$

2.3 Viscous boundary-layer problem in the liquid phase

The equations (2.37*a, b*), together with conditions (2.30*b, c, f*), constitute a viscous boundary-layer problem. The boundary layer is present due to the assumption that the Prandtl number is small, which is typical of liquid metal flows. Apart from the nondimensionalisation scheme, the present viscous boundary-layer problem is the same as that studied by Löfgren (2001). As Löfgren (2001), we derive the asymptotic self-similar solutions for the velocity, temperature and concentration fields in the limit of small Prandtl number. Due to the different scaling chosen, however, the asymptotic regime considered here is, in fact, different.

2.3.1 Stream-function formulation

The flow under consideration is incompressible and two-dimensional, hence we can express the flow velocity $\boldsymbol{u}$ in terms of a scalar stream function $\psi(x,z)$ as

$$u = \frac{\partial\psi}{\partial z}, \quad v = -\frac{\partial\psi}{\partial x}. \tag{2.41a, b}$$

Such a velocity field automatically satisfies the incompressibility condition (2.37*b*).

We will seek the solution to (2.37*a, b*) and (2.30*b, c, f*) in terms of a self-similar variable ζ, defined in (2.32), such that $u(x,z) = u(\zeta)$. Integrating (2.41*a*) we obtain

$$\begin{aligned}\psi(x,z) - \psi(x,b(x)) &= \int_{b(x)}^{z} u\left(\frac{\sigma}{2x^{1/2}}\right)\mathrm{d}\sigma \\ &= 2x^{1/2}\int_{\lambda_b}^{\zeta} u(s)\,\mathrm{d}s.\end{aligned}$$

Differentiating the expression $\psi(x,b(x))$, we get

$$\begin{aligned}\frac{\mathrm{d}}{\mathrm{d}x}\psi\left(x,b(x)\right) &= \left.\frac{\partial\psi}{\partial x}\right|_{z=b(x)} + \left.\frac{\partial\psi}{\partial z}\right|_{z=b(x)}\frac{\mathrm{d}b}{\mathrm{d}x} \\ &= \frac{\lambda_b}{x^{1/2}},\end{aligned}$$

where we have made use of the boundary conditions (2.30*b, c*) and the definition of $b(x)$. Hence the values of stream function at the mush/liquid interface can be expressed as

$$\psi\left(x,b(x)\right) = 2\lambda_b x^{1/2} + K.$$

where K is an arbitrary constant. From (2.41a, b), however, we see that if ψ is a stream function, then $\psi + K$ is also a stream function for any value of K. Therefore we can set $K = 0$. Finally, the stream function has the following form

$$\psi(x, z) = 2x^{1/2} \left[\lambda_b + \int_{\lambda_b}^{\zeta} u(s)\, \mathrm{d}s \right], \tag{2.42}$$

or equivalently,

$$\psi(x, z) = 2x^{1/2} f(\zeta; Pr), \tag{2.43}$$

where $f(\zeta; Pr) \equiv \lambda_b + \int_{\lambda_b}^{\zeta} u(s)\, \mathrm{d}s$. Using (2.41$a$, b) and (2.43), we can express the velocity field as

$$u = f', \tag{2.44a}$$

$$v = \frac{1}{x^{1/2}} (\zeta f' - f), \tag{2.44b}$$

where $f' \equiv \mathrm{d}f/\mathrm{d}\zeta$.

In terms of the stream function, the equation (2.37a) can be formulated in the following way

$$\frac{\partial \psi}{\partial z} \frac{\partial^2 \psi}{\partial x \partial z} - \frac{\partial \psi}{\partial x} \frac{\partial^2 \psi}{\partial z^2} = Pr \frac{\partial^3 \psi}{\partial z^3}.$$

Using the relations

$$\frac{\partial^2 \psi}{\partial x \partial z} = -\frac{\zeta}{2x} f'', \quad \frac{\partial^2 \psi}{\partial z^2} = \frac{1}{2x^{1/2}} f'', \quad \frac{\partial^3 \psi}{\partial z^3} = \frac{1}{4x} f''',$$

we obtain a third-order differential equation for the function f

$$Pr f''' + 2 f f'' = 0, \tag{2.45}$$

subject to boundary conditions

$$\zeta = \lambda_b : \quad f = \lambda_b, \tag{2.46a}$$

$$f' = 1, \tag{2.46b}$$

$$\zeta \to \infty : \quad f' \to \mathscr{U}. \tag{2.46c}$$

The condition (2.46a) follows from the fact that $\psi|_{z=b(x)} = b(x)$. Moreover, from (2.46a) and (2.44b), we can see that the condition $v|_{z=b(x)} = 0$ is automatically satisfied.

2.3.2 Asymptotic solution as $Pr \to 0$

Outer solution

We shall seek an outer solution of the boundary-layer problem (2.45) in the form of a regular asymptotic expansion

$$f_{\mathrm{out}}(\zeta; Pr) \sim f_1(\zeta) + Pr f_2(\zeta) + O(Pr^2), \quad \zeta = O(1),\ Pr \to 0, \tag{2.47}$$

where $f_i(\zeta) = O(1)$ for $\zeta = O(1)$ as $Pr \to 0$. From (2.46c) we obtain

$$\mathscr{U} \sim f_1'(\infty) + Pr f_2'(\infty) + O(Pr^2), \quad Pr \to 0,$$

whence

$$\begin{aligned} f_1'(\infty) &= \mathscr{U}, \\ f_i'(\infty) &= 0, \text{ for } i \geq 2. \end{aligned}$$

We insert the expansion (2.47) into the equation (2.45) to obtain

$$Pr\left[f_1''' + Pr f_2''' + O(Pr^2)\right] + 2\left[f_1 + Pr f_2 + O(Pr^2)\right]\left[f_1'' + Pr f_2''' + O(Pr^2)\right] = 0,$$

or, after some rearrangement,

$$2f_1 f_1'' + Pr\left[f_1''' + 2f_1 f_2'' + 2f_2 f_1''\right] + O(Pr^2) = 0.$$

$O(Pr^0)$ **solution** In the zeroth order, we have a differential equation along with one boundary condition

$$\begin{aligned} 2f_1 f_1'' &= 0, \quad f_1 \not\equiv 0, \\ f_1'(\infty) &= \mathscr{U}. \end{aligned}$$

Thus $f_1'' = 0$ and therefore $f_1(\zeta) = \mathscr{U}\zeta + A$, where A is a constant that is yet to be determined.

$O(Pr^1)$ **solution** The differential equation arising at the first order, along with appropriate boundary condition, has the form

$$\begin{aligned} f_1''' + 2f_1 f_2'' + 2f_2 f_1'' &= 0, \\ f_2'(\infty) &= 0, \end{aligned}$$

which yields

$$(\mathscr{U}\zeta + A) f_2'' = 0,$$

and thus $f_2'' = 0$. From that we have $f_2(\zeta) = d$, for some unknown constant d.

Inner solution

We assume that there is a boundary layer of thickness $O[\Omega(Pr)]$, adjacent to the mush/liquid interface $\zeta = \lambda_b^+$. To resolve this boundary layer, we define a scaled inner coordinate

$$\eta \equiv \frac{\zeta - \lambda_b}{\Omega(Pr)}, \quad \text{where} \quad \Omega(Pr) \to 0 \quad \text{as} \quad Pr \to 0.$$

Rescaling the equation (2.45), we get

$$Pr f_{\text{in}}^{(3)} + 2\Omega f_{\text{in}} f_{\text{in}}^{(2)} = 0, \tag{2.48}$$

where $f_{\text{in}}(\eta) \equiv f(\lambda_b + \Omega\eta)$, with $\eta = O(1)$ as $Pr \to 0$, and $f_{\text{in}}^{(i)} \equiv \mathrm{d}^i f_{\text{in}}/\mathrm{d}\eta^i$. This equation is subject to boundary conditions

$$f_{\text{in}}(0) = \lambda_b, \tag{2.49b}$$

$$f_{\text{in}}^{(1)}(0) = \Omega(Pr). \tag{2.49c}$$

We seek an asymptotic expansion of the inner solution

$$f_{\text{in}}(\eta; Pr) \sim \Delta_1(Pr)F_1(\eta) + \Delta_2(Pr)F_2(\eta) + O[\Delta_3(Pr)], \tag{2.50}$$

for $\eta = O(1)$ as $Pr \to 0$. To obtain consistent asymptotic balances upon inserting (2.50) into (2.48), we set

$$\Delta_1(Pr) = 1, \quad \Delta_2(Pr) = \Omega(Pr) = Pr \tag{2.51a, b}$$

$$F_1(0) = \lambda_b, \quad F_n(0) = 0 \ (n \geq 2), \tag{2.51c, d}$$

$$F_1^{(1)}(0) = 0, \quad F_2^{(1)}(0) = 1. \tag{2.51e, f}$$

After inserting (2.50) into (2.48), we obtain the following sequence of problems

$$O(Pr^1): \quad F_1^{(3)} + 2F_1F_1^{(2)} = 0, \tag{2.52a}$$

$$O(Pr^2): \quad F_2^{(3)} + 2F_1F_2^{(2)} + 2F_2F_1^{(2)} = 0. \tag{2.52b}$$

$O(Pr^1)$ solution First, assume that $F_1^{(2)}(0) \neq 0$. Then the solution of (2.52a) can be shown to satisfy the following integro-differential equation

$$F_1^{(1)}(\eta) = F_1^{(2)}(0) \int_0^\eta \exp\left(-2\int_0^\sigma F_1(s)\,\mathrm{d}s\right)\mathrm{d}\sigma, \tag{2.53}$$

which can be equivalently expressed as

$$F_1(\eta) = \lambda_b + F_1^{(2)}(0) \int_0^\eta \int_0^\omega \exp\left(-2\int_0^\sigma F_1(s)\,\mathrm{d}s\right)\mathrm{d}\sigma\,\mathrm{d}\omega. \tag{2.54}$$

The above equation contains an unknown constant $F_1^{(2)}(0)$. However, it turns out that this constant is, in fact, equal to zero. In that case we get

$$F_1(\eta) \equiv \lambda_b. \tag{2.55}$$

We will now show that $F_1^{(2)}(0) = 0$. First, we know from the boundary conditions, that $f(\lambda_b) = \lambda_b > 0$. So the values of the stream function at the interface satisfy $\psi(x, b(x)) = b(x)$. Therefore, ψ must be positive in the whole boundary layer and so must be the values of function f (see figure 2.3) – see (2.43). Moreover, in the boundary layer $f \sim f_{\text{in}}$ as $Pr \to 0$ and from (2.50) we know that $f_{\text{in}} \sim F_1$. Thus $F_1 > 0$ for all $\eta > 0$. The inner and outer solutions must match so that

$$\lim_{\eta\to\infty} f_{\text{in}}(\eta) = \lim_{\zeta\to 0^+} f_{\text{out}}(\zeta) < \infty.$$

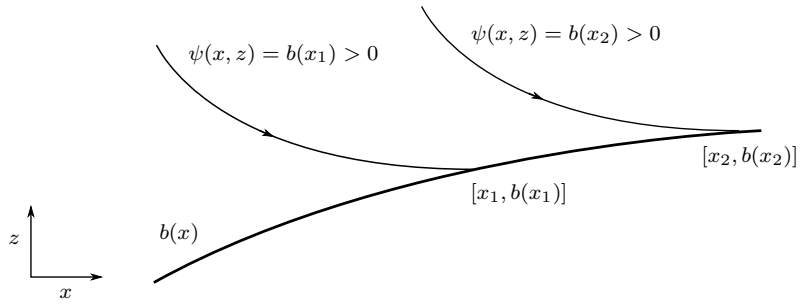

Figure 2.3: Each point within the boundary layer lies on a streamline terminating at the interface. As each streamline corresponds to a contour of the stream function, values of ψ in the boundary layer must be strictly positive.

Hence F_1 must be bounded for $\eta \to \infty$, i.e. there must exist a constant $K > 0$ such that

$$0 < F_1(\eta) < K, \quad \forall \eta > 0. \tag{2.56}$$

Now, assume that $F_1^{(2)}(0) \neq 0$. Then, by integrating both sides of (2.56), we get

$$\exp\left(-2\int_0^\sigma F_1(s)\,\mathrm{d}s\right) > \mathrm{e}^{-2K\sigma},$$

which, after double integration, yields an inequality

$$\int_0^\eta \int_0^\omega \exp\left(-2\int_0^\sigma F_1(s)\,\mathrm{d}s\right)\,\mathrm{d}\sigma\,\mathrm{d}\omega > \frac{\eta}{2K} + \frac{1}{4K^2}(\mathrm{e}^{-2K\eta} - 1).$$

Finally, using (2.54), we have

$$F_1(\eta) - \lambda_b < F_1^{(2)}(0)\left[\frac{\eta}{2K} + \frac{1}{4K^2}(\mathrm{e}^{-2K\eta} - 1)\right], \quad \text{if} \quad F_1^{(2)}(0) < 0,$$

$$F_1(\eta) - \lambda_b > F_1^{(2)}(0)\left[\frac{\eta}{2K} + \frac{1}{4K^2}(\mathrm{e}^{-2K\eta} - 1)\right], \quad \text{if} \quad F_1^{(2)}(0) > 0.$$

Thus, for $\eta \to \infty$, the right hand-side of the above inequalities tends to $+\infty$ when $F_1^{(2)}(0) > 0$, and to $-\infty$ when $F_1^{(2)}(0) < 0$. In both cases we get a contradiction with the boundedness of F_1. Hence we must set $F_1^{(2)}(0) = 0$.

$O(Pr^2)$ solution Using (2.55), the equation (2.52b) takes the form

$$F_2^{(3)} + 2\lambda_b F_2^{(2)} = 0,$$

subject to initial conditions

$$F_2(0) = 0, \quad F_2^{(1)}(0) = 0.$$

The explicit solution is as follows

$$F_2(\eta) = (1 + 2\lambda_b B)\eta + B(\mathrm{e}^{-2\lambda_b \eta} - 1),$$

where B is a constant that is yet to be determined by matching of the inner and outer solutions. Thus, the solution, correct to $O(Pr^2)$, in the inner region is as follows

$$f_{\mathrm{in}}(\eta; Pr) \sim \lambda_b + Pr\left[(1 + 2\lambda_b B)\eta + B\left(\mathrm{e}^{-2\lambda_b \eta} - 1\right)\right], \quad \eta = O(1),\ Pr \to 0.$$

Matching of the inner and outer solutions

The outer solution expressed in terms of the inner variable η has the form

$$f_{\rm out}(\zeta \mapsto \lambda_b + Pr\,\eta; Pr) \sim A + \mathscr{U}\,\lambda_b + Pr\,d + Pr\,\mathscr{U}\,\eta.$$

The inner solution expressed in the outer region has an expansion of the form

$$\begin{aligned} f_{\rm in}\left(\eta \mapsto \frac{\zeta - \lambda_b}{Pr}; Pr\right) &\sim -2\lambda_b^2 B + (1+2\lambda_b)\zeta - Pr\,B \\ &= \lambda_b - PrB + Pr(1+2\lambda_b B)\eta. \end{aligned}$$

To match the inner solution with the outer one, we must set

$$\mathscr{U} = 1 + 2\lambda_b B, \quad Pr\,d = -PrB, \quad \mathscr{U}\,\lambda_b + A = \lambda_b,$$

whence

$$B = \frac{\mathscr{U} - 1}{2\lambda_b}, \quad d = \frac{1 - \mathscr{U}}{2\lambda_b}, \quad A = \lambda_b(1 - \lambda_b).$$

Finally, the outer, inner and composite solutions, expressed in terms of the outer variable, are

$$f_{\rm out}(\zeta; Pr) \sim \lambda_b(1 - \mathscr{U}) + \mathscr{U}\,\zeta + Pr\frac{1 - \mathscr{U}}{2\lambda_b}, \quad \zeta = O(1), \tag{2.57a}$$

$$f_{\rm in}(\eta; Pr) \sim \lambda_b + Pr\left[\mathscr{U}\,\eta + \frac{1 - \mathscr{U}}{2\lambda_b}(1 - {\rm e}^{-2\lambda_b\eta})\right], \quad \eta = O(1), \tag{2.57b}$$

$$f(\zeta; Pr) \sim \lambda_b(1 - \mathscr{U}) + \mathscr{U}\,\zeta + Pr\frac{1 - \mathscr{U}}{2\lambda_b}\left[1 - \exp\left(-2\lambda_b\frac{\zeta - \lambda_b}{Pr}\right)\right]. \tag{2.57c}$$

Note that above asymptotic solutions are valid only if $\lambda_b \gg Pr/\lambda_b$ as $Pr \to 0$, or, equivalently

$$Pr \ll \lambda_b^2 \quad \text{for} \quad Pr \to 0. \tag{2.58}$$

Velocity field

The asymptotic solution for the velocity field is

$$u \sim 1 + (1 - \mathscr{U})\left[\exp\left(-2\lambda_b\frac{\zeta - \lambda_b}{Pr}\right) - 1\right], \tag{2.59a}$$

$$v \sim -\frac{1 - \mathscr{U}}{x^{1/2}}\left\{\lambda_b + \frac{Pr}{2\lambda_b} - \left(\zeta + \frac{Pr}{2\lambda_b}\right)\exp\left(-2\lambda_b\frac{\zeta - \lambda_b}{Pr}\right)\right\}. \tag{2.59b}$$

For fixed values of x, the limiting form of the velocity field, as $\zeta \to \infty$, is

$$u \to \mathscr{U}, \quad v \to \frac{\mathscr{U} - 1}{x^{1/2}}\left(\lambda_b + \frac{Pr}{2\lambda_b}\right).$$

Note that $v > 0$ ($v < 0$) when $\mathscr{U} > 1$ ($\mathscr{U} < 1$), see figure 2.4. Moreover, for $\mathscr{U} = 1$, the flow is trivial relative to the solid phase, in which case the problem studied by Worster (1986) of self-similar growth of a planar solid-liquid interface is reproduced, with his time variable replaced with our x.

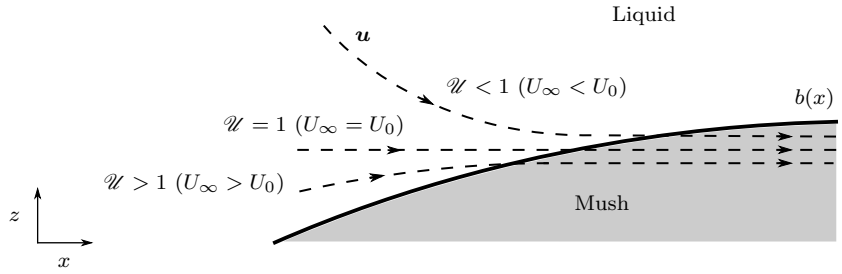

Figure 2.4: Sketch of representative streamlines for qualitatively different values of $\mathscr{U}$. In the mushy layer, the velocity field is equal to the velocity of moving substrate.

2.4 Thermal boundary-layer problem in the liquid phase

When formulated using the stream function ψ, the equation (2.36a) takes the form

$$\frac{\partial\psi}{\partial z}\frac{\partial\theta}{\partial x} - \frac{\partial\psi}{\partial x}\frac{\partial\theta}{\partial z} = \frac{\partial^2\theta}{\partial z^2}.$$

Using (2.32), this is transformed to an ordinary differential equation

$$\theta'' = -2f\theta' \tag{2.60}$$

with $\theta = \theta(\zeta)$, which is subject to

$$\zeta = \lambda_b : \quad \theta = \theta_b, \tag{2.61a}$$

$$\zeta \to \infty : \quad \theta = 1, \tag{2.61b}$$

with θ_b being a part of the solution. The solution of (2.60) and (2.61a,b) is of the form

$$\theta(\zeta; Pr) = \theta_b + (1-\theta_b)\frac{J(\zeta; Pr)}{J(\infty; Pr)}, \tag{2.62}$$

where

$$J(\zeta; Pr) \equiv \int_{\lambda_b}^{\zeta} \exp\left(-2\int_{\lambda_b}^{s} f\,\mathrm{d}\sigma\right)\,\mathrm{d}s. \tag{2.63}$$

The integral $\int_{\lambda_b}^{s} f\,\mathrm{d}\sigma$ can be approximated, using (2.57c), in the following way

$$\int_{\lambda_b}^{s} f\,\mathrm{d}\sigma \sim \frac{\mathscr{U}}{2}(s-\lambda_b)^2 + \Lambda(\lambda_b)(s-\lambda_b) + O(Pr^2), \tag{2.64}$$

with

$$\Lambda(\lambda) \equiv \lambda + Pr\frac{1-\mathscr{U}}{2\lambda}. \tag{2.65}$$

Therefore, by inserting (2.64) into (2.62) and dropping the $O(Pr^2)$ term, we get, after some manipulation, the asymptotic form of the temperature field as $Pr \to 0$

$$\theta(\zeta) \sim 1 + (\theta_b - 1)\frac{\operatorname{erfc}\left[\mathscr{U}^{1/2}(\zeta-\lambda_b) + \mathscr{U}^{-1/2}\Lambda(\lambda_b)\right]}{\operatorname{erfc}\left[\mathscr{U}^{-1/2}\Lambda(\lambda_b)\right]}, \quad \zeta > \lambda_b, \tag{2.66}$$

where

$$\mathrm{erfc}(\lambda) = 1 - \mathrm{erf}(\lambda), \quad \mathrm{erf}(\lambda) = \frac{2}{\pi^{1/2}} \int_0^{\lambda} \mathrm{e}^{-s^2}\, \mathrm{d}s.$$

Note that the Prandtl number affects the temperature field through the quantity $\Lambda(\lambda_b) \sim \lambda_b + O(Pr)$, provided $\lambda_b = O(1)$.

2.5 Compositional boundary-layer problem in the liquid phase

The equation (2.36b) is transformed into the following ordinary differential equation

$$\varepsilon \Theta'' = -2f\Theta', \tag{2.67}$$

with $\Theta = \Theta(\zeta)$, which is subject to

$$\zeta = \lambda_b : \quad \Theta = \Theta_b, \tag{2.68a}$$

$$\zeta \to \infty : \quad \Theta \to 1, \tag{2.68b}$$

with Θ_b being a part of the solution. The solution to (2.67) is

$$\Theta(\zeta; Pr, \varepsilon) = \Theta_b + (1 - \Theta_b) \frac{I(\zeta; Pr, \varepsilon)}{I(\infty; Pr, \varepsilon)}, \tag{2.69}$$

with

$$I(\zeta; Pr, \varepsilon) \equiv \int_{\lambda_b}^{\zeta} \exp\left(-\frac{2}{\varepsilon} \int_{\lambda_b}^{s} f \, \mathrm{d}\sigma \right) \mathrm{d}s. \tag{2.70}$$

Using (2.64) and dropping the $O(Pr^2)$-term, we obtain, after some manipulation, the following form of the concentration field in the liquid phase

$$\Theta(\zeta) \sim 1 + (\Theta_b - 1) \frac{\mathrm{erfc}\left[(\mathscr{U}/\varepsilon)^{1/2} (\zeta - \lambda_b) + (\mathscr{U}\varepsilon)^{-1/2} \Lambda(\lambda_b) \right]}{\mathrm{erfc}\left[(\mathscr{U}\varepsilon)^{-1/2} \Lambda(\lambda_b) \right]}, \quad \zeta > \lambda_b. \tag{2.71}$$

2.6 Temperature field in the solid phase

The heat equation (2.38) is transformed into the ordinary differential equation

$$\theta'' + 2\zeta\theta' = 0, \tag{2.72}$$

subject to boundary conditions

$$\zeta = 0 : \quad \theta = 0, \tag{2.73a}$$

$$\zeta = \lambda_a : \quad \theta = \theta_a, \tag{2.73b}$$

which has the solution

$$\theta = \theta_a \frac{\mathrm{erf}(\zeta)}{\mathrm{erf}\,(\lambda_a)}, \quad \zeta < \lambda_a, \tag{2.74}$$

with θ_a yet to be determined from the conditions at the solid/mush interface.

Chapter 3

Solidification with a solid/liquid interface

3.1 Introduction

Before focusing our attention on the self-similar solutions of the mushy layer problem formulated in the preceding chapter, we take a look at the situation when there are only solid and liquid phases present in the system. The problem was originally formulated by Löfgren (2001), but employing a different scaling of the governing equations as that used in this thesis. Though the limit of small Prandtl number is singular for the velocity field in the liquid phase, it is regular for the temperature and concentration fields as well as for the growth constant λ_h. However, from the experimental point of view, of central importance is the ratio of the horizontal flow velocity forced at infinity to the pulling rate of the substrate, $\mathscr{U}$, introduced in the previous chapter. It is through this velocity ratio that the flow controls the solidification. We shall study the dependence of the solidifying system on $\mathscr{U}$ and we also derive some approximate results in case when $\mathscr{U}$ is small. The the influence of $\mathscr{U}$ was not studied by Löfgren (2001).

3.2 Mathematical formulation

The governing equations in the liquid and solid phases are the same as those in the problem with a mushy layer, the only difference is in the conditions at the solid/liquid interface – however, these can be obtained from those at the solid/mush interface by setting $\chi_{a^+} = 1$. Thus the dimensionless conservation of heat and solute at the solid/liquid interface take the form

$$\mathscr{S}\frac{\mathrm{d}h}{\mathrm{d}x} = \left.\frac{\partial\theta}{\partial z}\right|_{h^-} - \left.\frac{\partial\theta}{\partial z}\right|_{h^+}, \tag{3.1a}$$

$$(\mathscr{C} - \Theta_h)\frac{\mathrm{d}h}{\mathrm{d}x} = \varepsilon \left.\frac{\partial\Theta}{\partial z}\right|_{h^+}, \tag{3.1b}$$

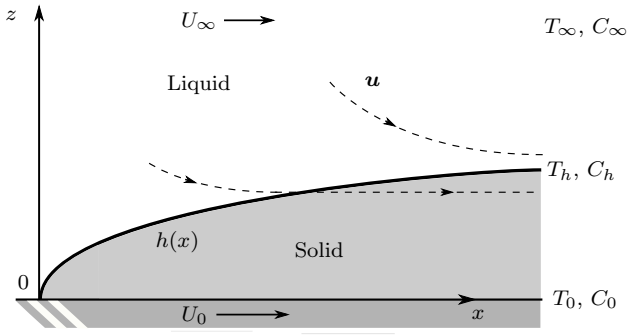

Figure 3.1: Definition sketch for the problem of solidification of a binary alloy over a horizontally moving substrate. A semi-infinite region $x > 0$, $z > 0$ is filled with a binary alloy of far-field solute concentration C_∞ and temperature T_∞ (for $z \to \infty$ and x fixed). The cooled lower boundary lies in the plane $z = 0$ and is moving in horizontal direction at a constant speed U_0. The stationary solid/liquid interface is located at $z = h(x)$. The horizontal flow velocity at $z \to \infty$ is U_∞.

with the dimensionless self-similar interface position

$$h(x) = 2\lambda_h x^{1/2} \tag{3.2}$$

for some positive growth constant λ_h. The dimensional liquidus relationship at the interface is

$$T_h = T_L(C_h) \equiv T_0 - \hat{\Gamma}(C_h - C_0), \tag{3.3}$$

where $\hat{\Gamma} = (T_h - T_0)/(C_0 - C_h)$ is the dimensional liquidus slope. The dimensionless liquidus takes the form

$$\theta_h = \theta_L(\Theta_h) \equiv \Gamma\Theta_h. \tag{3.4}$$

All the dimensional scales and dimensionless numbers are the same as that defined in the previous chapter. A definition sketch for the present problem is shown in figure 3.1.

3.3 Self-similar solutions

The temperature field in the liquid phase has the following approximate form (cf. (2.66))

$$\theta(\zeta) \sim 1 + (\theta_h - 1)\frac{\operatorname{erfc}\left[\mathscr{U}^{1/2}(\zeta - \lambda_h) + \mathscr{U}^{-1/2}\Lambda(\lambda_h)\right]}{\operatorname{erfc}\left[\mathscr{U}^{-1/2}\Lambda(\lambda_h)\right]}, \quad \text{as} \quad Pr \to 0 \tag{3.5}$$

and the concentration field (cf. (2.71))

$$\Theta(\zeta) \sim 1 + (\Theta_h - 1)\frac{\operatorname{erfc}\left[(\mathscr{U}/\varepsilon)^{1/2}(\zeta - \lambda_h) + (\mathscr{U}\varepsilon)^{-1/2}\Lambda(\lambda_h)\right]}{\operatorname{erfc}\left[(\mathscr{U}\varepsilon)^{-1/2}\Lambda(\lambda_h)\right]}, \quad \text{as} \quad Pr \to 0. \tag{3.6}$$

Note that general forms of these solutions are the same as (2.62) and (2.69) with λ_b replaced by λ_h. In the solid phase, the temperature field is (cf. (2.74))

$$\theta = \theta_h \frac{\operatorname{erf}(\zeta)}{\operatorname{erf}(\lambda_h)}. \tag{3.7}$$

The Stefan condition (3.1a), expressed in terms of ζ, reads

$$2\mathscr{S}\lambda_h = \theta'|_{h^-} - \theta'|_{h^+}, \tag{3.8}$$

where the temperature gradients on either sides of the interface can be expressed, using the general-form solution in the liquid phase, as

$$\theta'|_{h^-} = \frac{2\lambda_h\theta_h}{G(\lambda_h)}, \qquad \theta'|_{h^+} = \frac{1-\theta_h}{J(\infty;Pr)}, \tag{3.9a,b}$$

with

$$G(\lambda) = \pi^{1/2}\lambda\,\mathrm{e}^{\lambda^2}\,\mathrm{erf}(\lambda). \tag{3.10}$$

Thus the Stefan condition can be cast into the following form

$$\left[\frac{2\lambda_h}{G(\lambda_h)} + \frac{1}{J(\infty;Pr)}\right]\theta_h - \frac{1}{J(\infty;Pr)} - 2\mathscr{S}\lambda_h = 0. \tag{3.11}$$

The solute conservation at the interface transforms as

$$2(\mathscr{C} - \Theta_h)\lambda_h = \varepsilon\Theta'_h, \tag{3.12}$$

with the concentration gradient on the liquid side of the interface given by

$$\Theta'_h = \frac{1-\Theta_h}{I(\infty;Pr,\varepsilon)}. \tag{3.13}$$

Combining (3.13) with (3.12) we obtain the concentration at the interface as

$$\Theta_h = 1 + (1-\mathscr{C})\frac{2\lambda_h I(\infty;Pr,\varepsilon)}{\varepsilon - 2\lambda_h I(\infty;Pr,\varepsilon)}. \tag{3.14}$$

The nonlinear equation (3.11), along with the liquidus relationship $\theta_h = \Gamma\Theta_h$, serves as the equation from which λ_h can be sought for. The integrals $J(\infty;Pr)$ and $I(\infty;Pr,\varepsilon)$ can be approximated for $Pr \to 0$ in the following way[1]

$$J(\infty;Pr) \sim \frac{1}{2\Lambda(\lambda_h)}F\left[\frac{\Lambda(\lambda_h)}{\mathscr{U}^{1/2}}\right], \tag{3.17a}$$

[1]The quantity $\Lambda(\lambda_h)$ in fact crosses out from the denominators in (3.17a,b) and the integrals $J(\infty;Pr)$ and $I(\infty;Pr,\varepsilon)$ can then be expressed as

$$J(\infty;Pr) \sim \frac{\pi^{1/2}}{2}\mathscr{U}^{-1/2}\exp\left[\frac{\Lambda^2(\lambda_h)}{\mathscr{U}}\right]\mathrm{erfc}\left[\frac{\Lambda(\lambda_h)}{\mathscr{U}^{1/2}}\right], \tag{3.15}$$

$$I(\infty;Pr,\varepsilon) \sim \frac{\pi^{1/2}}{2}\left(\frac{\varepsilon}{\mathscr{U}}\right)^{1/2}\exp\left[\frac{\Lambda^2(\lambda_h)}{\varepsilon\mathscr{U}}\right]\mathrm{erfc}\left[\frac{\Lambda(\lambda_h)}{(\varepsilon\mathscr{U})^{1/2}}\right]. \tag{3.16}$$

However, the reason for introducing the function F in (3.17a,b) is that F is easier to be manipulated with and facilitates straightforward asymptotic calculations since $F(x) \sim 1$ as $x \to \infty$ (cf. Boisvert et al. 2010). Though, one must be aware that the forms (3.17a,b) introduce an artificial root $\lambda_h = [\frac{1}{2}Pr(\mathscr{U}-1)]^{1/2}$ in (3.19), corresponding to $\Lambda(\lambda_h) = 0$, which exists for $\mathscr{U} > 1$. In the next two chapters, however, we shall be interested only in cases when $\mathscr{U} < 1$.

$$I(\infty; Pr, \varepsilon) \sim \frac{\varepsilon}{2\Lambda(\lambda_h)} F\left[\frac{\Lambda(\lambda_h)}{(\varepsilon\mathscr{U})^{1/2}}\right]. \tag{3.17b}$$

with

$$F(\lambda) = \pi^{1/2}\lambda\, \mathrm{e}^{\lambda^2}\, \mathrm{erfc}(\lambda). \tag{3.18}$$

Using these, together with the liquidus relationship (3.4), we can write (3.11) as

$$\Gamma\left[\lambda_h \frac{F[\Lambda(\lambda_h)/\mathscr{U}^{1/2}]}{G(\lambda_h)} + \Lambda(\lambda_h)\right]\Theta_h - \Lambda(\lambda_h) - \mathscr{S}\lambda_h F\left[\frac{\Lambda(\lambda_h)}{\mathscr{U}^{1/2}}\right] = 0. \tag{3.19}$$

and the concentration and its gradient at the interface, respectively, are given as

$$\Theta_h \sim 1 + (1-\mathscr{C})\frac{\lambda_h F\left[\Lambda(\lambda_h)/(\varepsilon\mathscr{U})^{1/2}\right]}{\Lambda(\lambda_h) - \lambda_h F\left[\Lambda(\lambda_h)/(\varepsilon\mathscr{U})^{1/2}\right]}, \tag{3.20}$$

$$\Theta_h' \sim \varepsilon^{-1}(\mathscr{C}-1)\frac{2\lambda_h\Lambda(\lambda_h)}{\Lambda(\lambda_h) - \lambda_h F\left[\Lambda(\lambda_h)/(\varepsilon\mathscr{U})^{1/2}\right]}. \tag{3.21}$$

3.4 Asymptotic approximations

In typical experiments, the velocity ratio $\mathscr{U}$ can take both small and large values (cf. Löfgren 2001). In what follows, we shall focus our analysis on the case when $\mathscr{U}$ is small since it facilitates a relatively simple asymptotic approximations. Investigation of solutions for finite values of $\mathscr{U}$, namely $\mathscr{U} > 1$, is a difficult task since numerical calculations show multiplicity of solutions for λ_h and their nonexistence for sufficiently large values of $\mathscr{U}$. In the rest of this chapter, we will assume the regular limit of negligible latent heat release, i.e. we set $\mathscr{S} = 0$.

The numerical solution for λ_h as a function of Pr is depicted in figure 3.2(a) for various values of $\mathscr{U}$. The numerical results in figure 3.2(a) along with scaling analysis suggest that the limit $Pr \to 0$ for nonzero values of $\mathscr{U}$ is regular in (3.19), so that

$$\lambda_h \sim \lambda_0 + O(Pr), \quad \text{as} \quad Pr \to 0, \tag{3.22}$$

with $\lambda_0 = O(1)$ as $Pr \to 0$. The leading-order forms of the interfacial concentration and its gradient on the liquid side of the interface are

$$\Theta_h \sim 1 + (1-\mathscr{C})\frac{F[\lambda_0/(\varepsilon\mathscr{U}^{1/2})]}{1 - F[\lambda_0/(\varepsilon\mathscr{U}^{1/2})]}, \tag{3.23a}$$

$$\Theta_h' \sim \varepsilon^{-1}(\mathscr{C}-1)\frac{2\lambda_0}{1 - F[\lambda_0/(\varepsilon\mathscr{U}^{1/2})]}. \tag{3.23b}$$

To the leading order in Pr, the equation (3.19) becomes

$$\Gamma F\left(\frac{\lambda_0}{\mathscr{U}^{1/2}}\right)\left\{1 - \mathscr{C}F\left[\frac{\lambda_0}{(\varepsilon\mathscr{U})^{1/2}}\right]\right\} = G(\lambda_0)\left\{1 - \Gamma + (\Gamma\mathscr{C}-1)F\left[\frac{\lambda_0}{(\varepsilon\mathscr{U})^{1/2}}\right]\right\}.$$

Appearance of ratio $\lambda_0/\mathscr{U}^{1/2}$ in the above equation suggest a rescaling $\lambda_0 = \mathscr{U}^{1/2}\hat{\lambda}_0$ so that the equation becomes

$$\Gamma F(\hat{\lambda}_0)\left[1 - \mathscr{C}F(\hat{\lambda}_0/\varepsilon^{1/2})\right] = G(\mathscr{U}^{1/2}\hat{\lambda}_0)\left[1 - \Gamma + (\Gamma\mathscr{C}-1)F(\hat{\lambda}_0/\varepsilon^{1/2})\right].$$

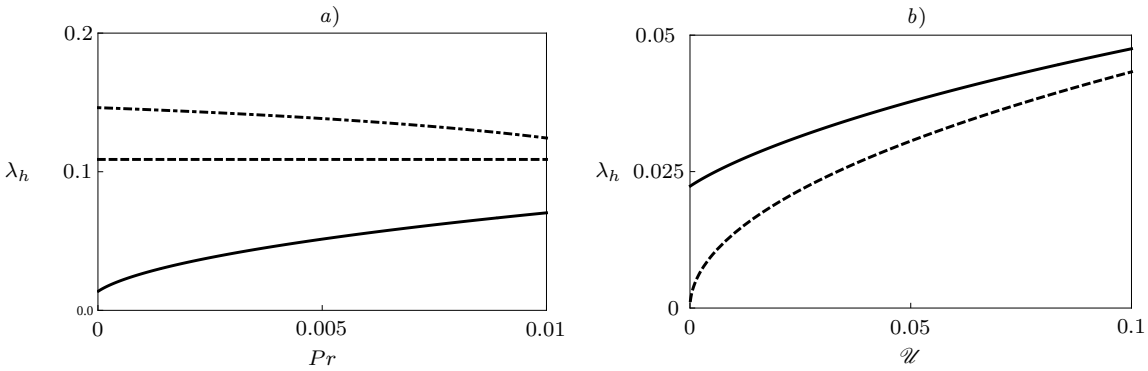

Figure 3.2: (a) The growth rate λ_h as a function of Prandtl number, calculated numerically from (3.19), shown for various values of velocity ratio: $\mathscr{U} = 10^{-2}$ (solid), $\mathscr{U} = 1$ (dashed) and $\mathscr{U} = 10$ (dot-dashed). Note that at non-zero $\mathscr{U}$, the value of λ_h attains finite values as $Pr \to 0$. Moreover, for $\mathscr{U} = 1$ the growth rate is independent of Pr owing to the fact that the Prandtl number affects the temperature and concentration fields only through the quantity $\Lambda(\lambda_h)$. (b) The values of the leading order solution λ_0 (dashed line), given by (3.26), compared with the numerical solution of (3.19) for $Pr = 10^{-3}$ (solid line), both as functions of $\mathscr{U}$. The values of the other physical parameters in all the computations are set to $\varepsilon = 10^{-1}$, $\mathscr{C} = 2$ and $\Gamma = 0.5$.

In the limit $\mathscr{U} \to 0$ with $\hat{\lambda}_0 = O(1)$, the dominant balance in the above equation is

$$F(\hat{\lambda}_0/\varepsilon^{1/2}) = \frac{1}{\mathscr{C}}, \tag{3.24}$$

with the high order terms being of $O(\mathscr{U})$. To derive (3.24), we used the following approximation

$$G(\lambda) = 2\lambda^2 + O(\lambda^4), \tag{3.25}$$

valid for small λ. Thus to leading order we have

$$\lambda_h \sim \varepsilon^{1/2} F_{\text{inv}}(\mathscr{C}^{-1}) \mathscr{U}^{1/2}, \quad \mathscr{U} \to 0, \tag{3.26}$$

with F_{inv} denoting the inverse of F. We can combine (3.26) with (3.23b) to obtain

$$\Theta_h' \sim 2\varepsilon^{-1/2} \mathscr{C} F_{\text{inv}}(\mathscr{C}^{-1}) \mathscr{U}^{1/2}, \quad \mathscr{U} \to 0. \tag{3.27}$$

The joint limit $Pr \to 0$, $\mathscr{U} \to 0$ requires more careful consideration. While the limit $Pr \to 0$ is regular for λ_h and the temperature and concentration fields, it is singular for the velocity field. Since the growth constant can be expressed as $\lambda_h = \lambda_0 + O(Pr)$, where $\lambda_0 = O(\mathscr{U}^{1/2})$ as $\mathscr{U} \to 0$, we have to ensure that this expansion, along with that of f in (2.57c), is asymptotic. To do this, we must require $\lambda_h \gg Pr/\lambda_h$, so that

$$Pr \ll \mathscr{U} \ll 1. \tag{3.28}$$

In case when $\mathscr{U} = 0$, obtained by letting $\mathscr{U} \to 0$ in (3.19), the root of (3.19) is $O(Pr^{1/2})$, thus violating the asymptotic constraint $\lambda_h \gg Pr/\lambda_h$. However, as we will show in the next chapter, when a mushy layer is present in the system, the solutions corresponding to $\mathscr{U} = 0$ are asymptotically consistent.

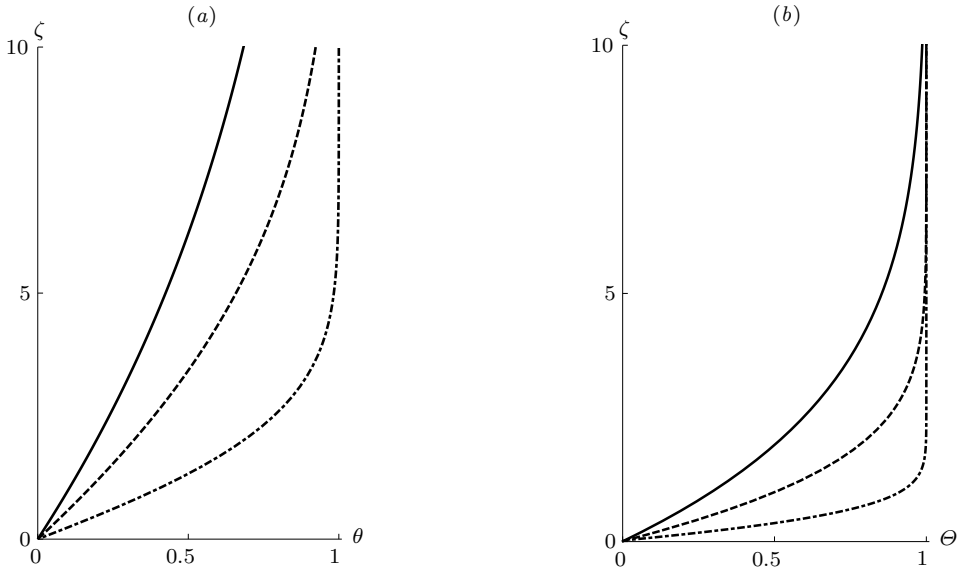

Figure 3.3: Temperature (a) and concentration (b) fields in liquid, evaluated from the asymptotic solutions (3.5) and (3.6), respectively, for different values of small velocity ratios. In both plots, we use the following values of $\mathscr{U}$: $\mathscr{U} = 10^{-3}$ (solid), $\mathscr{U} = 10^{-2}$ (dashed) and $\mathscr{U} = 10^{-1}$ (dot-dashed). The other quantities are set to $Pr = 10^{-4}$, $\varepsilon = 10^{-1}$, $\mathscr{C} = 2$ and $\Gamma = 0.5$. The values of λ_h are of order $O(10^{-2})$, therefore the solid phase is not visible in the plots.

To see how small $\mathscr{U}$ affects the temperature and concentration fields, we approximate the leading-order forms (i.e. we set $Pr = 0$) of (3.5) and (3.6) for $\mathscr{U} \to 0$ and $\zeta = O(1)$. For the temperature we obtain

$$\theta \sim \frac{2\varepsilon^{1/2} F_{\mathrm{inv}}(\mathscr{C}^{-1})}{F[\varepsilon^{1/2} F_{\mathrm{inv}}(\mathscr{C}^{-1})]}(\zeta - \lambda_h)\mathscr{U}^{1/2} \tag{3.29}$$

and for the concentration

$$\Theta \sim 2\varepsilon^{-1/2}\mathscr{C} F_{\mathrm{inv}}(\mathscr{C}^{-1})(\zeta - \lambda_h)\mathscr{U}^{1/2}. \tag{3.30}$$

In deriving (3.29) and (3.30) we used the fact that for $Pr = 0$ both θ_h and Θ_h are $O(\mathscr{U})$ when $\mathscr{U} \to 0$. The thickness of both thermal and concentration boundary layers is stretched by factor $\mathscr{U}^{-1/2}$. Thus the decrease in $\mathscr{U}$ has the effect of reducing the concentration gradient at the interface. The temperature and concentration fields are depicted in figures 3.3(a,b). Moreover, we see from (2.57c) that small $\mathscr{U}$ modifies the viscous boundary layer such that its effective thickness is $O(Pr/\mathscr{U}^{1/2}) \ll O(1/\mathscr{U}^{1/2})$. Therefore, the asymptotic condition (3.28) can be interpreted such that Pr and $\mathscr{U}$ must be small in such a way that the viscous boundary layer resides within the concentration one. As a result, the effect of the viscous boundary layer on the transport of heat and solute is negligible in the leading order (cf. Löfgren 2001) and it is through the velocity ratio that the flow affects the solidification. Therefore, the concentration and thermal fields together with the growth rate λ_h can well be approximated by their leading-order forms in Pr.

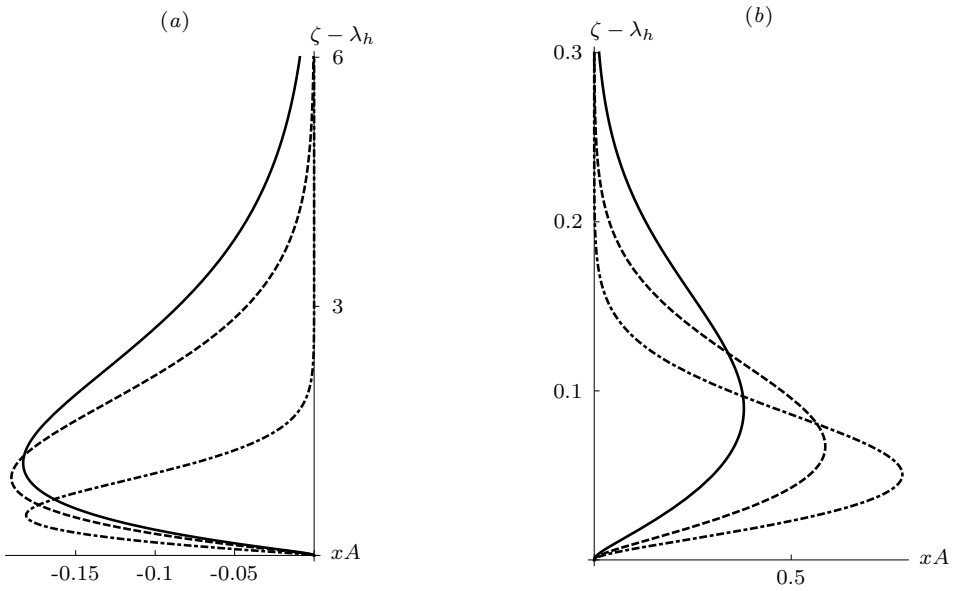

Figure 3.4: The advective flux of solute with respect to the moving solid phase, scaled with the x-coordinate, for (a) $\mathscr{U} < 1$ and (b) $\mathscr{U} > 1$. The curves shown in (a) correspond to $\mathscr{U} = 10^{-3}$ (solid), $\mathscr{U} = 10^{-2}$ (dashed) and $\mathscr{U} = 10^{-1}$ (dot-dashed); those in (b) correspond to $\mathscr{U} = 5$ (solid), $\mathscr{U} = 10$ (dashed) and $\mathscr{U} = 20$ (dot-dashed). The values of physical parameters are set to $Pr = 10^{-3}$, $\varepsilon = 10^{-1}$, $\mathscr{C} = 2$ and $\Gamma = 0.5$.

An important physical characteristic of the system is the dimensionless advective flux A of solute with respect to the moving substrate, defined by

$$A \equiv -(\boldsymbol{u} - \boldsymbol{u}_0) \cdot \boldsymbol{\nabla}\Theta = \tfrac{1}{2}x^{-1}(f - \zeta)\Theta'. \tag{3.31}$$

The minus sign in (3.31) reflects the minus sign in the definition of Θ. In figure 3.4 we plot the values of A, scaled with the x-coordinate, as a function of $\xi - \lambda_h$, for qualitatively different values of $\mathscr{U}$. Note that this scaled flux does not depend on x. Moreover, A is zero at the interface and attains a local extremum at a finite distance from the interface. When $\mathscr{U} < 1$, the streamlines of $\boldsymbol{u} - \boldsymbol{u}_0$ are oriented outwards from the interface, so the advective flux relative to the interface is negative. However, any fluid element eventually reaches the interface since in the frame moving with the solid, the interface position evolves proportionally to $t^{1/2}$. For $\mathscr{U} \to 0$, the scaled advective flux can be approximated as

$$xA \sim \varepsilon^{-1/2}\mathscr{C}F_{\mathrm{inv}}(\mathscr{C}^{-1})(f - \zeta)\exp\left(-\frac{2}{\varepsilon}\int_{\lambda_h}^{\zeta} f\,\mathrm{d}s\right)\mathscr{U}^{1/2}$$

provided $Pr \ll \mathscr{U}$. Note that xA scales with $\mathscr{U}^{1/2}$, not $\mathscr{U}$. When $\mathscr{U} > 1$, the fluid elements move faster than the moving substrate, so the streamlines of $\boldsymbol{u} - \boldsymbol{u}_0$ are directed towards the interface and the relative advective flux of solute is positive. Another feature that can be seen in figure 3.4 is that the thickness of the region where xA is effectively non-zero decreases with increasing $\mathscr{U}$. Also note that, while for $\mathscr{U} > 1$ the maximum values of xA are monotonically increasing with $\mathscr{U}$, it is not so for $\mathscr{U} < 1$. In case when $\mathscr{U} = 1$, there is zero advective flux of solute relative to

the moving substrate. Moreover, note that for $\mathscr{U} \uparrow 1$ the thickness of the region with effectively non-zero advective flux decreases, while it increases for $\mathscr{U} \downarrow 1$.

Chapter 4

Mushy layer with solute diffusion

4.1 Introduction

In this chapter, we return back to the situation where the solid and liquid phases are separated by the mushy layer. The self-similar solutions in the solid phase and mushy layer turn out to be, up to the dimensionless scaling, formally the same as that derived by Gewecke & Schulze (2011*b*) for a mushy layer in a semi-infinite domain, with their time variable in the definition of ζ replaced by our spatial variable x. The difference is in the conditions at the mush/liquid interface, through which the temperature and concentration fields in the liquid phase influence the mushy layer.

We shall also address questions concerning the properties of the liquid fraction at the solid/mush interface, which apply also to the models with planar interfaces and have not been addressed by the other authors so far. Throughout the chapter, as well as in the next one, we will assume that $0 \leq \mathscr{U} \leq 1$.

4.2 Self-similar solutions with nonzero Stefan number

4.2.1 Governing equations in the mushy layer

Since the temperature and concentration fields in the mushy layer are tied together via the liquidus relationship (2.35*c*), the equation (2.35*b*) is in fact a governing equation for the liquid fraction and can be cast, after the self-similar transformation, to the following form

$$\frac{\chi'}{\chi} = \frac{2\zeta\Theta' + \varepsilon\Theta''}{2\zeta(\mathscr{C} - \Theta) - \varepsilon\Theta'}, \tag{4.1}$$

which can be readily integrated to yield

$$\chi = \chi_{b^-} \exp\left(-\int_{\zeta}^{\lambda_b} \frac{2s\Theta' + \varepsilon\Theta''}{2s(\mathscr{C} - \Theta) - \varepsilon\Theta'}\,\mathrm{d}s\right). \tag{4.2}$$

The governing equation for the temperature field in the mushy layer becomes

$$\theta'' + 2\zeta\theta' = -2\mathscr{S}\zeta\chi', \tag{4.3}$$

which, due to the liquidus relationship, also determines the governing equation for the concentration field

$$\Theta'' + 2\zeta\Theta' = -2\frac{\mathscr{S}}{\Gamma}\zeta\chi'. \tag{4.4}$$

4.2.2 Conditions at the interfaces

Solid/mush interface

The condition (2.40a), expressing the conservation of heat at the solid/mush interface, transforms via (2.32) into the following form

$$2\mathscr{S}\chi_{a^+}\lambda_a = \theta'_{a^-} - \theta'_{a^+}. \tag{4.5}$$

The temperature gradient on the solid side of the interface can be expressed, using (2.74), as

$$\theta'_{a^-} = \frac{2\lambda_a\theta_a}{G(\lambda_a)}. \tag{4.6}$$

Inserting the above expression into (4.5) leads to the following equation

$$(2\mathscr{S}\lambda_a\chi_{a^+} + \Gamma\Theta'_{a^+})G(\lambda_a) = 2\Gamma\lambda_a\Theta_a, \tag{4.7}$$

where we have used the liquid relationship (2.35c), applied on θ_a and θ'_a. The conservation of solute, expressed by (2.40b), transforms into the equation

$$\left[2\lambda_a(\mathscr{C} - \Theta_a) - \varepsilon\Theta'_{a^+}\right]\chi_{a^+} = 0. \tag{4.8}$$

Mush/liquid interface

The conservation of heat, given by (2.39a), transforms to

$$2\mathscr{S}(1-\chi_{b^-})\lambda_b = \theta'_{b^-} - \theta'_{b^+}. \tag{4.9}$$

At this point we take into account the condition of marginal equilibrium, given by (1.19). In the present scaling, this condition can be expressed as

$$\theta'_{b^+} = \Gamma\Theta'_{b^+}. \tag{4.10}$$

Using (4.10), we can rewrite (4.9) as

$$2\mathscr{S}(1-\chi_{b^-})\lambda_b = \Gamma\left(\Theta'_{b^-} - \Theta'_{b^+}\right). \tag{4.11}$$

The conservation of solute (2.39b) takes the form

$$2(\mathscr{C} - \Theta_b)(1-\chi_{b^-})\lambda_b = \varepsilon\left(\Theta'_{b^+} - \chi_{b^-}\Theta'_{b^-}\right). \tag{4.12}$$

4.2.3 Integral equation for the liquid fraction in the mushy layer

At this point, it is instructive to re-write the equation (4.1) as

$$\varepsilon(\chi\Theta')' = 2\zeta\left[(\mathscr{C}-\Theta)\chi\right]', \tag{4.13}$$

which after integration yields the following integral equation

$$\left[2\zeta(\mathscr{C}-\Theta)-\varepsilon\Theta'\right]\chi = 2\int_{\lambda_a}^{\zeta}(\mathscr{C}-\Theta)\chi\,\mathrm{d}s, \tag{4.14}$$

which will prove useful in further analysis of the interfacial conditions. To derive (4.14), we used per-partes integration together with (4.8)[1]. Note that the integral in (4.14) is always positive for $\zeta > \lambda_a$ and so is the left-hand side of this equation[2]. Expressing (4.14) at the mush/interface yields

$$\left[2\lambda_b(\mathscr{C}-\Theta_b)-\varepsilon\Theta'_{b^-}\right]\chi_{b^-} = 2\int_{\lambda_a}^{\lambda_b}(\mathscr{C}-\Theta)\chi\,\mathrm{d}s. \tag{4.15}$$

The integral at the right hand-side of the above equation represents, apart from the numerical factor, the total amount of solute contained within the mushy layer.

Using (4.15), we can prove that the liquid fraction at the mush/liquid interface is equal to unity for any value of Stefan number and that the concentration gradient is continuous across the interface, i.e.

$$\chi_{b^-} = 1 \quad \text{and} \quad \Theta'_{b^-} = \Theta'_{b^+} \equiv \Theta'_b, \quad \text{for } \mathscr{S} \geq 0. \tag{4.16a, b}$$

To see that, we can express from (4.12) the liquid fraction at the mush/liquid interface as

$$\chi_{b^-} = 1 + \frac{\varepsilon(\Theta'_{b^-}-\Theta'_{b^+})}{2\lambda_b(\mathscr{C}-\Theta_b)-\varepsilon\Theta'_{b^-}}. \tag{4.17}$$

The last term in the above equation is non-negative, since (4.11) implies that the numerator in non-negative and (4.15) implies that the denominator is always positive. On the other hand, $\chi_{b^-} \in \langle 0,1\rangle$, so the nominator must be zero. The liquid fraction in mush is therefore

$$\chi = \exp\left(-\int_{\zeta}^{\lambda_b}\frac{2s\Theta'+\varepsilon\Theta''}{2s(\mathscr{C}-\Theta)-\varepsilon\Theta'}\,\mathrm{d}s\right). \tag{4.18}$$

The condition (4.8) states that at least one of the quantities $2\lambda_a(\mathscr{C}-\Theta_a)-\varepsilon\Theta'_{a^+}$ or χ_{a^+} is zero. However, in Appendix A.1 we prove, with the use of (4.14), that the former is always zero for general values of Stefan number, i.e.

$$2\lambda_a(\mathscr{C}-\Theta_a)-\varepsilon\Theta'_{a^+} = 0. \tag{4.19}$$

[1]Note that (4.14) is consistent with (4.8).

[2]Recall that $\mathscr{C}-\Theta > 0$ for all $\zeta > \lambda_a$.

This result extends that of Gewecke & Schulze (2011*a*) to the case when Stefan number is non-zero. In Appendix A.1 we also show that $2\zeta\Theta'_{a^+} + \Theta''_{a^+} \leq 0$ and that $2\zeta\Theta'_{a^+} + \varepsilon\Theta''_{a^+} \geq 0$, from which we derive that Θ''_{a^+} is negative and bounded for $\mathscr{S} \geq 0$ and that χ'_{a^+} is bounded for $\mathscr{S} > 0$. Though the sign and the boundedness of Θ''_{a^+} can be as well deduced from the physical character of the solution, however, the boundedness of the gradient of the liquid fraction as $\zeta \to \lambda_a^+$ for positive values of Stefan number is not an obvious fact and is our original result.

The determine whether $\chi_{a^+} = 0$ for general values of Stefan number is a more delicate task. In the next section, we shall discuss the values of χ_{a^+} in case when Stefan number is negligible.

4.3 Self-similar solutions with zero Stefan number

The coupling in the equations (4.1) and (4.4) vanishes when $\mathscr{S} = 0$. However, since the orders of all the governing equations are retained, the asymptotic limit $\mathscr{S} \to 0$ is regular. The rationale behind this limit lies mostly in the fact that the uncoupled system, unlike the coupled one, can be solved explicitly. The numerical solution of the coupled system would require application of a complicated shooting scheme (see Worster 1986 for the numerical solution of a general system of mushy-layer equations with different thermal properties of each phases and a non-zero Stefan number).

4.3.1 Solutions with $\varepsilon = O(1)$

Temperature and concentration fields in the mushy layer

The equation (4.3) becomes

$$\theta'' + 2\zeta\theta' = 0, \tag{4.20}$$

with the solution

$$\theta = \theta_a \frac{\operatorname{erf}(\zeta)}{\operatorname{erf}(\lambda_a)}, \tag{4.21}$$

where we have used the condition (4.5), which reduces simply to the continuity of the temperature gradient across the solid/mush interface. Thus the temperature field in both solid and mush is given by

$$\theta = \theta_a \frac{\operatorname{erf}(\zeta)}{\operatorname{erf}(\lambda_a)}, \quad 0 \leq \zeta \leq \lambda_b \tag{4.22}$$

and the concentration field

$$\Theta = \Theta_a \frac{\operatorname{erf}(\zeta)}{\operatorname{erf}(\lambda_a)}, \quad \lambda_a \leq \zeta \leq \lambda_b. \tag{4.23}$$

The equations (4.7) and (4.19) can be solved for Θ_a and Θ'_{a^+} to obtain

$$\Theta_a = \frac{\mathscr{C}G(\lambda_a)}{G(\lambda_a) + \varepsilon} \qquad \text{and} \quad \Theta'_{a^+} = \frac{2\lambda_a\mathscr{C}}{G(\lambda_a) + \varepsilon}. \tag{4.24a,b}$$

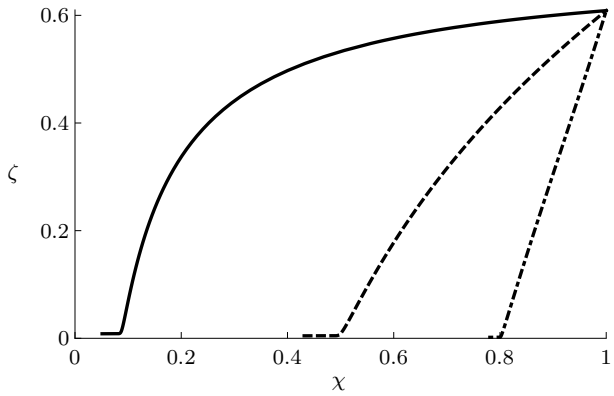

Figure 4.1: The liquid fraction in the mushy layer as a function of ζ, calculated from (4.18) for zero Stefan number and different values of $\mathscr{C}$: $\mathscr{C} = 1.1$ (solid line), $\mathscr{C} = 2$ (dashed line) and $\mathscr{C} = 5$ (dot-dashed line). The values of the other parameters are set to $Pr = 10^{-2}$, $\varepsilon = 10^{-2}$, $\mathscr{U} = 10^{-2}$ and $\Gamma = 0.5$. In all calculations $\chi_{a^+} = 0$, however, the singularity at $\zeta = \lambda_a^+$ disrupts the calculation of the integral in (4.18) near the solid/mush interface.

Liquid fraction at the solid/mush interface

One way to find χ_{a^+} is to calculate the integral in (4.18) numerically. However, due to the condition (4.19) the integral has a singularity at $\zeta = \lambda_a^+$, which complicates the numerical integration in the vicinity of this point. Another way is to derive the information about χ_{a^+} analytically. Gewecke & Schulze (2011*a*) analysed the liquid fraction at the solid/mush interface in a model with planar interfaces, zero latent-heat release and uniform thermal properties. Under such conditions, the temperature field decoupled completely from the rest of the system, being given by the same function in all phases. That allowed the authors to show that the governing equation for the liquid fraction had a singularity with a simple pole located at the solid/mush interface. Therefore they were able to derive a series solution for χ, using which they found that $\chi_{a^+} = 0$. In Appendix A.2 we again use the integral equation (4.14) to show that $\chi_{a^+} = 0$ when Stefan number is zero. Unlike Gewecke & Schulze (2011*a*), our derivation uses only the governing equations without the need to know their explicit solutions. In addition to this, in Appendix A.3 we also make some remarks concerning the values of χ_{a^+} for positive values of Stefan number, though the determination of χ_{a^+} in such case is still an open task.

In figure 4.1 we plot the liquid fraction in the mushy layer as a function of ζ for different values of $\mathscr{C}$ with $\mathscr{S} = 0$. Though the liquid fraction at the mush side of the solid/mush interface is zero, the singularity at $\zeta = \lambda_a^+$ in the integral in (4.18) complicates the numerical reproduction of this result. The most significant feature is the steep gradient of χ near the solid/mush interface (cf. Worster 1986 and Gewecke & Schulze 2011*a*). Note the behaviour of χ with the increasing $\mathscr{C}$: the larger values of $\mathscr{C}$ result in larger values of liquid fraction in the mushy layer. Recall that increasing $\mathscr{C}$ corresponds to decreasing the overall concentration variation ΔC in the system. Thus the smaller ΔC results in melting of dendrites of the mushy layer.

Algebraic equation for λ_a

The relations (4.24*a, b*) express the concentration and its gradient on the mush side of the solid/mush interface as functions of the growth constant λ_a, which is still left undetermined. To derive an algebraic equation from which λ_a can be calculated, we express (4.23) at the mush/liquid interface to obtain

$$\frac{\Theta_a}{\mathrm{erf}(\lambda_a)} = \frac{\Theta_b}{\mathrm{erf}(\lambda_b)}, \tag{4.25}$$

which can be combined with (4.24*a*) to get

$$\left[\Theta_b - \mathscr{C}\frac{\mathrm{erf}(\lambda_b)}{\mathrm{erf}(\lambda_a)}\right] G(\lambda_a) + \varepsilon\Theta_b = 0. \tag{4.26}$$

Algebraic equation for λ_b

The condition of marginal equilibrium, given by (4.10), together with the continuity of the concentration gradient across the mush/liquid interface, imply

$$\theta'_{b^-} = \theta'_{b^+}. \tag{4.27}$$

The temperature gradients on the mush and liquid sides of the mush/liquid interface, respectively, can be expressed, using (4.22), as

$$\theta'_{b^-} = \frac{2\lambda_b\theta_b}{G(\lambda_b)}, \qquad \theta'_{b^+} = \frac{1-\theta_b}{J(\infty;Pr)}. \tag{4.28a,b}$$

To derive (4.28*b*), we used (2.62). The continuity of temperature gradients then yields

$$\theta_b = \frac{G(\lambda_b)}{2\lambda_b J(\infty;Pr) + G(\lambda_b)}. \tag{4.29}$$

The concentration gradients on the both sides of the mush/liquid interface can be expressed as

$$\Theta'_{b^-} = \frac{2\lambda_b\Theta_b}{G(\lambda_b)}, \qquad \Theta'_{b^+} = \frac{1-\Theta_b}{I(\infty;Pr,\varepsilon)}. \tag{4.30a,b}$$

Using these, the continuity of concentration gradients across the mush/liquid interface yields

$$\Theta_b = \frac{G(\lambda_b)}{2\lambda_b I(\infty;Pr,\varepsilon) + G(\lambda_b)}. \tag{4.31}$$

By combining (4.29) and (4.31) via the liquidus relationship (2.35*c*) we finally obtain the algebraic equation for the growth constant λ_b as follows

$$2\lambda_b\left[I(\infty;Pr,\varepsilon) - \Gamma J(\infty;Pr)\right] + (1-\Gamma)G(\lambda_b) = 0. \tag{4.32}$$

The integrals $J(\infty;Pr)$ and $I(\infty;Pr,\varepsilon)$ can be approximated for $Pr \to 0$ in the following way (cf. (3.17*a, b*))

$$J(\infty;Pr) \sim \frac{F\left[\Lambda(\lambda_b)/\mathscr{U}^{1/2}\right]}{2\Lambda(\lambda_b)}, \tag{4.33a}$$

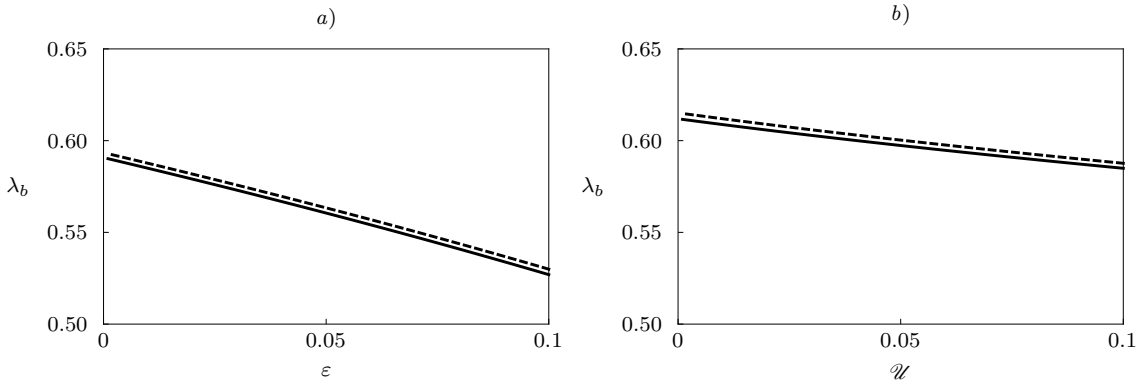

Figure 4.2: *a*) The growth constant λ_b as a function of the inverse Lewis number ε, calculated from (4.34) for $Pr = 10^{-2}$ (solid line) and $Pr = 0$ (dashed line). The values of the other parameters are set to $\mathscr{U} = 10^{-1}$, $\Gamma = 0.5$ and $\mathscr{C} = 2$. *b*) The growth constant λ_b as a function of $\mathscr{U}$, calculated from (4.34) for $Pr = 10^{-2}$ (solid line) and $Pr = 0$ (dashed line). The values of the other parameters are set to $\varepsilon = 10^{-2}$, $\Gamma = 0.5$ and $\mathscr{C} = 2$.

$$I(\infty; Pr, \varepsilon) \sim \frac{\varepsilon F\left[\Lambda(\lambda_b)/(\varepsilon\mathscr{U})^{1/2}\right]}{2\Lambda(\lambda_b)}. \tag{4.33b}$$

Using these, (4.32) becomes

$$\varepsilon\lambda_b F\left[\frac{\Lambda(\lambda_b)}{(\varepsilon\mathscr{U})^{1/2}}\right] - \Gamma\lambda_b F\left[\frac{\Lambda(\lambda_b)}{\mathscr{U}^{1/2}}\right] + (1-\Gamma)\Lambda(\lambda_b)G(\lambda_b) = 0 \tag{4.34}$$

and the temperature and concentration at the interface are

$$\theta_b = 1 - \frac{\lambda_b F\left[\Lambda(\lambda_b)/\mathscr{U}^{1/2}\right]}{\lambda_b F\left[\Lambda(\lambda_b)/\mathscr{U}^{1/2}\right] + \Lambda(\lambda_b)G(\lambda_b)}, \tag{4.35a}$$

$$\Theta_b = 1 - \frac{\varepsilon\lambda_b F\left[\Lambda(\lambda_b)/(\varepsilon\mathscr{U})^{1/2}\right]}{\varepsilon\lambda_b F\left[\Lambda(\lambda_b)/(\varepsilon\mathscr{U})^{1/2}\right] + \Lambda(\lambda_b)G(\lambda_b)}. \tag{4.35b}$$

Note that the growth constant λ_b appears explicitly in (4.26) but not vice versa, i.e. we can compute λ_b from (4.34) without any knowledge of λ_b.

Before we move further, we point out that the equation (4.34) admits, besides the physical one, two solutions that we shall not take into account: the first one is $\lambda_b = 0$, which is not physical since we require $\lambda_a < \lambda_b$, and the second one is $\lambda_b = [\frac{1}{2}Pr(\mathscr{U}-1)]^{1/2}$, which is also not a relevant solution (see the footnote before (3.17*a, b*)). However, this root exists only for $\mathscr{U} \geq 1$, which is a parametric regime that we shall not address.

In figure 4.2(a, b) we plot the growth constant λ_b, calculated numerically from (4.34), as a function of ε and $\mathscr{U}$, for both small and zero values of Prandtl number. We see that the solutions corresponding to small Pr are very close to that with $Pr = 0$. Therefore we can approximate the values of λ_b for small Pr by those with $Pr = 0$. Moreover, the plots suggest that the limits $\varepsilon \to 0$ and $\mathscr{U} \to 0$ are both regular for λ_b and thus interchangeable, a fact that will allow us to find an approximate solution of (4.34) in a relatively simple form – see the following subsection.

4.3.2 Solutions in the limit $\varepsilon \to 0$

Since the diffusion of heat is typically more rapid than that of solute, the inverse Lewis number, ε, is small. However, the growth of the mushy layer is governed primarily by the thermal balances at the interfaces. Therefore the advance of the mush/liquid interface is not restricted by the diffusion of solute away from the interface. As a result, the mushy layer exists even when the diffusion of solute is negligible, with no solid phase present in the system — such situation corresponds to setting $\varepsilon = 0$ (cf. Gewecke & Schulze 2011*a* for the case of a mushy layer on a finite domain). We shall discuss the case $\varepsilon = 0$ in the next chapter. However, the limit $\varepsilon \to 0$ is singular in the liquid phase, the concentration field having the boundary layer of thickness $O(\varepsilon^{1/2})$. At this moment, we restrict our attention to showing that the limit $\varepsilon \to 0$ is regular for the growth constants λ_a and λ_b.

We shall prove that $\lambda_a \to 0$ as $\varepsilon \to 0$, provided λ_b is finite. First, we conclude from (4.35*b*) that $\Theta_b \to 1$ as $\varepsilon \to 0$. Next, assume that λ_a is finite, and so is $G(\lambda_a)$, as $\varepsilon \to 0$. Then, (4.26) implies

$$\frac{\mathrm{erf}(\lambda_b)}{\mathrm{erf}(\lambda_a)} \to \frac{1}{\mathscr{C}} < 1 \quad \text{as} \quad \varepsilon \to 0,$$

which, since $\mathrm{erf}(\lambda)$ is an increasing function, is a contradiction with the requirement that $\lambda_a < \lambda_b$. Thus we have shown that $\lambda_a \to 0$ as $\varepsilon \to 0$. For small values of λ_a, the following approximations are valid

$$\mathrm{erf}(\lambda_a) = \tfrac{2}{\pi^{1/2}}\lambda_a + O(\lambda_a^3), \qquad G(\lambda_a) = 2\lambda_a^2 + O(\lambda_a^4). \tag{4.36a,b}$$

Inserting these into (4.26), with $\Theta_b \approx 1$, we obtain a quadratic equation with one root satisfying $\lambda_a \to 0$ as $\varepsilon \to 0$, which has the following aproximate form

$$\lambda_a = \frac{\varepsilon}{\pi^{1/2}\mathscr{C}\,\mathrm{erf}(\lambda_b)} + O(\varepsilon^2) \quad \text{as} \quad \varepsilon \to 0. \tag{4.37}$$

Inserting (4.37) into (4.24*a*, *b*), we can express the concentration and its gradient at the bottom of the mushy layer as

$$\Theta_{a^+} \approx \frac{2\mathscr{C}\varepsilon}{2\varepsilon + \pi\mathscr{C}^2\,\mathrm{erf}^2(\lambda_b)} \qquad \text{and} \quad \Theta'_{a^+} \approx \frac{2\pi^{1/2}\mathscr{C}^2\,\mathrm{erf}(\lambda_b)}{2\varepsilon + \pi\mathscr{C}^2\,\mathrm{erf}^2(\lambda_b)} \tag{4.38a,b}$$

as $\varepsilon \to 0$.

We see from (4.37) that increasing $\mathscr{C}$, which is equivalent to a decreasing variation of concentration, ΔC, in the system, results in a decreasing thickness of the solid phase. Since λ_b is a decreasing function of $\mathscr{U}$, we infer from (4.37) that λ_a is an increasing function of $\mathscr{U}$, as was the growth constant λ_h, discussed in the previous chapter, in case when $\mathscr{U} < 1$. However, unlike the problem with a solid/liquid interface, here we have that $\lambda_a = O(1)$ as $Pr \to 0$, $\mathscr{U} \to 0$. Therefore we do not need any additional restriction such as (3.28) to retain the asymptotic character of the expansion of function f, given by (2.57*c*), as $Pr \to 0$, $\mathscr{U} \to 0$.

To see that λ_b is finite as $\varepsilon \to 0$, we realize that the term $F[\Lambda(\lambda_b)/(\varepsilon\mathscr{U})^{1/2}]$ in (4.34) is bounded whatever the value of λ_b as $\varepsilon \to 0$. To see this, we used the

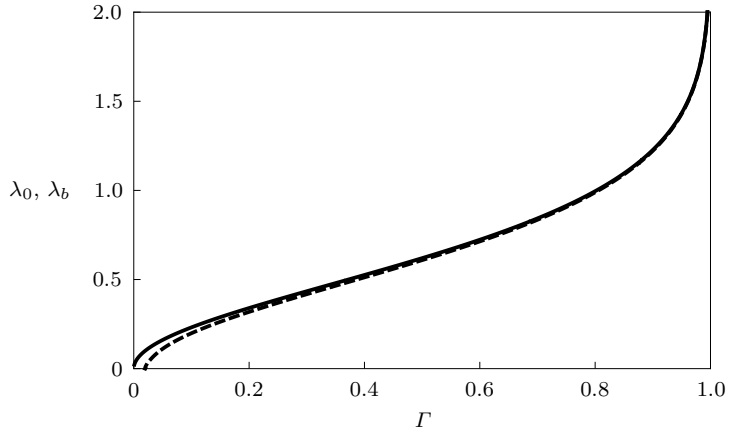

Figure 4.3: The leading-order solution of (4.40a), calculated from (4.42) as a function of Γ (solid line), compared with the solution of (4.34) with $Pr = 10^{-2}$, $\varepsilon = 10^{-2}$ and $\mathscr{U} = 10^{-2}$ (dashed line). Note that λ_0, $\lambda_b \to \infty$ as $\Gamma \to 1^-$. Also note that positive solutions of (4.34) exist for $\Gamma > \Gamma_{\min}$, with $\Gamma_{\min}$ given by (4.44).

asymptotic approximation $F(s) \sim 1$ as $s \to \infty$. Thus the limit $\varepsilon \to 0$ is regular in (4.34), the corresponding leading-order solution being the root of

$$-\Gamma\lambda_b F\left[\frac{\Lambda(\lambda_b)}{\mathscr{U}^{1/2}}\right] + (1-\Gamma)\Lambda(\lambda_b)G(\lambda_b) = 0. \tag{4.39}$$

Note that the trivial solution $\lambda_b = 0$ corresponds to the trivial solution of (4.34) and is not physical. Thus the only consistent solution of the above equation is the finite one.

Though the equation (4.34) cannot be solved explicitly for λ_b, we can find λ_b in a simple approximate form when ε and $\mathscr{U}$ are small. Since the limit $Pr \to 0$ is regular for λ_b and figures 4.2(a, b) show that the dependence of λ_b on Pr is weak, we set $Pr = 0$ in (4.34) and (4.39), respectively, to obtain

$$\varepsilon F\left[\frac{\lambda_b}{(\varepsilon\mathscr{U})^{1/2}}\right] - \Gamma F\left(\frac{\lambda_b}{\mathscr{U}^{1/2}}\right) + (1-\Gamma)G(\lambda_b) = 0, \tag{4.40a}$$

$$-\Gamma F\left(\frac{\lambda_b}{\mathscr{U}^{1/2}}\right) + (1-\Gamma)G(\lambda_b) = 0. \tag{4.40b}$$

As we stated at the end of the previous subsection, the figures 4.2(a, b) suggest that the limits $\varepsilon \to 0$ and $\mathscr{U} \to 0$ are interchangeable. Therefore we can approximate the solution of (4.40a) as

$$\lambda_b \approx \lambda_0 - \frac{\lambda_0\varepsilon}{\Gamma + 2\lambda_0^2} - \frac{\Gamma\mathscr{U}}{2\lambda_0(\Gamma + 2\lambda_0^2)} \quad \text{as} \quad \varepsilon \to 0,\ \mathscr{U} \to 0, \tag{4.41}$$

with λ_0 being the root of

$$G(\lambda_0) = \frac{\Gamma}{1-\Gamma}. \tag{4.42}$$

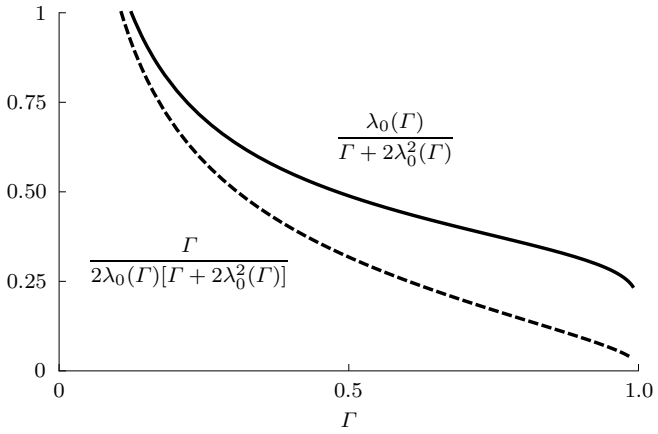

Figure 4.4: The magnitudes of the first-order effects of small ε (solid line) and small $\mathscr{U}$ (dashed line) in the approximation (4.41) of the growth constant λ_b for $Pr = 0$. Note that both effects are unbounded as $\Gamma \to 0$.

Note that $\Gamma/(1-\Gamma) \to 0$ as $\Gamma \to 0$ and that $\Gamma/(1-\Gamma) \to \infty$ as $\Gamma \to 1^-$. Since $G(\lambda_0) \geq 0$ for all $\lambda_0 \geq 0$, there exists a unique solution of (4.42) for every $\Gamma \in (0,1)$. To derive (4.41), we used the following asymptotic approximation (cf. Boisvert et al. 2010)

$$F(x) \sim 1 - \tfrac{1}{2}x^{-2} + O(x^{-4}), \quad \text{as} \quad x \to \infty \tag{4.43}$$

and the fact that $\lambda_b = O(1)$ as $\varepsilon \to 0$, $\mathscr{U} \to 0$. The solution to (4.42) is shown in figure 4.3, together with the solution of (4.34) for small values of Pr, ε and $\mathscr{U}$. Note that $\lambda_0 \to \infty$ as $\Gamma \to 1^-$. To interpret this result, recall the definition of Γ, given by (2.22d). The limit $\Gamma \to 1^-$ corresponds to the dimensional situation when $T_\infty = T_b$ so that there are zero temperature and concentration gradients in the liquid phase, the temperature being equal to $T_L(C_\infty)$. In the dimensionless formulation, this is equivalent to $\theta_b \to 1$ and $\Theta_b \to 1$, which is consistent with (4.35a, b), since the denominators grow faster that the numerators as $\lambda_b \to \infty$.

Note that positive solutions of (4.34) exists only for $\Gamma > \Gamma_{\min}$, where the lower bound

$$\Gamma_{\min} \equiv \frac{\varepsilon + Pr(1-\mathscr{U})}{1 + Pr(1-\mathscr{U})} \tag{4.44}$$

can be derived by letting $\lambda_b \to 0$ in (4.34), provided $Pr > 0$ and $\mathscr{U} \neq 1$[3]. The magnitudes of the first-order effects of ε and $\mathscr{U}$ in (4.41) are monotonically decreasing functions of Γ, as can be seen from figure 4.4. Note that for small Γ, both effects are unbounded. However, to retain the asymptotic character of (4.41), one must keep Γ fixed while performing the limit $\varepsilon \to 0$.

As can be seen from figure (4.3), the equation (4.42) captures the essential structure of (4.34), with Pr, ε and $\mathscr{U}$ providing the small corrections. This result confirms that the growth of the mush/liquid interface is primarily determined by the thermal field (cf. Worster 2000 for a mushy layer with planar interfaces). Recall that $\Theta_b \to 1$ as $\varepsilon \to 0$, whence $\theta_b \to \Gamma$ as $\varepsilon \to 0$. Therefore for small values of ε, the dimensionless liquidus slope Γ approximates the temperature at the mushy/liquid interface. Finally,

[3]When $\mathscr{U} = 1$, taking the limit $\lambda_b \to 0$ in (4.34) yields $\Gamma_{\min} = \varepsilon^{1/2}$.

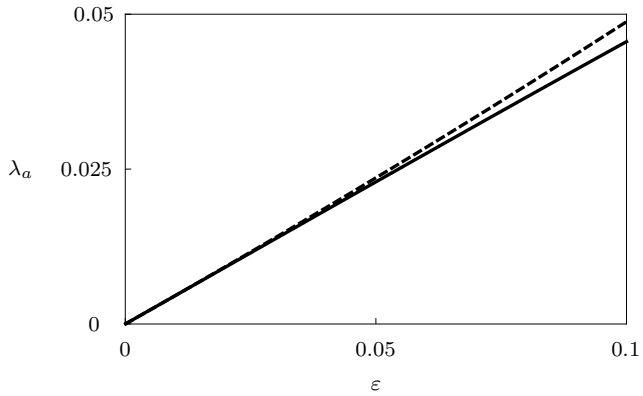

Figure 4.5: Growth constant λ_a as a function of ε, calculated numerically from (4.26) (solid line), with λ_b calculated numerically from (4.34), compared with the approximate form (4.37), with λ_b given by (4.41) (dashed line). The values of the other parameters are set to $Pr = 10^{-2}$, $\mathscr{U} = 10^{-2}$, $\mathscr{C} = 2$ and $\Gamma = 0.5$.

in figure 4.5 we plot the growth constant λ_a as a function of ε. Both the solution of (4.26) and the approximate solution (4.37), with λ_b given by (4.41), are shown.

4.3.3 Solutions with $\mathscr{U} = 0$

All the solutions discussed so far corresponded to positive values of $\mathscr{U}$. However, it is instructive to investigate separately the case when $\mathscr{U} = 0$. In dimensional world, such situation corresponds to $U_\infty = 0$, i.e. setting the far-field horizontal velocity to zero. The motivation behind such choice is twofold: it provides simpler explicit forms for temperature and concentration fields in the liquid phase than that with $\mathscr{U} > 0$, and it enables determination of a closed-form dependence of the dimensional positions of the solid/mush and mush/liquid interfaces on the substrate speed U_0. For example, the dimensional form of the mush/liquid interface is

$$b(x) = 2\lambda_b \left(\frac{\kappa}{U_0} x\right)^{1/2}, \tag{4.45}$$

with λ_b being independent of U_0 since the dimensionless problem is independent of $\mathscr{U}$. Therefore

$$b(x) \sim \frac{1}{U_0^{1/2}} \tag{4.46}$$

for $U_\infty = 0$ and fixed x. The same is true for the dimensional position of the solid/mush interface, given by function $z = a(x)$.

The asymptotic procedure for solving the third-order differential equation (2.45) is valid also for $\mathscr{U} = 0$ provided $\lambda_b \gg Pr$ as $Pr \to 0$. The function f has the asymptotic expansion

$$f(\zeta; Pr) \sim \lambda_b + \frac{Pr}{2\lambda_b}\left[1 - \exp\left(-2\lambda_b \frac{\zeta - \lambda_b}{Pr}\right)\right] \quad \text{as} \quad Pr \to 0. \tag{4.47}$$

The integrals $J(\zeta; Pr)$ and $I(\zeta; Pr, \varepsilon)$ can be calculated explicitly as

$$J(\zeta; Pr) \sim \frac{\lambda_b}{2\lambda_b^2 + Pr}\left\{1 - \exp\left[-\frac{2\lambda_b^2 + Pr}{\lambda_b}(\zeta - \lambda_b)\right]\right\}, \tag{4.48a}$$

$$I(\zeta; Pr, \varepsilon) \sim \frac{\varepsilon\lambda_b}{2\lambda_b^2 + Pr}\left\{1 - \exp\left[-\frac{2\lambda_b^2 + Pr}{\varepsilon\lambda_b}(\zeta - \lambda_b)\right]\right\} \tag{4.48b}$$

for $Pr \to 0$. The corresponding limits for $\zeta \to \infty$ are

$$J(\infty; Pr) \sim \frac{\lambda_b}{2\lambda_b^2 + Pr}, \qquad I(\infty; Pr, \varepsilon) \sim \frac{\varepsilon\lambda_b}{2\lambda_b^2 + Pr}. \tag{4.49a,b}$$

Inserting these into (4.28b) and (4.30b), we obtain the corresponding gradients on the liquid side of the mush/liquid interface

$$\theta'_{b^+} = (1 - \theta_b)\frac{2\lambda_b^2 + Pr}{\lambda_b}, \qquad \Theta'_{b^+} = (1 - \Theta_b)\frac{2\lambda_b^2 + Pr}{\varepsilon\lambda_b}. \tag{4.50a,b}$$

The corresponding gradients on the mush side of the mush/liquid interface are given by (4.28a,b), since the forms of the temperature and concentration fields in the mush are unaffected by the choice $\mathscr{U} = 0$. Combining (4.50a,b) with the marginal equilibrium (4.10) we get the interfacial temperature and concentration at the interface in the following forms

$$\theta_b = 1 - \frac{1 - \Gamma}{1 - \varepsilon}, \qquad \Theta_b = 1 - \frac{\varepsilon(1 - \Gamma)}{\Gamma(1 - \varepsilon)}. \tag{4.51a,b}$$

Finally, using (2.62) and (2.69) we can express the temperature and concentration fields in the liquid phase as

$$\theta \sim 1 - \frac{1 - \Gamma}{1 - \varepsilon}\exp\left[-\frac{2\lambda_b^2 + Pr}{\lambda_b}(\zeta - \lambda_b)\right], \tag{4.52a}$$

$$\Theta \sim 1 - \frac{\varepsilon(1 - \Gamma)}{\Gamma(1 - \varepsilon)}\exp\left[-\frac{2\lambda_b^2 + Pr}{\varepsilon\lambda_b}(\zeta - \lambda_b)\right]. \tag{4.52b}$$

Note the presence of factor ε^{-1} in the exponent of (4.52b), in contrast to the factor $\varepsilon^{-1/2}$ in (2.71). Typical profiles of the temperature and concentration fields, given by (4.52a, b), are depicted in figure 4.6 together with the profiles corresponding to positive values of $\mathscr{U}$. The algebraic equation for λ_b is derived from the continuity of the temperature gradients across the mush/liquid interface and has the following form

$$G(\lambda_b)\left(1 + \frac{Pr}{2\lambda_b^2}\right) = \frac{\Gamma - \varepsilon}{1 - \Gamma}, \tag{4.53}$$

which has a positive solution only if its right-hand side is positive, i.e. for $\Gamma > \varepsilon$, cf. (4.44). Note that $\lambda_b = O(1)$ as $Pr \to 0$, thus satisfying the constraint $\lambda_b \gg Pr$ so that the expansion (4.47) remains asymptotic. The solutions in the mushy layer and the solid phase, together with the equation for λ_a, are affected by the choice $\mathscr{U} = 0$

only through the values of λ_b. Note that for $Pr \to 0$ and $\varepsilon \to 0$ the equation (4.53) turns into (4.42).

We can combine (4.50b) and (4.51b) with the integral relation (4.15) to obtain the total dimensionless amount of solute contained within the mushy layer, given by the following integral

$$\int_{\lambda_a}^{\lambda_b} (\mathscr{C} - \Theta)\chi \, \mathrm{d}s = \lambda_b(\mathscr{C} - 1) - \frac{\varepsilon Pr(1-\Gamma)}{2\lambda_b \Gamma(1-\varepsilon)}. \tag{4.54}$$

Recall that, in terms of dimensional quantities, $\mathscr{C} - \Theta = C/\Delta C$. We can use (4.54) to study how the physical parameters affect the redistribution of solute within the mushy layer. First note that the value of the integral (4.54) is determined dominantly by the concentration ratio, with the other effects being of order $O(\varepsilon Pr)$ as ε, $Pr \to 0$. Moreover, we point out that the effect of $\mathscr{C}$ increases with λ_b, i.e. with the increasing thickness of the mushy layer, while the effect of the inverse Lewis number and Prandtl number decreases with λ_b (the large values of λ_b can be obtained, for example, by Γ being close to unity, but fixed).

The average bulk composition in the mushy layer is, to the leading order in small Pr, $\mathscr{U}$ and ε, determined by the concentration ratio, i.e.

$$\frac{1}{\lambda_b - \lambda_a} \int_{\lambda_a}^{\lambda_b} (\mathscr{C} - \Theta)\chi \, \mathrm{d}s = \mathscr{C} - 1 + O(Pr) + O(\mathscr{U}) + O(\varepsilon), \tag{4.55}$$

with Γ fixed.

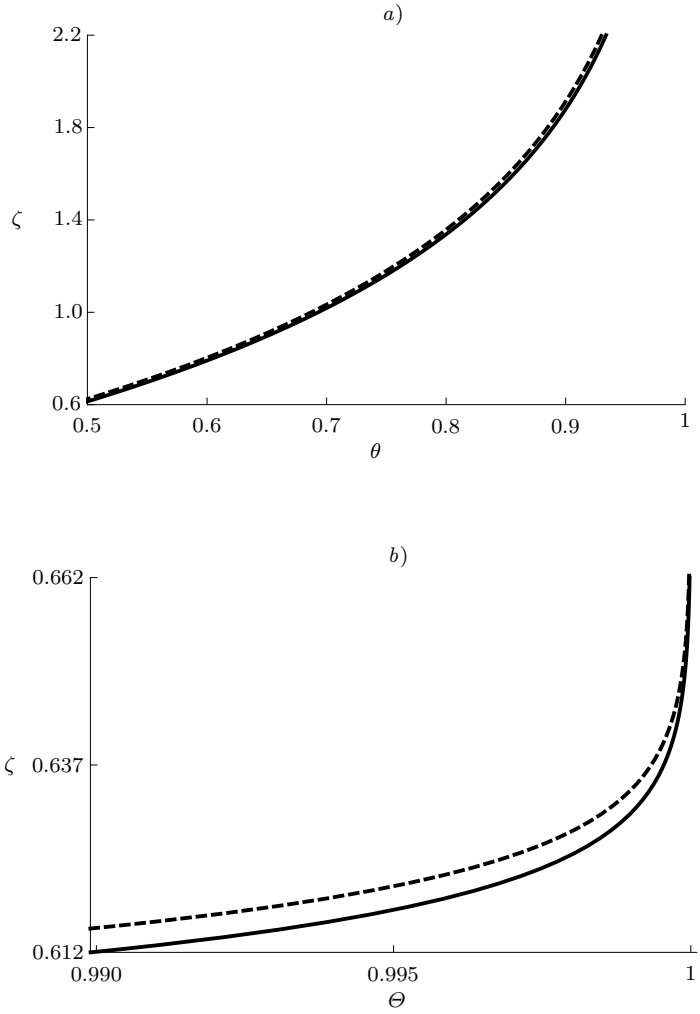

Figure 4.6: Temperature (a) and concentration (b) fields in the liquid phase as functions of ζ, given by (2.66) and (2.71) for $\mathscr{U} = 10^{-2}$ (solid lines), compared with the forms (4.52a, b) (dashed lines). The values of the other parameters are set to $Pr = 10^{-2}$, $\varepsilon = 10^{-2}$, $\mathscr{S} = 0$ and $\Gamma = 0.5$.

Chapter 5

Mushy layer with no solute diffusion

5.1 Introduction

The diffusion of solute is typically negligibly small compared to the diffusion of heat. It is therefore reasonable to investigate the limit of large Lewis number, which is equivalent to the limit $\varepsilon \to 0$. While this limit is regular in the mushy layer, it is singular in the liquid phase, resulting in formation of a thin concentration boundary layer adjacent to the mush/liquid interface. However, if we adopt the assumption that the scale on which the properties of mushy layer are homogenized is comparable to the scale of solute variations within the compositional boundary layer, then we can set $\varepsilon = 0$. In such case the compositional boundary layer remains unresolved within the homogenization limit (cf. Worster 2002).

When the solute diffusion is neglected, we can model the conservation of solute in the mushy layer in two different ways: locally and globally. The models hitherto discussed were all local as they assumed the conservation of solute within infinitesimal volume elements. While the local conservation of solute is possible in both cases of zero and non-zero solute diffusion, the global model is applicable only under the assumption of zero solute diffusion. The idea of the global conservation model was first introduced by Huppert & Worster (1985). Another useful reference can be found in the review by Huppert (1993). Thompson, Huppert & Worster (2003) developed a global conservation model for diffusion-controlled growth of a ternary alloy under the assumption that the temperature profile in the mushy layer was linear.

Here, we use the global approach to investigate the effect of the forced boundary-layer flow in the liquid phase, represented by the dimensionless numbers Pr and $\mathscr{U}$, on the characteristics of the mushy layer. Then we discuss the local conservation model and its relation to the global one. Though the local model with negligible solute diffusion has already been studied by other authors, new in our investigation are the dimensionless scalings and the explicit relation between the liquid fractions in the local and global models in case when Stefan number is negligible.

5.2 Global conservation model with no solute diffusion

In the global conservation model, we require that the average bulk concentration (per unit length in the horizontal direction) within the mushy layer is equal to that in the liquid phase, C_∞[1], and that the volume fraction $\chi = \chi_{\rm glob}$ is uniform, i.e.

$$\frac{1}{b(x)}\int_0^{b(x)} C(x,z)\chi_{\rm glob}\,{\rm d}z = C_\infty, \quad \text{for all} \quad x > 0. \tag{5.1}$$

The formulation above hinges on the assumption that there is no advective transport of solute relative to the solid portion of the mush, which is true since, in the mush, $\boldsymbol{u} = \boldsymbol{1}$. Moreover, we assume that there is no solid phase present as there is no diffusion mechanism that would enable the transport of solute away from the solid/mush interface to the mushy layer.[2] In dimensionless formulation, the equation (5.1) reads

$$\frac{1}{b(x)}\int_0^{b(x)} (\mathscr{C} - \Theta)\chi_{\rm glob}\,{\rm d}z = \mathscr{C} - 1, \quad \text{for all} \quad x > 0. \tag{5.2}$$

The dimensionless governing equation for the temperature field in the mushy layer is

$$\frac{\partial\theta}{\partial x} = \frac{\partial^2\theta}{\partial z^2}. \tag{5.3}$$

The term $\mathscr{S}\partial_x\chi$, which would normally be present in the above equation, cf. (2.35a), is zero since χ is uniform in the mush, so there is no internal phase change that would result in the release of latent heat, even when the Stefan number is positive. After the self-similar transformation, (5.3) becomes

$$\theta'' + 2\zeta\theta' = 0, \tag{5.4}$$

with the solution

$$\theta(\zeta) = \theta_b\frac{{\rm erf}(\zeta)}{{\rm erf}(\lambda_b)}, \tag{5.5}$$

where the interfacial temperature θ_b is yet to be determined. The temperature and concentration fields in the mush are tied through the liquidus relationship

$$\theta = \Gamma\Theta, \tag{5.6}$$

therefore the concentration field satisfies

$$\frac{\partial\Theta}{\partial x} = \frac{\partial^2\Theta}{\partial z^2}, \tag{5.7}$$

[1] The concentration of solute in the liquid phase is uniform when there is no solute diffusion; it is a direct consequence of the equations governing the concentration field in the liquid phase.

[2] In the local conservation model with no solute diffusion, the absence of solid phase is a direct consequence of the local conservation of solute at the solid/mush interface – see section 5.3 of the present chapter.

or

$$\Theta'' + 2\zeta\Theta' = 0. \tag{5.8}$$

The governing equation for the temperature field in the liquid phase is the same as we have hitherto used. However, the equation for concentration reduces to $\Theta' = 0$. Therefore the concentration is homogenous, equal to its far-field value, i.e.

$$\Theta \equiv 1, \quad \text{for} \quad \zeta \geq \lambda_b. \tag{5.9}$$

In the present case with no solute diffusion, the principle of marginal equilibrium, discussed in detail by Worster (2002), implies continuity of concentration across the mush/liquid interface, so that

$$\Theta_{b^-} = \Theta_{b^+} = \Theta_b = 1 \tag{5.10}$$

and therefore the temperature at the mush/liquid interface is given by the dimensionless liquidus slope as

$$\theta_b = \mathit{\Gamma}. \tag{5.11}$$

Finally, the concentration field in the mush is

$$\Theta(\zeta) = \frac{\operatorname{erf}(\zeta)}{\operatorname{erf}(\lambda_b)}. \tag{5.12}$$

Expressing (5.2) using the self-similar variable, we get

$$\frac{1}{\lambda_b}\int_0^{\lambda_b} (\mathscr{C} - \Theta)\chi_{\text{glob}}\,\mathrm{d}\zeta = \mathscr{C} - 1. \tag{5.13}$$

Note that (5.13) is consistent with (4.55), which reduces to (5.2) when $\varepsilon = 0$. The above relation provides an alternative interpretation of the dimensionless parameter $\mathscr{C}$: the value by which it excesses unity is equal to the average dimensionless bulk concentration of the mushy layer. The integral on the left-hand side can be calculated using per-partes in the following way

$$\begin{aligned}\int_0^{\lambda_b} (\mathscr{C} - \Theta)\,\mathrm{d}\zeta &= (\mathscr{C} - 1)\lambda_b + \int_0^{\lambda_b} \zeta\Theta'\,\mathrm{d}\zeta \\ &= (\mathscr{C} - 1)\lambda_b - \tfrac{1}{2}(\Theta'_{b^-} - \Theta'_{0^+}),\end{aligned} \tag{5.14}$$

where we have used (5.8) and (5.10). The concentration gradients at the lower and upper boundaries of the mushy layer can be obtained from the corresponding explicit solutions as

$$\Theta'_{0^+} = \frac{2\lambda_b\,\mathrm{e}^{\lambda_b^2}}{G(\lambda_b)}, \quad \text{and} \quad \Theta'_{b^-} = \frac{2\lambda_b}{G(\lambda_b)}. \tag{5.15}$$

Using the expressions above, together with (5.13) and (5.14), we obtain the volume fraction of the liquid phase in the mushy layer as

$$\chi_{\text{glob}} = \frac{\mathscr{C} - 1}{\mathscr{C} - 1 + H(\lambda_b)}, \tag{5.16}$$

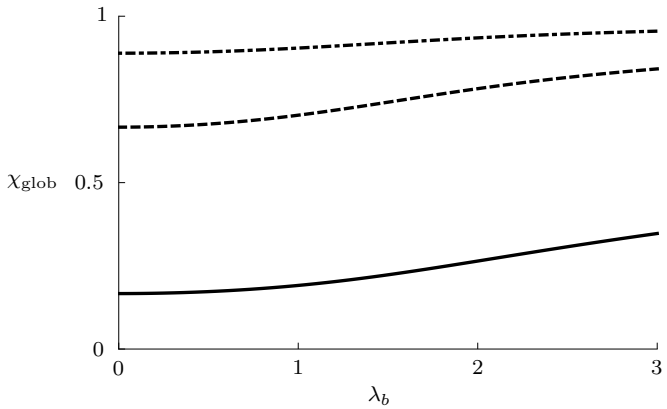

Figure 5.1: The volume fraction of liquid in the global conservation model, given by (5.16), as a function of the self-similar thickness of the mushy layer in case when $\mathscr{S} = 0$, for different values of concentration ratio: $\mathscr{C} = 1.1$ (solid line), $\mathscr{C} = 2$ (dashed line) and $\mathscr{C} = 5$ (dot-dashed line). For given $\mathscr{C}$, the minimum value of χ corresponds to the solution discussed by Worster (2000) under the assumption of linear temperature profile in the mush (for details, see text).

with

$$H(\lambda_b) \equiv \frac{\mathrm{e}^{\lambda_b^2} - 1}{G(\lambda_b)}. \tag{5.17}$$

It is straightforward to show that $\chi_{\rm glob}$ is always positive and less than unity. Moreover, note that $H(\lambda_b) \to 1/2$ as $\lambda_b \to 0$ and $H(\lambda_b) \to 0$ as $\lambda_b \to \infty$.

The Stefan condition at the mush/liquid interface reads

$$\mathscr{S}(1 - \chi_{\rm glob})\frac{\mathrm{d}b}{\mathrm{d}x} = \left.\frac{\partial\theta}{\partial z}\right|_{b^-} - \left.\frac{\partial\theta}{\partial z}\right|_{b^+}. \tag{5.18}$$

Note that, unlike the local conservation model, in which $\chi_{b^-} = 1$, in the global model the left hand-side of the Stefan condition is always nonzero when $\mathscr{S} > 0$. Indeed, in the global model, the solidification occurs only at the interface and the global conservation forces the uniform volume fraction to be less than unity in the mush. Using (5.5), we can express the condition (5.18) as

$$\mathscr{U}^{1/2}\frac{\mathrm{e}^{\lambda_b^2}\,\mathrm{erf}(\lambda_b)}{\mathrm{e}^{\Lambda^2(\lambda_b)/\mathscr{U}}\,\mathrm{erfc}[\Lambda(\lambda_b)/\mathscr{U}^{1/2}]} = \frac{1}{1-\Gamma}\left[\Gamma + \mathscr{S}\frac{1 - \mathrm{e}^{\lambda_b^2}}{\mathscr{C} - 1 + H(\lambda_b)}\right]. \tag{5.19}$$

5.2.1 Solutions with zero Stefan number

To simplify the mathematical problem, we will consider the regular limit of negligible Stefan number. In this limit, the thickness of the mushy layer is independent of $\mathscr{C}$. Moreover, the concentration ratio affects the system only through the quantity $\chi_{\rm glob}$. This allows us, for given $\mathscr{C}$, to plot $\chi_{\rm glob}$ as a function of the dimensionless mushy layer thickness λ_b (see figure 5.1). Note that

$$\chi_{\rm glob} \to 1 - \frac{1}{2\mathscr{C} - 1} \quad \text{as} \quad \lambda_b \to 0, \tag{5.20}$$

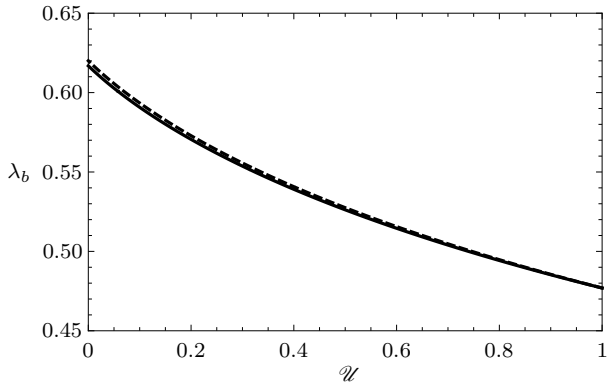

Figure 5.2: Growth constant λ_b in the case when $\mathscr{S} = 0$, calculated from (5.21) as a function of $\mathscr{U}$, for $Pr = 10^{-2}$ (solid line) and $Pr = 0$ (dashed line). In calculations we set $\Gamma = 0.5$.

which is the value obtained by Worster (2000) under the quasi-stationary approximation, in which the temperature profile in the mush could be well approximated by its steady form owing to the fact that the heat conduction was rapid compared to the rate of solidification. One way to ensure a slow solidification rate is to assume large values of Stefan number, resulting in a thin mushy layer. Though in the present case we have $\mathscr{S} = 0$, the temperature profile in the mush can be treated as linear provided λ_b is small enough.

With $\mathscr{S} = 0$, the nonlinear equation for λ_b becomes

$$\Gamma\lambda_b F\left[\frac{\Lambda(\lambda_b)}{\mathscr{U}^{1/2}}\right] + (\Gamma - 1)\Lambda(\lambda_b)G(\lambda_b) = 0. \tag{5.21}$$

We can make further simplification by taking the regular limit $Pr \to 0$ in the above equation to obtain

$$\Gamma F\left(\frac{\lambda_b}{\mathscr{U}^{1/2}}\right) + (\Gamma - 1)\lambda_b G(\lambda_b) = 0. \tag{5.22}$$

In figure 5.2, solutions to (5.21) with small Pr and to (5.22) are shown as functions of $\mathscr{U}$.

It can be shown that $\lambda_b = O(1)$ as $\mathscr{U} \to 0$ such that (5.22) reduces to a simple equation

$$G(\lambda_b) = \frac{\Gamma}{1 - \Gamma} \quad \text{for} \quad \mathscr{S} = 0,\ Pr \to 0,\ \mathscr{U} \to 0, \tag{5.23}$$

which is the same as (4.42).

Before we move further, it is instructive to have a closer look at the definitions of dimensionless numbers $\mathscr{C}$ and Γ. It is straightforward to show that these numbers are, in fact, not independent, since

$$\mathscr{C}\Gamma = \frac{\hat{\Gamma}C_0}{\Delta T}. \tag{5.24}$$

The relation stated above will prove useful in the physical interpretation of different asymptotic limits, which we shall discuss below.

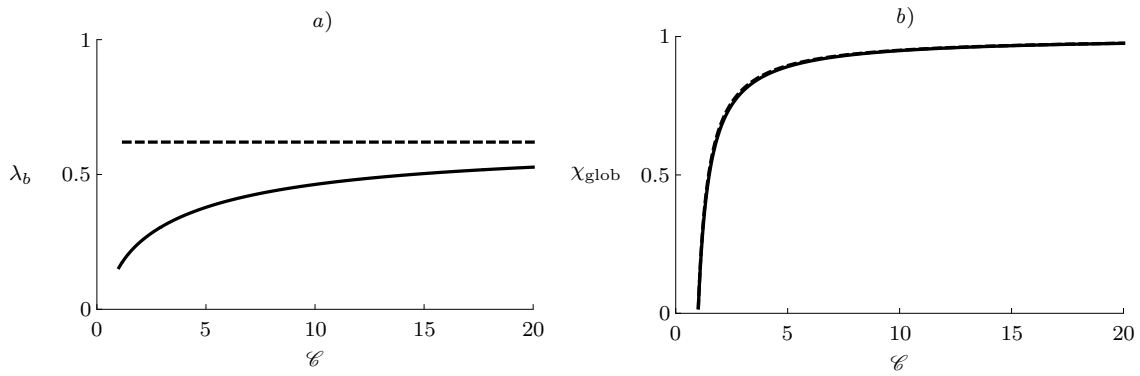

Figure 5.3: *a*) Growth constant λ_b as a function of $\mathscr{C}$, calculated from (5.25) with $\mathscr{S} = 10$ (solid line) and from (5.23) (dashed line). Note that the solution of (5.23) does not depend on $\mathscr{C}$. *b*) Liquid volume fraction as a function of $\mathscr{C}$, calculated using the values of λ_b from *a*): $\mathscr{S} = 10$ (solid line) and $\mathscr{S} = 0$ (dashed line). Note, that there is virtually no difference between the two curves. In all calculations, we set $\Gamma = 0.5$.

$\mathscr{C} \to 1$ with Γ fixed

This limit is equivalent to $C_\infty \to 0$ so that the bulk composition in the system decreases to zero; this can be seen also from (5.2). Moreover, (5.16) implies that $\chi \to 0$: as the initial composition decreases, there is less solute to be rejected upon solidification and hence the growth of dendrites is enhanced.

$\mathscr{C} \to \infty$ with Γ fixed

This limit is equivalent to $C_\infty \to C_0$ with λ_b fixed. Moreover, (5.24) implies $\hat{\Gamma} C_0/\Delta T \sim \mathscr{C} \to \infty$ so that $\Delta T \to 0$ (recall that $\Delta T \equiv T_\infty - T_0$). Finally, (5.16) implies $\chi \to 1$: increasing the far-field concentration (and hence the bulk concentration in the mush) results in melting of dendrites. In order to keep the thickness (in terms of λ_b) of the mushy layer unaffected, we need to decrease the far-field temperature of the melt.

$\mathscr{C} \to \infty$ with $\mathscr{C}\Gamma$ fixed

In this limit, $\Gamma \sim \mathscr{C}^{-1} \to 0$ with $\hat{\Gamma} C_0/\Delta T$ kept fixed. As in the limit with fixed Γ discussed above, the liquid fraction tends to unity ($\chi \to 1$). However, (5.23) implies that $\lambda_b \to 0$. Thus, when $C_\infty \to C_0$ with C_0, ΔT and $\hat{\Gamma}$ kept fixed, the thickness of mushy layer decreases.

5.2.2 Effect of nonzero Stefan number

To include the effect of latent heat release when as $\mathscr{U} \to 0$, the equation (5.19) can be approximated, to leading order, as follows

$$G(\lambda_b)\left(1 + \frac{Pr}{2\lambda_b^2}\right) = \frac{1}{1-\Gamma}\left[\Gamma + \mathscr{S}\frac{1 - \mathrm{e}^{\lambda_b^2}}{\mathscr{C} - 1 + H(\lambda_b)}\right]. \tag{5.25}$$

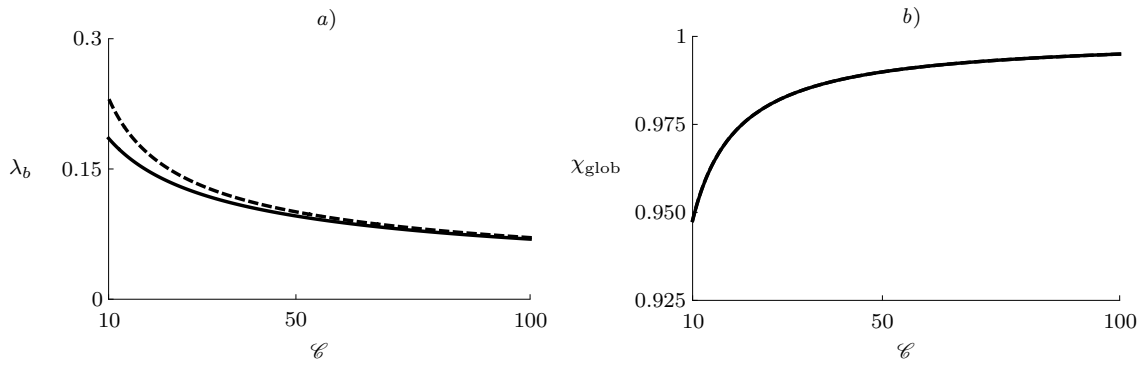

Figure 5.4: *a*) Growth constant λ_b as a function of $\mathscr{C}$, calculated from (5.25) with $\mathscr{S} = 10$ (solid line) and from (5.23) (dashed line). In both computations we set $\mathscr{C}\Gamma = 1$. *b*) Liquid volume fraction as a function of $\mathscr{C}$, calculated using the values of λ_b from *a*): $\mathscr{S} = 10$ (solid line) and $\mathscr{S} = 0$ (dashed line). Note that both curves are virtually the same.

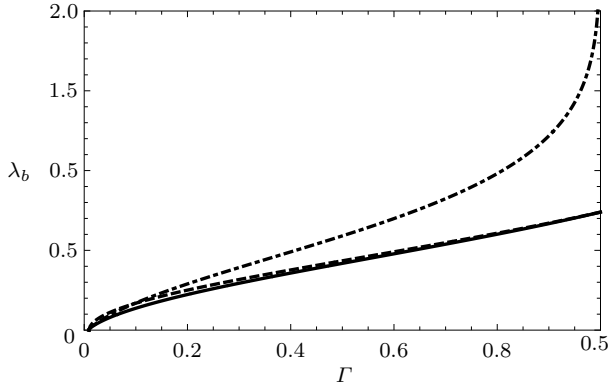

Figure 5.5: The numerical solution of the full equation (5.19) as a function of Γ (solid line), together with the zero-$\mathscr{U}$ solution, given by (5.25) (dashed line), and the leading-order solution, given by (5.23) (dot-dashed line). The values of dimensionless numbers are set to $Pr = 10^{-2}$, $\mathscr{U} = 10^{-1}$, $\mathscr{S} = 1$ and $\mathscr{C} = 2$. Note the regularizing effect of nonzero Stefan number on the values of λ_b.

In figure 5.3(a) we plot the solution of (5.25) with $Pr = 0$ as a function of $\mathscr{C}$ with Γ fixed, along with the solution of (5.23). The corresponding values of χ_{glob} are shown in figure 5.3(b). In figure 5.4(a) we plot the solution of (5.25) with $Pr = 0$ as a function of $\mathscr{C}$ with $\mathscr{C}\Gamma$ fixed. The corresponding values of χ_{glob} are shown in figure 5.4(b). Note that in both cases the positive values of Stefan number result in the decreasing thickness of the mushy layer, however, the extent of the internal phase change, represented by the values of χ, is almost unaffected.

The numerical solutions of (5.19), (5.25) and (5.23) are shown in figure 5.5 as functions of Γ. We have already stated in Chapter 4 that the singularity in λ_b as $\Gamma \to 1^-$ is the consequence of the zero Stefan number. As can be seen in the global model, positive values of Stefan number result in finite values of λ_b as $\Gamma \to 1^-$. The same effect of nontrivial latent-heat release can be anticipated in the local model discussed in Chapter 4.

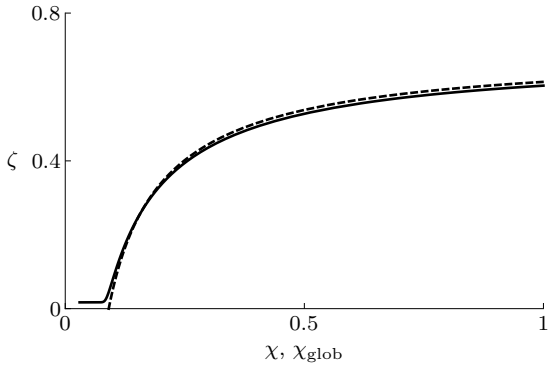

Figure 5.6: The local liquid fraction in the mushy layer, calculated from (5.32) (dashed line), compared with that given by (4.18) in the case when solute diffusion is present (solid line) with $\varepsilon = 0.5 \times 10^{-2}$. Note that apart from the narrow region ahead the solid/mush interface, where the solid curve exhibits steep gradients, there is virtually no differences between the two cases.

5.3 Local conservation model with no solute diffusion

In section 4.3.2 we discussed the asymptotic limit $\varepsilon \to 0$ in the local conservation model of a mushy layer. We showed that the thickness of the solid phase tended to zero in this limit, with the thickness of the mushy layer being finite. In this section we shall focus our attention on the limiting case when the solute diffusion is negligible, i.e. we set $\varepsilon = 0$. While in the global conservation model the absence of the solid phase in the system was assumed a priori, however, in the local model it is a direct consequence of the conservation of solute at the solid/mush interface. The retreat of the solid phase in case when the solute diffusion is negligible was also discussed by Gewecke & Schulze (2011*a*) for the mushy layer in a vertically bounded domain.

In the local conservation model with zero solute diffusion, the bulk composition in the mushy layer is constant, i.e.

$$\frac{\partial}{\partial x}[(\mathscr{C} - \Theta)\chi] = 0. \tag{5.26}$$

The above equation follows from (2.35*b*) by setting $\varepsilon = 0$. The temperature field in the mushy layer is governed by

$$\frac{\partial \theta}{\partial x} = \frac{\partial^2 \theta}{\partial z^2} - \mathscr{S}\frac{\partial \chi}{\partial x}. \tag{5.27}$$

However, since the limit $\mathscr{S} \to 0$ is regular, in what follows, we set $\mathscr{S} = 0$ in order to derive explicit solutions. The governing equations in the liquid phase does not differ from those used in the global model, with homogenous concentration $\Theta \equiv 1$.

The equation (5.26) expressed using the self-similar variable reads

$$2\zeta[(\mathscr{C} - \Theta)\chi]' = 0, \tag{5.28}$$

which after integration becomes

$$(\mathscr{C} - \Theta)\chi - (\mathscr{C} - 1)\chi_{b^-} = 0, \tag{5.29}$$

where we have used that $\Theta_b = 1$. The value of liquid fraction at the interface can be deduced from the local conservation of solute at the interface

$$(\mathscr{C} - 1)(1 - \chi_{b^-})\frac{\mathrm{d}b}{\mathrm{d}x} = 0, \tag{5.30}$$

so that

$$\chi_{b^-} = 1 \tag{5.31}$$

is the only consistent solution. Thus the liquid fraction in the mush can be expressed as

$$\chi = \frac{\mathscr{C} - 1}{\mathscr{C} - \Theta}. \tag{5.32}$$

Note that upon integrating (5.29) we obtain the same form of the average bulk composition within the mushy layer as the leading order one in (4.55).

The local conservation of solute at the solid/mush interface implies

$$(\mathscr{C} - \Theta_a)\chi_{a^+}\frac{\mathrm{d}a}{\mathrm{d}x} = 0. \tag{5.33}$$

However, from (5.32) we have $\chi_{a^+} = (\mathscr{C}-1)/(\mathscr{C}-\Theta_a)$, which is nonzero since $\mathscr{C} > 1$. Thus the only way to satisfy the above equation is to set $\mathrm{d}a/\mathrm{d}x = 0$ so that

$$\lambda_a = 0, \tag{5.34}$$

which implies that there is no solid in the system in case when the solute diffusion is neglected. Since $\Theta_0 = 0$, we obtain the liquid fraction at the bottom of the mushy layer

$$\chi_{0^+} = 1 - \frac{1}{\mathscr{C}}. \tag{5.35}$$

Note that χ_{0^+} is always positive even for positive values of Stefan number since to derive (5.35), we only used (5.28), which does not depend on $\mathscr{S}$.

The temperature field in the mushy layer has the form

$$\theta = \Gamma\frac{\mathrm{erf}(\zeta)}{\mathrm{erf}(\lambda_b)} \tag{5.36}$$

and the concentration field

$$\Theta = \frac{\mathrm{erf}(\zeta)}{\mathrm{erf}(\lambda_b)}. \tag{5.37}$$

Recall that $\theta_b = \Gamma$ due to the liquidus relationship between the temperature and concentration fields and the fact that $\Theta_b = 1$. In figure 5.6 we compare the liquid fraction given by (5.32) with that in case when the solute diffusion is not neglected, given by (4.18). Note that the two solutions are almost the same, except a narrow region ahead of the solid/mush interface.

Since we assume $\mathscr{S} = 0$, the Stefan condition at the mush/liquid interface implies the continuity of temperature gradient at this interface, as was also the case in the global conservation model. Using the explicit solutions derived above together with the solution for the temperature field in the liquid, the continuity of temperature

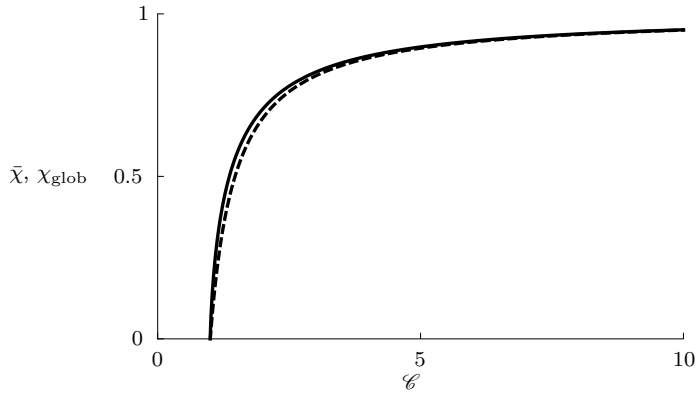

Figure 5.7: The average local volume fraction $\bar{\chi}$ as a function of $\mathscr{C}$ compared with the volume fraction $\chi_{\rm glob}$ in the corresponding global conservation model. The values of the other parameters are $Pr = 10^{-2}$, $\mathscr{U} = 10^{-1}$, $\mathscr{S} = 0$ and $\Gamma = 0.5$.

gradient can be used to derive an algebraic equation for the growth constant λ_b in the following form

$$\Gamma\lambda_b F\left[\frac{\Lambda(\lambda_b)}{\mathscr{U}^{1/2}}\right] + (\Gamma - 1)\Lambda(\lambda_b)G(\lambda_b) = 0. \tag{5.38}$$

We obtained the equation that is the same as (5.21) that we derived for the global conservation model. However, this is not surprising since the only difference between the global and local models is in the liquid fractions in the mush. Particularly, the Stefan condition has the same mathematical expression in both models. When $\mathscr{S} = 0$, the liquid fractions does not enter the Stefan conditions as the left hand-sides of these conditions are zero.

We have just shown that for zero Stefan number and for given values of Γ, $\mathscr{C}$, Pr and $\mathscr{U}$ the thickness of the mushy layer in the local conservation model is the same as that in the global one, as well as the temperature and concentration fields. Using this information, we can derive a relationship between the liquid fractions in the global and local models. Since λ_b and the concentration field in the global and local models are the same, we can combine (5.13) with (5.32) to obtain

$$\frac{1}{\lambda_b}\int_0^{\lambda_b}\frac{\mathrm{d}\zeta}{\chi} = \frac{1}{\chi_{\rm glob}}, \tag{5.39}$$

that is, the reciprocal liquid fraction in the global model is equal to the average reciprocal liquid fraction in the local model. In figure 5.7 we plot the average local liquid volume fraction, defined by

$$\bar{\chi} = \frac{1}{\lambda_b}\int_0^{\lambda_b}\chi\,\mathrm{d}\zeta, \tag{5.40}$$

together with the liquid fraction in the global model, both as functions of $\mathscr{C}$. Note that there is only a slight difference between these quantities. Moreover, for $\mathscr{C} \to \infty$, this difference tends to zero.

Conclusions

The explicit solutions to the solidification problems are useful since they facilitate a straightforward analysis of the physical phenomena involved. Moreover, they can serve as benchmark for testing numerical solutions of more complicated problems for which closed-form solutions are not available.

In this thesis we made a contribution to self-similar solutions describing solidification phenomena already known. The specific features of the present setting are the two-dimensional solid/mush and mush/liquid interfaces along with the two-dimensional flow in the liquid phase. Although the problem involves two-dimensional interfaces, when the velocity ratio is equal to unity, however, the governing equations turn out to be the same as that for the problem with planar interfaces, already studied by other authors. Therefore, some of our new results can be applied also for planar interfaces. In what follows we would like to point out the main contributions of the present study.

Unlike Cheung *et al.* (2002) and Cheung & Tangthieng (2003), we used the local conservation of solute to model the liquid fraction in the mushy layer instead of the lever rule, though the application of the lever rule is a common practice in metallurgical literature. However, we use the approach of Worster (1986) and model the local liquid fraction by a hyperbolic partial differential equation.

The problem with solid/liquid interface, discussed in Chapter 3, was previously studied by Löfgren (2001). Our main contribution consist in the analysis of the way the velocity ratio influences the temperature and concentration fields (stretching of the thermal and viscous boundary layers) and the position of the solid/liquid interface. Moreover, one can take the zero-Prandtl number solutions for the temperature and concentration fields and the growth rate as good approximations of full solutions. Such a simplification enables one to find the leading-order solutions in relatively simple forms, appropriate for further investigation. Another important feature is the different signs of the solutal advective flux for $\mathscr{U} > 1$ and $\mathscr{U} < 1$.

In Chapter 4, we showed that the liquid fraction at the solid/mush interface is zero when Stefan number is negligible. Gewecke & Schulze (2011*a*) showed this for the self-similar solution of the mushy-layer problem in the semi-infinite region with planar phase interfaces. However, we showed that this result can be derived directly from the governing equations without any knowledge of the explicit solutions. The key step was the transformation of the local conservation equation for the liquid fraction to an integral equation, which is our own result. The integral equation for liquid fraction also facilitated a relatively simple proof that the liquid fraction at the mush/liquid interface is equal to unity for any value of Stefan number. Though this

result was derived by Worster (1986), however, our derivation is less technical than that by Worster (1986) and does not require any knowledge of explicit solutions since it is based only on the formulation of the conservation laws at the interface.

In the case when Stefan number is positive, our new result is that the gradient of the liquid fraction at solid/mush interface is bounded, unlike the case when the Stefan number is negligible, in which case the numerical solutions indicate that the gradient is infinite. The boundedness of the liquid-fraction gradient for positive Stefan numbers is a direct consequence of the coupling between the liquid fraction and the temperature field, represented by the heat equation with the source term due to the local latent-heat release. Therefore the singularity of the liquid-fraction gradient turns out to be the consequence of the negligible Stefan number. Though the analysis presented in this thesis focused on a mushy layer with two-dimensional interfaces, however, the self-similar form of the mushy-layer equations was the same as that for a mushy layer with planar interfaces, the only difference being in the definition of the self-similar variable. Therefore the discussion regarding the values of the liquid fraction on the solid/mush interface is relevant also for the systems with planar interfaces.

In the situation with the solid/liquid interface, the thickness of the solid phase decreases to zero as $Pr \to 0$ and $\mathscr{U} \to 0$ with $Pr \ll \mathscr{U}$. However, when the mushy layer is present, the thickness of the solid phase and the mushy layer tends to a finite value in this limit. Moreover, the limit becomes regular.

Since the solutal diffusivity is typically small compared to the thermal diffusivity, we studied the asymptotic limit of small inverse Lewis number ε. In such case we found that the normalized thickness of the solid phase, λ_a, scales with ε. Therefore the growth of the solid phase is controlled by solute diffusion. Since this result holds also when $\mathscr{U} = 1$, the same scaling applies also to the problem of the mushy layer with planar interfaces, studied by Worster (1986) and Gewecke & Schulze (2011*b*). Moreover, when ε is small, the solid thickness decreases with the concentration ratio as $\mathscr{C}^{-1}$. On the other hand, the growth of the mushy layer is controlled by thermal diffusion, since λ_b is finite as $\varepsilon \to 0$. The dimensionless quantity that dominantly controls the growth of the mushy layer is the dimensionless liquidus slope Γ: while the thickness of the mushy layer attains finite values for all $\mathscr{U} \in \langle 0, 1\rangle$ with Γ fixed, it is unbounded for values of Γ close to unity. Thus to obtain thick mushy layers, the parameter Γ is the one that must be varied. However, the singularity in λ_b as $\Gamma \to 1^-$ is the consequence of the fact that there is no latent-heat release at the mush/liquid interface to inhibit the growth of the mush when there is no thermal gradient in the liquid. As can be seen in the global model, positive values of Stefan number result in finite values of λ_b as $\Gamma \to 1^-$.

The average bulk composition within the mush in the local conservation model is, to the leading order in small Pr, ε and $\mathscr{U}$, given by the concentration ratio. More specifically, the value by which $\mathscr{C}$ exceeds unity is equal (to the leading order) to the average dimensionless bulk composition. In the global model, this is an exact equality as a direct consequence of the global conservation of solute. Therefore, in general, the concentration ratio may serve as an indicator of the redistribution of the solute within the mushy layer.

One of the main contributions of our thesis is also the dimensionless formulation used. The typical scalings used so far by other authors were such that the temperature and concentration in the mushy layer were the same (cf. Worster 1991, Guba & Worster 2006*a* and Guba & Worster 2006*b*). However, we chose the scalings that distinguish between the temperature and concentration fields in the mushy layer. As a result, we were able to identify the dimensionless liquidus slope, to the leading order in ε, with the dimensionless temperature at the mush/liquid interface.

Nonetheless, one should have in mind the assumptions on which the mathematical formulation of the problem rested. The first one was stationarity in the laboratory frame of reference — we completely ignored the transient behaviour, which, in practice, can substantially influence the evolution of the system towards the steady state. The second assumption was the semi-infinity in both horizontal and vertical directions, which was essential for the self-similar analysis.

There are several problems still left open, which could motivate further investigation. The first one is the possibility of a nontrivial flow in the mushy layer, a question that in fact served as the original motivation for our thesis. In the present case, we did not consider the variations of density with temperature and concentration in order to simplify the problem. Since there was no horizontal pressure gradient to drive the flow (the flow was driven by moving substrate), the only flow in the mushy layer consistent with the boundary-layer reduction and the self-similar formulation was the uniform one (i.e. trivial with respect to the dendrites). Finding a nontrivial flow in the mushy layer, consistent with the self-similar formulation, will require incorporation of the buoyancy effects, i.e. the variations of the liquid density with temperature and concentration. A difficult task will also be to correctly determine the boundary conditions at the mush/liquid interface, since the nontrivial flow in the mushy layer can eventually cross the mush/liquid interface.

Another open task is the numerical analysis of the liquid fraction at the solid/mush interface in case when the Stefan number is positive. Though Worster (1986) solved a more general problem with planar interfaces numerically with positive values of Stefan number and distinct material properties of liquid and solid phases, however, the numerical solution of a simpler problem presented here would be useful for validation of our result that the gradient of liquid fraction is bounded towards the solid/mush interface.

Bibliography

Aitta, A., Huppert, H. & Worster, M. G. 2001 Diffusion-controlled solidification of a ternary melt from a cooled boundary. *J. Fluid Mech.* **432**, 201–217.

Anderson, D. M. 2003 A model for diffusion-controled solidification of ternary alloys in mushy layers. *J. Fluid Mech.* **483**, 165–197.

Anderson, D. M. & Schulze, T. P. 2005 Linear and nonlinear convection in solidifying ternary alloys. *J. Fluid Mech.* **545**, 213–243.

Aris, R. 1990 *Vectors, Tensors, and the Basic Equations of Fluid Mechanics*. Dover Publications.

Boisvert, R. F., Clark, Ch. W., Lozier, D. W. & Olver, F. W. J. 2010 *NIST Handbook of Mathematical Functions*. Cambridge University Press.

Cheung, F. B., Shiah, S. W. & Tangthieng, C. 2002 Behavior of the two-phase mushy zone during freeze coating on a continuous moving plate. *J. Heat Transfer* **124**, 111–119.

Cheung, F. B. & Tangthieng, C. 2003 Thermosolutal transport and macrosegregation during freeze coating of a binary substance on a continuous moving object. *Int. J. Heat Mass Transfer* **46**, 2313–2327.

Davis, S. H. 2001 *Theory of Solidification*. Cambridge University Press.

Fowler, A. C. 1985 The formation of freckles in binary alloys. *IMA J. Appl. Math.* **35**, 159–174.

Gewecke, N. R. & Schulze, T. P. 2011*a* The rapid advance and slow retreat of a mushy zone. *J. Fluid Mech.* **674**, 227–243.

Gewecke, N. R. & Schulze, T. P. 2011*b* Solid-mush interface conditions for mushy layers. *J. Fluid Mech.* **689**, 357–375.

Guba, P. & Anderson, D. M. Convective instability of ternary mushy layer. In preparation.

Guba, P. & Worster, M. G. 2006*a* Free convection in laterally solidifying mushy regions. *J. Fluid Mech.* **558**, 69–78.

Guba, P. & Worster, M. G. 2006*b* Nonlinear oscillatory convection in mushy layers. *J. Fluid Mech.* **553**, 419–443.

Guba, P. & Worster, M. G. 2010 Interactions between steady and oscillatory convection in mushy layers. *J. Fluid Mech.* **645**, 411–434.

Huppert, H. E. 1990 Fluid mechanics of solidification. *J. Fluid Mech.* **212**, 209–240.

Huppert, H. E. 1993 Bulk Models of Solidification. In *Handbook of Crystal Growth. Volume 1: Fundamentals, A: Thermodynamics and Kinetics, B: Transport and Stability* (ed. D. T. J. Hurle), pp. 743–783. North Holland.

Huppert, H. E. & Worster, M. G. 1985 Dynamic solidification of a binary melt. *Nature* **314**, 703–707.

Kyselica, J. 2013 Evolution of the solidification front of a binary mixture. *Appl. Math. Model.* **37**, 3761–3776.

Kyselica, J. & Guba, P. 2014 Forced boundary-layer flow and solidification on a moving substrate. Under review for *Acta Mech.*

Löfgren, H. B. 2001 Ideal solidification of a liquid-metal boundary layer flow over a conveying substrate. *J. Fluid Mech.* **446**, 121–131.

Löfgren, H. B. & Åkerstedt, H. O. 2001 Initial solidification in liquid metal film flow over a moving boundary. *Int. J. Heat Mass Transfer* **44**, 837–842.

Schlichting, H. 1979 *Boundary-layer theory*, 7th edn. McGraw-Hill.

Schulze, T. P. & Worster, M. G. 2005 A time-dependent formulation of the mushy-zone free boundary problem. *J. Fluid Mech.* **541**, 193–202.

Steen, P. H. & Karcher, Ch. 1997 Fluid mechanics of spin casting of metals. *Annu. Rev. Fluid Mech.* **29**, 373–397.

Thompson, A. F., Huppert, H. E. & Worster, M. G. 2003 Appendix: A global conservation model for diffusion-controlled solidification of a ternary alloy. *J. Fluid Mech.* **483**, 191–197.

Worster, M. G. 1986 Solidification of an alloy from a cooled boundary. *J. Fluid Mech.* **167**, 481–501.

Worster, M. G. 1991 Natural convection in a mushy layer. *J. Fluid Mech.* **224**, 335–359.

Worster, M. G. 2000 Solidification of Fluids. In *Perspectives in Fluid Dynamics: A Collective Introduction to Current Research* (ed. G. K. Batchelor, H. K. Moffat & M. G. Worster), pp. 393–446. Cambridge University Press.

Worster, M. G. 2002 Interfaces on all scales during solidification and melting. In *Interfaces for the 21st Century* (ed. M. K. Smith, M. J. Miksis, G. P. Neitzel G. B. McFadden & D. R. Canright), pp. 187–201. Imperial College Press.

Appendix

A.1 Proof of equation (4.19) when $\mathscr{S} \geq 0$

The condition (4.8) states that at least one of the quantities $2\lambda_a(\mathscr{C} - \Theta_a) - \varepsilon\Theta'_{a^+}$ and χ_{a^+} must be zero. However, we shall prove that the former is always zero. To prove that, assume the converse was true, i.e. $2\lambda_a(\mathscr{C} - \Theta_a) - \varepsilon\Theta'_{a^+} \neq 0$, so that $\chi_{a^+} = 0$. Moreover, (4.14) implies that $2\zeta(\mathscr{C} - \Theta) - \varepsilon\Theta' > 0$ for $\zeta > \lambda_a$ since the integral on the right hand-size of (4.14) is always positive for $\zeta > \lambda_a$. Therefore we get from the continuity that $2\lambda_a(\mathscr{C} - \Theta_a) - \varepsilon\Theta'_{a^+} > 0$. To sum up, there must exist some constant $K > 0$ such that $2\zeta(\mathscr{C} - \Theta) - \varepsilon\Theta' > K$ for all $\zeta \geq \lambda_a$, from which we get

$$\left| \frac{2\zeta\Theta' + \varepsilon\Theta''}{2s(\mathscr{C} - \Theta) - \varepsilon\Theta'} \right| < \frac{1}{K} |2\zeta\Theta' + \varepsilon\Theta''|$$

for $\zeta \geq \lambda_a$. The expression on the right hand-side of the above inequality is bounded (we will prove it below) in the mushy layer so that

$$\lim_{\zeta \to \lambda_a^+} \int_{\zeta}^{\lambda_b} \frac{2s\Theta' + \varepsilon\Theta''}{2s(\mathscr{C} - \Theta) - \varepsilon\Theta'} \, \mathrm{d}s \neq \infty,$$

which contradicts the assumption that $\chi_{a^+} = 0$. Therefore the original assumption was false, i.e. (4.19) holds.

It remains to prove that $2\zeta\Theta' + \varepsilon\Theta''$ is bounded as $\zeta \to \lambda_a^+$. To show that, we first prove that $2\zeta\Theta' + \varepsilon\Theta'' \geq 0$ and $2\zeta\Theta' + \Theta'' \leq 0$ in a sufficiently small neighbourhood of $\zeta = \lambda_a$. We start with (4.4) and assume that $2\zeta\Theta' + \Theta'' > 0$. Hence we obtain that $\chi' < 0$, which together with (4.1) implies that $2\zeta\Theta' + \varepsilon\Theta'' < 0$. To sum up, the two inequalities that must hold simultaneously are

$$2\zeta\Theta' + \Theta'' > 0 \quad \text{and} \quad -2\zeta\Theta' - \varepsilon\Theta'' > 0 \quad \text{as} \quad \zeta \to \lambda_a. \tag{A.1a,b}$$

These can be added up to yield

$$(1 - \varepsilon)\Theta'' > 0, \tag{A.2}$$

which implies that $\Theta'' > 0$ since ε is typically small. But this violates the inequality $2\zeta\Theta' + \varepsilon\Theta'' < 0$ since Θ' must be positive for the model to be physically consistent.[3]

[3]Negative values of Θ' near the interface would correspond to positive dimensional concentration gradients, which would indicate the diffusive flux of solute towards the solid/mush interface.

Therefore $2\zeta\Theta' + \Theta'' \leq 0$, which together with (4.1) implies that $2\zeta\Theta' + \varepsilon\Theta'' \geq 0$. The two inequalities can be written as

$$2\zeta\Theta' + \Theta'' \leq 0 \quad \text{and} \quad -2\zeta\Theta' - \varepsilon\Theta'' \leq 0 \quad \text{as} \quad \zeta \to \lambda_a \qquad (A.3a,b)$$

and added up to yield

$$(1-\varepsilon)\Theta'' \leq 0, \qquad (A.4)$$

whence $\Theta'' \leq 0$. This last inequality forces the expression $2\zeta\Theta' + \varepsilon\Theta''$ to be bounded. To see this, first note that (4.5) implies that $0 \leq \theta'_{a^+} \leq \theta'_{a^-} < \infty$, which upon applying the liquidus relationship yields $0 \leq \Theta'_{a^+} = \Gamma\theta'_{a^+} < \infty$. Therefore Θ' is bounded as $\zeta \to \lambda_a^+$, so the only way for $2\zeta\Theta' + \varepsilon\Theta''$ to be unbounded is that Θ'' is unbounded, i.e. $\Theta'' \to -\infty$. However, this would violate the inequality (A.3b).

To summarize a rather formal discussion above, we have shown that both quantities $\Theta' \geq 0$ and $\Theta'' \leq 0$ are bounded as $\zeta \to \lambda_a^+$. Though, from the physical point of view, this is not surprising, it has some important consequences regarding the liquid fraction in the mushy layer — for that reason it deserved such a formal treatment. The inequality (A.3a) together with (4.4) implies that

$$0 \leq \chi'_{a^+} < \infty \quad \text{for} \quad \mathscr{S} > 0. \qquad (A.5)$$

However, note that to show this and the inequalities (A.3a, b), we needed that $\mathscr{S} > 0$ in (4.4). With $\mathscr{S} = 0$, the equation (4.4) becomes $2\zeta\Theta' + \Theta'' = 0$ and $2\zeta\Theta' + \varepsilon\Theta'' = -(1-\varepsilon)\Theta'' > 0$, which can be easily verified from the self-similar solutions, as well as the boundedness of $2\zeta\Theta' + \varepsilon\Theta''$. Therefore we conclude that (4.19) holds for any values of Stefan number, including the case when $\mathscr{S} = 0$. However, we do not know anything about the boundedness of χ'_{a^+} when $\mathscr{S} = 0$, since the coupling between χ' and the concentration field in (4.4) is lost in that case.

A.2 Liquid fraction at the solid/mush interface when $\mathscr{S} = 0$

Here we shall use the integral relation (4.14) to show that $\chi_{a^+} = 0$ in case when $\mathscr{S} = 0$. We denote the integrand of (4.18) as $q(\zeta)$, i.e.

$$q(\zeta) \equiv \frac{q_1(\zeta)}{q_2(\zeta)} \qquad (A.6)$$

with

$$q_1(\zeta) \equiv 2\zeta\Theta'(\zeta) + \varepsilon\Theta''(\zeta), \qquad (A.7a)$$
$$q_2(\zeta) \equiv 2\zeta[\mathscr{C} - \Theta(\zeta)] - \varepsilon\Theta'(\zeta). \qquad (A.7b)$$

Using the explicit solution (4.23) we obtain

$$q_1(\zeta) = (1-\varepsilon)\frac{4\zeta\Theta_a}{\pi^{1/2}\,\mathrm{erf}(\lambda_a)}\,\mathrm{e}^{-\zeta^2} > 0. \qquad (A.8)$$

Therefore $q_1(\lambda_a^+) > 0$. Now, assume that $\chi_{a^+} > 0$. Therefore the integral in (4.18) must be finite. From (4.14) we obtain

$$q_2(\zeta) = \frac{2}{\chi(\zeta)} \int_{\lambda_a}^{\zeta} [\mathscr{C} - \Theta(s)]\chi(s)\,\mathrm{d}s > 0. \tag{A.9}$$

Therefore

$$\frac{q_2(\zeta)}{\zeta - \lambda_a} = \frac{2}{\chi(\zeta)} \frac{1}{\zeta - \lambda_a} \int_{\lambda_a}^{\zeta} [\mathscr{C} - \Theta(s)]\chi(s)\,\mathrm{d}s.$$

Taking $\zeta \to \lambda_a^+$ we obtain a finite limit

$$\lim_{\zeta \to \lambda_a^+} \frac{q_2(\zeta)}{\zeta - \lambda_a} = 2(\mathscr{C} - \Theta_a). \tag{A.10}$$

To derive this, we used the assumption that $\chi_{a^+} > 0$ and the fact that

$$\lim_{\zeta \to \lambda_a^+} \frac{1}{\zeta - \lambda_a} \int_{\lambda_a}^{\zeta} \psi(s)\mathrm{d}s \equiv \frac{\mathrm{d}}{\mathrm{d}\zeta} \left(\int_{\lambda_a}^{\zeta} \psi(s)\mathrm{d}s \right) \Bigg|_{\zeta = \lambda_a^+} = \psi(\lambda_a)$$

holds for any continuous function ψ. We thus proved that

$$q(\zeta) = O[(\zeta - \lambda_a)^{-1}], \quad \text{as} \quad \zeta \to \lambda_a^+ \tag{A.11}$$

and therefore[4]

$$\int_{\zeta}^{\lambda_b} q(s)\mathrm{d}s \to +\infty, \quad \text{as} \quad \zeta \to \lambda_a^+, \tag{A.12}$$

which implies that $\chi_{a^+} = \exp(-\infty) = 0$, a contradiction with the assumption that $\chi_{a^+} > 0$. Thus we have proved that $\chi_{a^+} = 0$. To derive this result, the assumption of zero Stefan number allowed us to use the explicit solutions (4.23) to show that $q_1(\lambda_a^+) > 0$.

A.3 Liquid fraction at the solid/mush interface when $\mathscr{S} > 0$

We have already shown that χ'_{a^+} is bounded when Stefan number is nonzero. Though the determination whether χ_{a^+} is zero or not is still an open task, however, we shall make some remarks concerning this problem. First, note that to prove that $\chi_{a^+} = 0$, regardless the value of Stefan number, it is sufficient to show that

[4]Let the function $\psi\colon (a, b\rangle \to \mathbb{R}$ be integrable on any bounded interval $\langle \zeta, b\rangle$ with $a < \zeta < b$ and let $\psi(\zeta) = O[(\zeta - a)^{-p}]$ with $p \geq 1$ as $\zeta \to a^+$. Then the integral

$$\int_a^b \psi(s)\mathrm{d}s \equiv \lim_{\zeta \to a^+} \int_{\zeta}^b \psi(s)\mathrm{d}s$$

is divergent.

$2\lambda_a\Theta'_{a^+} + \varepsilon\Theta''_{a^+} > 0$. Second, from (4.4) we have, in the limit $\zeta \to \lambda_a^+$, the following equality

$$2\lambda_a\Theta'_{a^+} + \Theta''_{a^+} = -2\frac{\mathscr{S}}{\Gamma}\lambda_a\chi'_{a^+}. \tag{A.13}$$

The limits in (A.13) are well defined since we have already shown in A.1 that all the quantities in (4.4) are bounded as $\zeta \to \lambda_a^+$. If we could show that the right hand-side of (A.13) tends to zero as $\mathscr{S} \to 0$, we could use (A.13) to obtain

$$2\lambda_a\Theta'_{a^+} + \varepsilon\Theta''_{a^+} = -(1-\varepsilon)\Theta''_{a^+} + r(S), \tag{A.14}$$

with $r(S)$ denoting the right hand-side of (A.13). The first term in (A.14) tends to a positive number and the second one, according to the hypothesis, tends to zero. Thus we obtain that for sufficiently small values of Stefan number the quantity $\varepsilon\Theta''_{a^+} + 2\lambda_a\Theta'_{a^+}$ must be positive. It thus only remains to verify the hypothesis that $r(S) \to 0$ as $\mathscr{S} \to 0$. This is still an open task, which, for example, could be verified by direct numerical calculations.

A.4 Author's published and submitted papers

A.4.1 Published papers

Kyselica, J. 2013 Evolution of the solidification front of a binary mixture. *Appl. Math. Model.* **37**, 3761–3776

A.4.2 Submitted papers

Kyselica, J., Guba, P. 2014 Forced boundary-layer flow and solidification on a moving substrate. Under review for *Acta Mech.*